

**PRACTICAL APPLICATION OF PETROGRAPHIC METHODS TO CRUSHED
STONE AGGREGATE EXPLORATION: COMPARING MICROSTRUCTURES
AND GRAIN BOUNDARIES TO PHYSICAL QUALITY TESTING OF
AGGREGATE**

By

Nicholas Charles Nuño

A thesis submitted to the Graduate Faculty of
Auburn University
in partial fulfillment of
requirements for the Degree of
Master of Science

Auburn, Alabama
December 12, 2015

Copyright 2015 by Nicholas Charles Nuño

Approved by

Dr. Mark G. Steltenpohl, Professor of Geology, Department of Geosciences
Dr. Jim A. Saunders, Professor of Geology, Department of Geosciences
Robert S. Fousek, Geologist, President of FMR Inc., Auburn, Alabama
Dr. Randy C. West, Director of the National Center for Asphalt Technology, Civil
Engineering, Auburn University

ABSTRACT

This research attempts to compare and correlate microscopic properties of aggregate material to the aggregates physical engineering properties. Material was collected and tested to obtain physical and mechanical properties of the aggregate. Thin sections were prepared and studied documenting minerals present, internal microstructures, and mineral grain boundaries. The physical aggregate testing properties were compared to the microscopic properties to determine if there is a correlation between the microscopic properties and how the rock will perform in building materials.

A direct correlation exists between properties observed under the microscope and physical testing results. The use of microscopy in exploration can result in significant exploration cost savings. Observed properties of potential aggregate such as grain size, mineralogy, absorption, texture, and fractures can be correlated to the quality of potential aggregate and how it will perform.

ACKNOWLEDGEMENTS

Funding for this research was graciously provided by Vulcan Materials via a grant administered through the Auburn University Environmental Institute and the National Center for Asphalt Technology (NCAT). Marsha Andrews of Vulcan Materials Inc. provided access to the Notasulga Quarry where samples were collected for testing. Thanks are owed to Randy West and NCAT for providing the facilities and equipment for testing, as well as valuable instruction on the ASTM testing process. Special thanks are owed to Mark Steltenpohl for providing funding, valuable insights into the field area, and assistance in sample preparation. Thanks are also owed to thesis committee members Mark Steltenpohl, Randy West, Bob Fousek, and Jim Saunders for their valuable suggestions and comments that improved the quality of this thesis. Finally, thanks are owed to my parents, Albert and Laura Nuño, for providing every kind of support throughout my undergraduate and graduate studies.

TABLE OF CONTENTS

Abstract.....	ii
Acknowledgments.....	iii
List of Tables	vi
List of Figures.....	vii
Introduction	1
Objectives	5
Literature Review	7
Rock Composition and Texture	7
Petrographic Examination	7
Location Overview	12
Geographic Location	12
Geologic History	14
Site Specific	19
Methods	20
Sampling	20
Preparation	27
Gradation	29
Testing	30
ASTM C88	30

ASTM C127	33
ASTM C131	35
ASTM C295	39
Results	41
ASTM Testing	41
Petrographic Analysis	43
Discussion	120
Los Angeles Abrasion Percentage of Loss	120
Sodium Sulfate Soundness Percentage of Loss	121
Specific Gravity and Absorption	121
Conclusions	123
References	126
Appendix A: Sieve Analysis for Fine and Coarse Aggregate	129
Appendix B: Sodium Sulfate Soundness	138
Appendix C: Specific Gravity and Absorption	147
Appendix D: Los Angeles Abrasion	156

LIST OF TABLES

1. Summary results from the ASTM standard tests run on samples of aggregate material from the Notasulga Quarry. 41
2. Terminology used to describe textures in this petrographic report 44

LIST OF FIGURES

1.	Digital Elevation Map (DEM) showing the site location in regards to roads and topographic features (ESRI, 2012).....	13
2.	Photograph (taken Fall 2009) of the quarry site looking east from the west highwall.....	14
3.	Geologic map and cross-section of the Alabama Piedmont (modified after Osborne et al., 1988; Thomas and coworkers as presented in Hatcher et al., 1989; and Steltenpohl, 2005). The red circle indicates the approximate location of the Notasulga Quarry within the Farmville Metagranite.....	15
4.	Location of hand samples collected within the Notasulga quarry on April 10, 2010	22
5.	Sample crusher at the Alabama Department of Transportation (ALDOT), Montgomery, Alabama where samples were crushed by the author.	28
6.	Gilson Shakers at the Alabama DOT in Montgomery, AL	29
7.	Preparing each sample interval size for submersion into the sodium sulfate solution.....	31
8.	Sample sizes soaking in sodium sulfate solution.....	32
9.	Samples sitting in bath of sodium sulfate solution	32
10.	Testing apparatus used to weigh sample in water. The scale has a bucket which hangs in the water to determine weight of the sample under water	34
11.	The Los Angeles Machine used to determine wear and tear of an aggregate source material.....	36
12.	The Los Angeles Machine with the doors open. The sample material is placed into the feed along with steel balls and locked in place	36

13.	One steel ball weighing 390-445 grams. The appropriate numbers of balls are placed into the Los Angeles Machine with the sample and the balls are used to pulverize or grind and crush the sample in order to gather information on how the sample may perform in its intended use.....	37
14.	Eleven steel balls used to perform grading “B” of ASTM C131.....	37
15.	N1-4-10P, Typical view of sample. Photographed with crossed polars at 100X magnification	46
16.	N1-4-10P, Typical view of sample showing interlocking grain boundaries. Photographed under crossed polars at 100X magnification.	47
17.	N1-4-10P, Large medium grained quartz grain showing undulatory extinction. Plagioclase is undergoing altering to sericite and clay. Photographed under crossed polars at 100X magnification	47
18.	N1-4-10P, Muscovite intergrown with biotite. Photographed under plane polarized light at 40X magnification.	48
19.	N1-4-10P, Same view as above in Figure 18 but photographed under crossed polars at 40X magnification.	48
20.	N1-4-10P, Muscovite with symplectic texture. Photographed under plane polarized light at 100X magnification.	50
21.	N1-4-10P, Same view as above in Figure 20 but photographed under crossed polars at 100X magnification.....	50
22.	N1-4-10P, Plagioclase undergoing saussuritization producing fine grained sericite, albite, and clay. Photographed under plane polarized light at 100X magnification.	51
23.	N1-4-10P, Same view as above in Figure 22 but photographed under crossed polars at 100X magnification. The bright interference colors of the stand out in contrast to the plagioclase.	51
24.	N2-4-10P, A.) Biotite under plane polarized light showing dark brown pleochroism. B.) Same view as A. but rotated 90° to show the light brown pleochroism. C.) Typical view of sample showing minerals present. The quartz within this thin section has slightly undulatory extinction. Same view as A. but photographed under crossed polars at 40X magnification.	55
25.	N2-4-10P, Biotite interlocked with quartz grains. Apatite is present. Remnants of garnet can be seen within this slide. Photographed under plane polarized light at 100X magnification.	56

26.	N2-4-10P, Same view as above in Figure 25 but photographed under crossed polars at 100X magnification. Quartz shows slightly undulatory extinction.....	56
27.	N2-4-10P, Grungy plagioclase grain undergoing saussuritization producing clay and sericite. Healed fractures common in the thin section. Plagioclase grain boundaries interlock with the quartz and biotite grain boundaries. Photographed under plane polarized light at 100X magnification	58
28.	N2-4-10P, Same view as above in Figure 27 but photographed under crossed polars at 100X magnification.....	58
29.	N2-4-10P, Muscovite with some grains exhibiting symplectic texture. Isotropic garnet is present. Photographed under plane polarized light at 100X magnification	59
30.	N2-4-10P, Same view as above in Figure 29 but photographed under crossed polars at 100X magnification.....	59
31.	N3-4-10, Granophyric texture in alkali feldspar metagranite. Photographed under plane polarized light at 100X magnification.....	62
32.	N3-4-10, Same view as above in Figure 31 but photographed under crossed polars at 100X magnification.....	62
33.	N3-4-10, Symplectic texture in muscovite. Photographed under plane polarized light at 100X magnification.	63
34.	N3-4-10, Same view as above in Figure 33 but photographed under crossed polars at 100X magnification.....	63
35.	N3-4-10, Plagioclase undergoing saussuritization to sericite and clay. Photographed under plane polarized light at 40X magnification	64
36.	N3-4-10, Same view as above in Figure 35 but photographed under crossed polars at 40X magnification.....	64
37.	N3-4-10, Biotite that has altered to chlorite and plagioclase saussuritized to produce clay. Photographed under plane polarized at 100X magnification	65
38.	N3-4-10, Same view as above in Figure 37 but photographed under crossed polars at 100X magnification.....	65
39.	N3-4-10, Plagioclase having undergone saussuritization producing sericite and clay. Photographed under plane polarized light at 40X magnification.....	67

40.	N3-4-10, Same view as above in Figure 39 but photographed under crossed polars at 40X magnification.....	67
41.	N3-4-10, Biotite is pleochroic light brown to dark brown under plane polarized light at 40X magnification. Typical microcline and quartz interlocking grain boundaries.	68
42.	N3-4-10, Same view as above in Figure 41 but photographed under crossed polars at 40X magnification.....	68
43.	N4-4-10, Biotite completely altered to chlorite and plagioclase undergoing alteration to sericite and clay. Open fracture filled with blue epoxy. Photographed under plane polarized light at 40X magnification	74
44.	N4-4-10, Same view as above in Figure 43 but photographed under crossed polars at 40X magnification. Note the interlocking, embayed grain boundaries.....	74
45.	N4-4-10, Plagioclase grain with moderate alteration to sericite and clay. Photographed under plane polarized light at 40X magnification	75
46.	N4-4-10, Same view as above in Figure 45 but photographed under crossed polars at 40X magnification.....	75
47.	N4-4-10, Albite exsolving in microcline producing perthitic textures. Photographed under plane polarized light at 40X magnification	76
48.	N4-4-10, Same view as above in Figure 47 but photographed under crossed polars at 40X magnification.....	76
49.	N4-4-10, Biotite completely altered to chlorite intergrown with muscovite. Photographed under plane polarized light at 100X magnification	78
50.	N4-4-10, Same view as above in Figure 49 but photographed under crossed polars at 100X magnification. Here it is clear that microcline has interlocking, embayed boundaries with plagioclase and also with muscovite where the short axis has been exploited.....	80
51.	N4-4-10, A clot of garnet with intergrown biotite and muscovite. Biotite has undergone alteration to chlorite. Photographed under plane polarized light at 40X magnification.....	79
52.	N4-4-10, Same view as above in Figure 51 but photographed under crossed polars at 40X magnification.....	79

53.	N4-4-10, Chlorite replacing biotite and intergrowths of muscovite within a microcline grain. Photographed under plane polarized light at 100X magnification.	80
54.	N4-4-10, Same view as above in Figure 53 but photographed under crossed polars at 100X magnification.....	80
55.	N4-4-10, Chlorite replacing biotite and intergrowths of muscovite. Plagioclase undergoing alteration to sericite. Albite poikilitically enclosed in plagioclase. Photographed under plane polarized light at 100X magnification	81
56.	N4-4-10, Same view as above in Figure 55 but photographed under crossed polars at 100X magnification.....	81
57.	N1A-4-10, Typical view of sample matrix. Photographed under 100X magnification	84
58.	N1A-4-10, Same view as above in Figure 57 but photographed under crossed polars at 100X magnification. Grain boundaries are embayed and interlocking.	84
59.	N1A-4-10, Interlocking grain boundaries. Biotite has altered to chlorite and muscovite has symplectic texture. Photographed under 40X magnification.....	85
60.	N1A-4-10, Same view as above in Figure 59 but photographed under crossed polars at 40X magnification.....	85
61.	N1A-4-10, Highly altered plagioclase grains poikilitically enclosed in microcline. Photographed under plane polarized light at 40X magnification	86
62.	N1A-4-10, Same view as above in Figure 61 but photographed under crossed polars at 40X magnification.....	86
63.	N1A-4-10, Biotite altered to chlorite, the latter having a fibrous texture. Photographed under 40X magnification	88
64.	N1A-4-10, Same view as above in Figure 63 but photographed under crossed polars at 40X magnification. Plagioclase undergoing saussuritization to sericite and clay.....	88
65.	N1A-4-10, Epidote intergrown with biotite forming a clot within the thin section that has undergone alteration to chlorite. Photographed under plane polarized light at 40X magnification	89

66.	N1A-4-10, Same view as above in Figure 65 but photographed under crossed polars at 40X magnification.....	89
67.	N2A-4-10, Typical view of sample. Photographed under 40X magnification	92
68.	N2A-4-10, Same view as above in Figure 67 but photographed under crossed polars at 40X magnification. Plagioclase grain hosts myrmekitic texture.	92
69.	N2A-4-10, Biotite with intergrowths of muscovite with symplectic texture. Photographed under plane polarized light at 100X magnification	93
70.	N2A-4-10, Same view as above in Figure 69 but photographed under crossed polars at 100X magnification. Quartz has undulatory extinction with embayed and interlocking grain boundaries	93
71.	N2A-4-10, Biotite is pleochroic, light brown to dark brown. Photographed under plane polarized light at 100X magnification.....	94
72.	N2A-4-10, Same view as above in Figure 71 but photographed under crossed polars at 100X magnification.....	94
73.	N2A-4-10, Biotite intergrown with garnet and epidote. Photographed under plane polarized light at 100X magnification.....	95
74.	N2A-4-10, Same view as above in Figure 75 but photographed under crossed polars at 100X magnification.....	95
75.	N2A-4-10, Plagioclase with intergrowths of muscovite with symplectic texture. Photographed under plane polarized light at 100X magnification	96
76.	N2A-4-10, Same view as above in Figure 75 but photographed under crossed polars at 100X magnification.....	96
77.	N2A-4-10, Biotite has straight grain boundaries. Most other grain boundaries in the thin section are embayed and interlocking. Photographed under plane polarized light at 100X magnification.....	98
78.	N2A-4-10, Same view as above in Figure 77 but photographed under crossed polars at 100X magnification.....	98
79.	N2A-4-10, Plagioclase with moderate alteration to sericite, clay and carbonate. Photographed under plane polarized light at 100X magnification.....	99
80.	N2A-4-10, Same view as above in Figure 79 but photographed under crossed polars at 100X magnification.....	99

81.	N2A-4-10, Euhedral sphene that has been altered to opaque minerals. Photographed under plane polarized light at 100X magnification	101
82.	N2A-4-10, Same view as above in Figure 81 but photographed under crossed polars at 100X magnification.....	101
83.	N3A-4-10, Typical view of sample illustrating an abundance of fractures present. Photographed under 40X magnification.....	104
84.	N3A-4-10, Same view as above in Figure 83 showing fractures cutting across multiple grains photographed under crossed polars at 40X magnification	104
85.	N3A-4-10, Fractures healed with carbonate, quartz, and opaque minerals traversing microcline and plagioclase. Photographed at 40X magnification	105
86.	N3A-4-10, Same view as above in Figure 85 but photographed under crossed polars at 40X magnification.....	105
87.	N3A-4-10, Albite exsolution resulting in perthitic texture within microcline. Photographed under plane polarized light at 40X magnification	106
88.	N3A-4-10, Same view as above in Figure 87 but photographed under crossed polars at 40X magnifications. Note the myrmekite in plagioclase	106
89.	N3A-4-10, Healed fractures extending through quartz and microcline. Photographed under 40X magnification	107
90.	N3A-4-10, Same view as above in Figure 89 but photographed under crossed polars at 40X magnification. Note the interlocking and embayed boundaries between the quartz and microcline grains	107
91.	N3A-4-10, Biotite altered to chlorite. Muscovite with symplectic textures. Photographed under 40X magnification	109
92.	N3A-4-10, Same view as above in Figure 91 but photographed under crossed polars at 40X magnification. Note the symplectic texture within the muscovite	109
93.	N3A-4-10, Chlorite showing light green to dark green pleochroism. Photographed under 40X magnification	110
94.	N3A-4-10, Same view as above in Figure 93 but photographed under crossed polars at 40X magnification. Quartz has undulose extinction	101

95.	N4A-4-10, Embayed and interlocking plagioclase and quartz with undulatory extinction. Photographed under 40X magnification.....	113
96.	N4A-4-10, Same view as above in Figure 95 but photographed under crossed polars at 40X magnification. Plagioclase shows signs of oscillatory zoning. Note quartz grains with embayed boundaries	113
97.	N4A-4-10, Typical view of sample. Microcline has a perthitic texture and myrmekite is present in plagioclase. Photographed under 40X magnification	114
98.	N4A-4-10, Same view as above in Figure 97 but photographed under crossed polars at 40X magnification. Note the perthitic texture within the microcline	114
99.	N4A-4-10, Myrmekite in plagioclase adjacent to microcline. Photographed under 100X magnification	115
100.	N4A-4-10, Same view as above in Figure 99 but photographed under crossed polars at 100X magnification.....	115
101.	N4A-4-10, Muscovite with symplectic texture and myrmekite in plagioclase. Photographed under 40X magnification	116
102.	N4A-4-10, Same view as above in Figure 101 but photographed under crossed polars at 40X magnification. Note the embayed boundaries with surrounding grains of quartz and microcline and straight boundaries with muscovite and biotite	116
103.	N4A-4-10, Chloritic alteration of biotite with muscovite intergrowths. Photographed under 100X magnification	118
104.	N4A-4-10, Same view as above in Figure 103 but photographed under crossed polars at 100X magnification. Muscovite has symplectic texture	118

INTRODUCTION

Since the beginning of civilization, people have been mining earth's mineral resources to better their lives. Whether it is mining gold and other precious stones and metals for royalty, uranium to make weapons for defense, or aggregate for concrete, hot mix asphalt to make roads, or for other construction uses, mining is essential. For aggregate mining companies to remain competitive and profitable, they must always be looking for additional reserves of high quality stone or sand and gravel. Aggregate exploration is a high cost endeavor so mining companies must continually seek new technology and methods to save exploration costs.

Aggregate is an essential ingredient in making ready mix concrete and hot mix asphalt products which are needed in our modern society. Aggregate comprises seventy-five to eighty percent of concrete (Dolar-Mantuanui, 1983), and ninety to ninety-five percent of hot mix asphalt (Barksdale, 2001). Most concrete and hot mix asphalt is needed for urban areas that are developing, and since transportation of rock is costly, quarries need to be located nearby. As these urban areas grow larger, new aggregate sites with quality stone must be found. Likewise, tightening of government standards and regulations protecting the environment has resulted in increased mining costs. As quality stone reserves are depleted through time, new quarry sites will need to be located and permitted.

Performance of quality aggregate is represented by its ability to withstand handling and associated production activities as well as degradation of the aggregate particles within completed structures due to physical and environmental forces. Important mechanical properties of aggregate include 1) strength and interconnectedness of the assembly of particles, and 2) resistance to breakage and abrasion of the individual particles. The first category is affected primarily by particle gradation and shape. Different rocks have different physical properties which influence aggregate material performance. Many of these properties can be measured using standardized tests (Langer & Knepper, 1995). The second category is affected by rock composition and texture. Petrographic analysis is useful in evaluating the second of these two categories.

Petrographic examination is the visual examination and analysis of the material to determine the lithology and properties of the aggregate being considered for use in ready-mix concrete, hot-mix asphalt, and other construction uses. Petrographic examination allows the properties of specific aggregate types to be established. These include the physical and chemical characteristics such as particle shape, surface texture, pore features, hardness, and potential for alkali-aggregate reactivity; coatings on sand and gravel particles; and the presence of contaminating substances (Mielenz, 1955). The procedure for conducting a petrographic examination requires at a minimum the use of a hand lens and petrographic and stereoscopic microscopes.

Examination of a rock in hand sample and in thin section provides information that is essential in the evaluation of aggregate physical performance tests. For example, an understanding of a rock's mineral composition and texture, as well as physical properties such as hardness, durability, and porosity, which can be obtained from

petrographic examination, will give a better understanding of how the rock will perform as aggregate for use as a building material.

Petrographic analyses, including hand sample and thin section analysis, were conducted on the rock samples used in this report. Background information on the major rock types and geologic history are provided to assist in the understanding of the petrographic summaries presented. The information obtained from the petrographic analysis, specifically texture, mineral composition, grain boundaries, and microstructures within the rock, will be analyzed and compared to the aggregate performance test results. The objective of this study is to explore for correlations between rock composition, microstructures and related properties, and the results of the physical testing conducted on the samples to establish guidelines for use in evaluating new aggregate sources prior to expensive drilling and associated exploration costs. Guidelines developed in this report can be used to make a determination early in the exploration phase if additional drilling costs are justified or if the proposed source has a low probability of producing an aggregate that will meet applicable specifications.

The American Society for Testing Material (ASTM) has created a set of standards and test methods for aggregate used in construction. The tests include ASTM standards C 127, *Standard Test Method for Density, Relative Density (Specific Gravity), and Absorption of Coarse Aggregate*; C 131, *Standard Test Method for Resistance to Degradation of Small Size Coarse Aggregate by Abrasion and Impact in the Los Angeles Machine*; and C 88, *Standard Test Method for Soundness of Aggregates by Use of Sodium Sulfate or Magnesium Sulfate* (ASTM, 2008).

ASTM C 127 is used to determine apparent specific gravity, bulk specific gravity, and surface saturated specific gravity. The specific gravity of aggregate is used to proportion aggregate with asphalt or cement and other additives to produce building materials (Barksdale, 2001). ASTM C 131 is used to determine the percent loss and the ability of the aggregate to resist degradation during production and subsequent handling. ASTM C 88 determines an aggregates ability to resist freezing and thawing. The sulfate solution penetrates the pore space within the rock and expands as it dries breaking the rock simulating water penetrating the pore space and expanding as it freezes rupturing the rock.

The rock types used in this study include metagranite from the Notasulga quarry near Loachapoka, Alabama. A wide range of samples were collected from the Farmville Metagranite and tested at the National Center for Asphalt Technology (NCAT) and the Alabama Department of Transportation (ALDOT) by the author and the results have not been previously reported. Comparisons between the tested aggregate and observed properties using petrographic analysis of the aggregate have been made and are presented in this report. Using these comparisons a mining geologist can predict how similar rocks may behave if tested and whether the rock will meet applicable specifications allowing mining companies to evaluate a potential deposit prior to expensive drilling and testing of the drill cores.

OBJECTIVES

This study compares and correlates microscopic properties of construction aggregate to physical properties of the aggregate. Metagranite was chosen as the study material. Vulcan Materials Inc. granted the author permission to allow access to their Notasulga quarry and sample the Farmville Metagranite for study and testing.

Samples for physical testing are traditionally obtained during exploration by use of core drilling. The recovered cores are split, crushed, composited into samples, and the samples subjected to testing to determine if the site is capable of producing a quality aggregate that will meet all required specifications. The cost of core drilling represents a significant investment whether quality material is found or not. Currently core drilling with ancillary road and drill pad building runs \$30.00 to \$40.00 per foot. A typical crushed stone quarry site is nominally 150 acres and often is over 500 acres. The industry recommended standard for core drill hole spacing is about 500 feet and holes may range up to 300 feet or more in depth requiring substantial investment for drilling and testing of the cores. A method of evaluating stone from outcrops before investing significant money into core drilling is needed. ASTM C 295 *Standard Guide for Petrographic Examination of Aggregates for Concrete* provides guidelines to be used in examining aggregates from both established locations and those being evaluated during exploration. However, ASTM C 295 is only used to quantify deleterious materials such as reactive minerals that can lead to alkali-aggregate reactions, pop outs in concrete,

shale, schist, mica, or swelling clays, among other problems. It does not address the potential of correlating the results of the petrographic examination with the physical testing results. The objectives of this study are as follows: (1) collect samples from the Notasulga quarry highwalls to make thin sections along with sufficient material for use in physical testing; (2) test the samples at the NCAT and ALDOT laboratories following ASTM standards to obtain physical and mechanical properties of the aggregate; (3) study thin sections and document microstructures, mineral grain boundaries, deleterious materials, and identify any alkali-aggregate reactive components; and (4) compare results of aggregate physical testing to the microscopic properties to determine any correlations between them.

LITERATURE REVIEW

Rock Composition and Texture

Previous experience with petrographic analysis for aggregate evaluation has suggested that knowledge of a rock's mineral composition, physical characteristics such as mineral grain boundaries relationships, bedding plane, foliation, absorption, and porosity, is useful in understanding how the rock will perform as a construction material.

A study by Tugrul and Zarif (1999) reports that petrographic analysis has been developed to quantify the relationships between the petrographic characteristics of rocks to the physical and mechanical properties of intact granite rocks from a location in Turkey. They found that a rock's average grain size alters the strength of the rock and in turn the strength of the aggregate. As grain size increases the strength of the material decreases and strength increases as the average grain size decreases. They found that mineralogical composition is one of the main properties controlling rock strength. Tugrul and Zarif (1999), as well as many others after them, state that the greater the degree of interlocking grains present in target rocks the greater the rock strength.

Petrographic Examinations

The purpose of conducting petrographic examinations is to aid the investigation, selection, testing, and control of aggregate material. The petrographic examination will

assist the geologist in determining the extent of an undeveloped deposit of aggregate material and indicate the relative quality of the aggregate compared to alternative sites. Examination of exposures in the field can provide the quality data and descriptions of variations in the material (if any) in order to determine the minimum program of exploration and sampling needed for acceptance or rejection of a deposit (Mielenz, 1955).

Since 1936, all aggregate material used in concrete construction by the Bureau of Reclamation and the United States Army Corps of Engineers (USACOE) were examined petrographically as part of the basis for their selection for aggregates (Mielenz & Witte, 1948). In 1952, the American Society for Testing Materials, ASTM, accepted a Recommended Practice for Petrographic Examination of Aggregates for Concrete (C295), which became a standard practice in 1954 (Mielenz, 1955). This standard was adopted to standardize the methods used by petrographers to conduct and report the results of petrographic examinations. The standard practice allows for unfamiliar geological deposits to be compared to known deposits that have been previously tested and have yielded either satisfactory or poor testing results.

Samples of aggregate for petrographic examination should be representative of the source of the materials being used. ASTM D75, *Standard Methods of Sampling Stone, Slag, Gravel, Sand, and Stone Block for use as Highway Materials*, gives the recommended procedure for sampling and for preparation of the sample for analysis (Mielenz, 1946). Preliminary petrographic examinations may be performed in the field or may be performed in the laboratory as part of the program of testing (Mielenz, 1955). Preliminary examinations are conducted with the aid of a hand lens, a 10% solution of

hydrochloric acid (HCl), and hardness points to identify lithology, general mineral composition, presence of deleterious materials and hardness.

Petrographic examination of samples in the field is usually qualitative with detailed quantitative work performed later in a laboratory. If the deposit being tested is variable, it is important to select samples from each zone, and detailed notes should be made noting the location of each sample, a description of the lithology and mineralogy, formation name if known, and any other relevant data. These notes and the results of the tests on the samples will allow for characterization of the deposit and a determination of whether it is economical to mine. It will show areas of undesirable material that should be avoided during mining (Mielenz, 1955). Rocks in the field may contain zones of faulting or jointing which allow water to penetrate into the rock resulting in weathering and/or alteration of minerals. Areas may contain deleterious substances such as excessive mica, chert, clay, shale, schist, friable stone, alkali-aggregate reactive materials, chlorite or other deleterious substances. These materials need to be identified by geologic and petrographic examinations of the outcrops in the field (Mielenz, 1955). A rock may look sound at first glance but upon detailed examination, may contain deleterious properties or constituents that make it unsuitable for use as an aggregate. Mielenz (1955) cites the Chiplima granite as a notable example. It is the source of aggregate used for the construction of the Hirakud Dam in India. Initial testing of the aggregate manufactured from the granite produced test results that met all specifications. However, when used in ready mix concrete (RMC) in the dam and after being subjected to one or more monsoon seasons, reactions occurred in the aggregate resulting in brown staining and the development of microfractures from the oxidation of jarosite in the

granite. Had an in-depth petrographic examination had been performed prior to the selection of the granite aggregate for the dam project the jarosite likely would have been noted and the conclusion drawn that this aggregate source contained deleterious materials and hence was unsuitable for use as a construction aggregate in the dam.

Petrographic examination of samples in the laboratory can be brief or very detailed. Brief examinations can determine the minerals in the material and supply validation for abandonment or continued investigation of undeveloped deposits (Mielenz, 1955). During analysis in the lab, the petrographer notes features such as: 1) friability in the fingers; 2) resonance when struck; 3) ease of fracturing; 4) nature of fracture surfaces and fracture fillings; 5) odor of fresh fractures; 6) color and its variation; 7) internal structure, such as porosity, granularity, or lamination; and 8) reaction to water, such as absorption of droplets on a fresh fracture, evolution of air on immersion, capillary suction against the tongue, slaking, softening, or swelling (Mielenz, 1955). Petrographic examination of crushed stone will establish the internal texture, particle size and shape, distribution of unsound or deleterious substances, and abundance of fines caused by the crusher.

The petrographic characteristics known to affect the mechanical properties of an aggregate include grain size, grain shape, packing density, degree of interlocking grains, types of contacts, amount and type of cement holding the grains together, and the mineralogical composition (Ulusay et al., 1994). Grain sizes and strength correlations have been studied previously on different types of sandstone, limestone and marble, and crystalline rock. Fahy and Guccione (1979) showed that sandstone with smaller grain sizes had higher strength values. Although grain size does play a role in strength, they

concluded that sphericity inversely correlates with compressive strength and shows the strongest correlation among the petrographic properties. In limestone and marble, Handlin and Hager (1957) found that strength increased as grain size increased. Their study, however, did not take into account the correlation between the amount of cement between the grains and the mechanical properties. In crystalline rock, Onodera and Asoka (1980) found similar results as Handlin and Hanger (1957), such that an increased grain size increases strength of the rock but concluded that matrix and cement had more to do with increases in strength. Bell (1978) looked at the packing density occupied by grains within the rock and correlated it to strength properties. He concluded that when the packing density increased, the strength of the material increased. This study shows, however, that as grain size increases, sulfate soundness and Los Angeles abrasion also increase (See Conclusions).

LOCATION OVERVIEW

Geographic Location

The study area is located in Lee County, Alabama west of the town of Loachapoka and within generally rolling hills of the piedmont physiographic province (Figure 1). The site is owned and operated by Vulcan Materials Inc. (VMC) who has produced construction aggregate from the site since 2005. The site is currently active and the necessary precautions must be taken in order to maintain safety around large equipment (Figure 2).

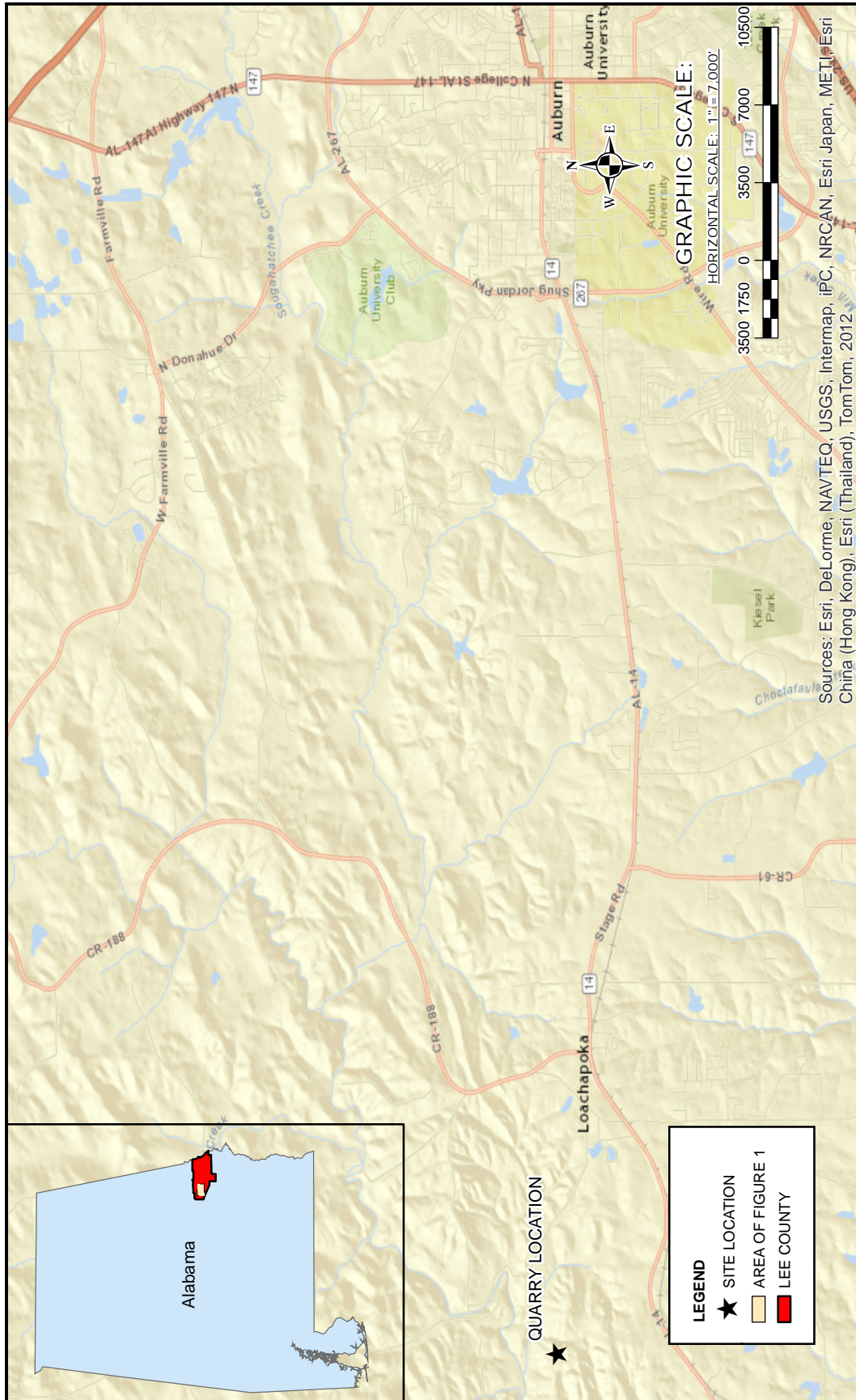


Figure 1. Digital Elevation Map (DEM) showing the site location in regards to roads and topographic features.



Figure 2. Photograph (taken Fall 2009) of the quarry site looking east from the west highwall.

Geologic History

The mine site is located within rocks of the Inner Piedmont terrane that lies between the Brevard fault zone to the west and the Towaliga fault zone to the east (Figure 3). The Inner Piedmont terrane of Alabama has been subdivided into the Dadeville and Opelika Complexes (Bentley & Neathery, 1970; Osborne et al., 1988), which are northeast trending sequences of metasedimentary and/or meta-igneous rocks (Cook et al., 2007). The post metamorphic Tallassee synform is composed of these two complexes and plunges shallowly toward the north-northeast (Grimes & Steltenpohl, 1993). As a result of the Tallassee synform, the outcrops in the quarry floor strike northeast and dip towards the northwest. These complexes contain kyanite and or sillimanite zone mineral assemblages (Cook et al., 2007). The timing of metamorphism and related deformation has been interpreted to be Ordovician, Devonian, and/or Carboniferous, but is not well

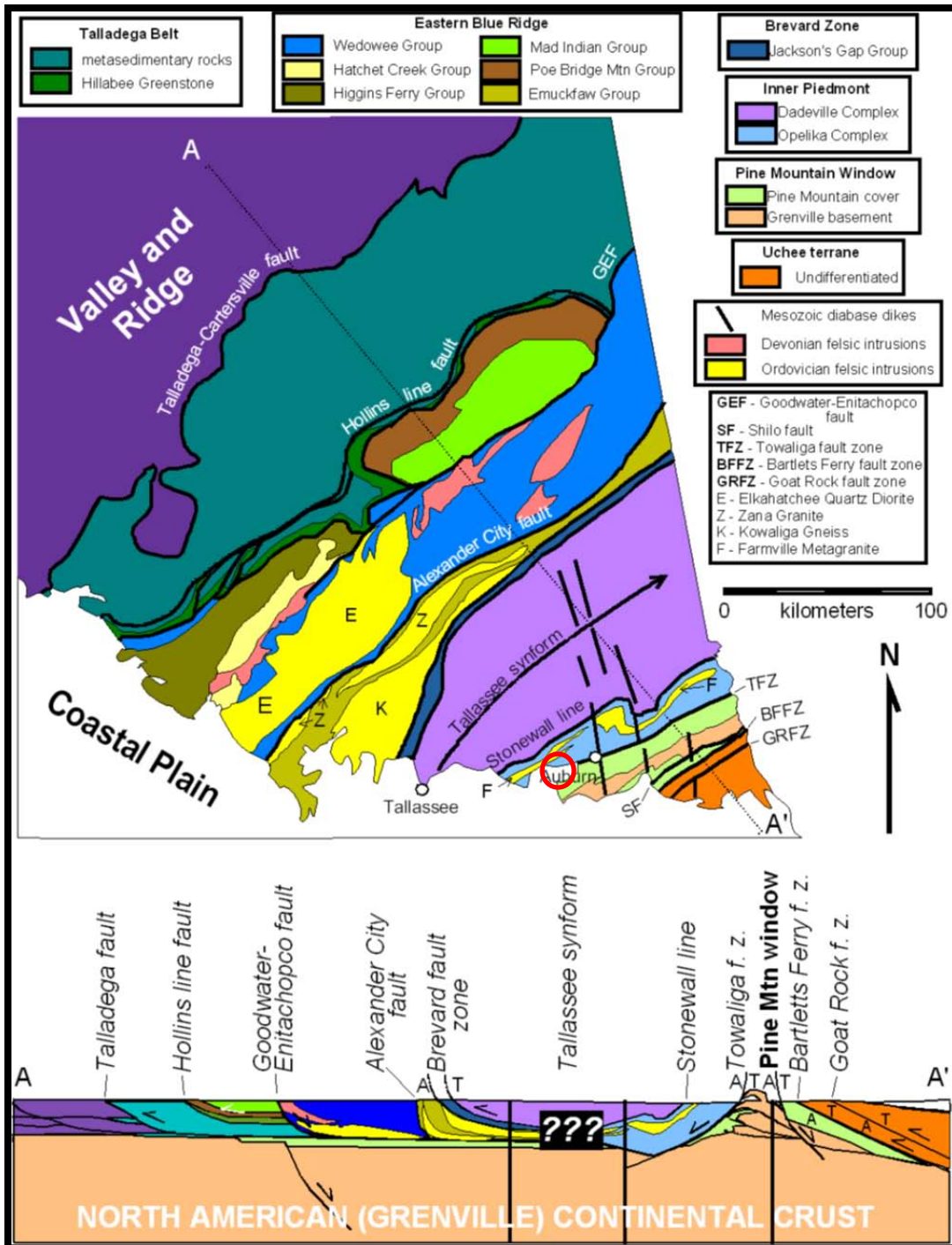


Figure 3. Geologic map and cross-section of the Alabama Piedmont (modified after Osborne et al., 1988; Thomas and coworkers as presented in Hatcher et al., 1989; and Steltenpohl, 2005). The red circle indicates the approximate location of the Notasulga Quarry within the Farmville Metagranite.

constrained due to lack of fossils in the rocks and reliable isotopic dates (Steltenpohl & Moore, 1988). The Inner Piedmont has been described as either an Iapetan suspect terrane that was thrust above the Laurentian margin or as part of the distal Laurentian slope rise facies itself (Steltenpohl et al., 1990). The rocks within the study area have been assigned to the Opelika Complex (Steltenpohl & Moore, 1988; Sterling & Steltenpohl, 2004). The Opelika Complex is divided into four lithologic packages (Bentley & Neathery, 1970; Steltenpohl et al., 1990) the Loachapoka Schist, the Auburn Gneiss, the Farmville Metagranite, and pegmatites of uncertain affinity (Bogdan, 2009). Previous studies by Grimes and Steltenpohl (1993) as well as others have suggested that the Opelika Complex may actually belong to the Emuckfaw Group of the Eastern Blue Ridge rather than the Inner Piedmont. Evidence supporting this hypothesis includes field mapping, age dating, and geologic observations. The Opelika Complex and Emuckfaw Group contain mostly repetitive meta-arkosic schist and gneiss which were intruded by large volumes of granitic magmas (Cook et al., 2007). The Emuckfaw Group lies on the west limb of the Tallassee synform while the Opelika Complex forms part of the east limb. The Dadeville Complex forms the synform's core. Thermal Ionization Mass Spectrometry (TIMS) U-Pb zircon dates from the Farmville Metagranite gives a crystallization date of 460 ± 16 Ma (Steltenpohl et al., 2005). This date indicates that Middle Ordovician magmatism was more widespread than previously believed and that the Opelika Complex and Emuckfaw Group likely are related.

The unit being mined for aggregate stone at the Notasulga quarry is the Farmville Metagranite (Steltenpohl et al., 1990), which was formerly known as the "Bottle Granite" of Bentley and Neathery (1970). The Farmville Metagranite is named for exposures in

and around Farmville City, Lee County, Alabama. Steltenpohl and others (1990) designate the type locality as the extensive roadway outcrops along and directly beneath the bridge over Saugahatchee Creek, Lee County, Alabama (SW1/4 sec. 18, T. 19N., R 25 E.).

The Farmville Metagranite, based upon proportions of modal quartz, alkali feldspar, and plagioclase, is classified as a granite (Goldberg & Burnell, 1987). Goldberg and Steltenpohl (1990) describe the major mineral assemblage as quartz, microcline, plagioclase (albite-oligoclase), biotite, muscovite and trace amounts of garnet, epidote, sphene, apatite, and zircon. The dominant phyllosilicate is biotite, with muscovite representing a minor phase (< 3%) and predominantly confined to the margins and within sheared zones of the metagranite. The same authors classify the metagranite as peraluminous (molar $Al/Na + K + Ca > 1.1$) and corundum-normative (0.8-6.4%) based upon major element data. The metagranite is thus characterized as having an S-type affinity denoting an origin through partial melting of a pelitic source (Goldberg & Burnell, 1987). The same authors also indicate that the schists of the Auburn Gneiss sequence could not have been source for the Farmville.

Goldberg and Steltenpohl (1990) recognized that the Farmville Metagranite occurs as smaller, ill-defined tabular bodies with highly mobilized margins against its host units rather than distinct, homogenous, regional scale individual plutons as depicted on the geologic map of Alabama (Osborne et al., 1988). Sills of Farmville are generally concordant to the regional foliation and exhibit a lit-par-lit relationship attributed to injection along foliation plane polarized lights and lithologic contacts in the country rock

(Colberg, 1989). These observations are supported by field relationships exposed at the study site.

Emplacement of the Farmville Metagranite was determined to be syntectonic by Goldberg and Steltenpohl (1990) based upon the criteria established by Patterson and Tobisch (1988) of: 1) continuity of dominant foliation in both the metagranite and country rock; 2) continuity of stretching lineations in both the metagranite and country rock; 3) the greatest intensities of strain occur along the margins of the metagranite bodies; and 4) the general concordance of the bodies within regional structures.

The Farmville Metagranite was originally interpreted to have intruded and crystallized in the Devonian based upon a Rb-Sr whole-rock isochron of 369 ± 5 Ma (Goldberg & Burnell, 1987). Steltenpohl and others (2005), however, report a TIMS U-Pb date on zircons from the Farmville Metagranite indicating igneous crystallization at 460 ± 16 Ma. This date further supports correlation of the Opelika Complex rocks with the Emuckfaw Group based upon mapping (Grimes & Steltenpohl, 1993; White, 2007) and Middle Ordovician granitic magmatism. Steltenpohl and others (2005) interpret remobilized parts of the Farmville as due to metamorphism and deformation circa 369 Ma. Goldberg and Steltenpohl (1990) report a 341 ± 10 Ma Rb-Sr isochron on rocks marginal to these remobilized Farmville bodies, which likely reflects mid-Mississippian fluid-driven shear deformation.

Site Specific

The Notasulga quarry is underlain by a northeast trending sequence of metasedimentary and metaigneous rocks associated with the Opelika Complex of the Inner Piedmont (Osborne et al., 1988). Bogdan (2009) determined and delineated various rock units on the site that may affect mining operations. Core holes were utilized to analyze the geology of the site and from the core holes he was able to separate the rock types into five rock packages (Rock Package 1 through Rock Package 5).

Rock Package 1 (RP1) was a metasedimentary package that was the lowermost unit in the lithologic section of rocks studied at the site. The metasedimentary lithologies found in RP1 include quartzite, quartz plagioclase paragneiss, and garnet muscovite schist. Rock Package 2 (RP2) includes augen gneiss with potassium feldspar augens and persistent concordant pegmatite layers approximately 15 cm in thickness. Rock Package 3 (RP3) is composed of a metasedimentary package of quartz biotite schist and leucosomal boudins. Quartz-plagioclase pegmatite boudins are common throughout the sequence. Rock Package 4 (RP4) is a meta-granite that is the target unit that Vulcan is currently mining. RP4 has been mapped by Sterling and Steltenpohl (2004) as part of the Farmville Metagranite. Rock Package 5 (RP5) is a pure muscovite paraquartzite that marks the top of the lithologic section.

The meta-granite mined at this site produces fine and coarse-grained aggregate to sell to the markets in Alabama and Florida. Vulcan is obligated to do quality control on the material sold so most of the samples in this study came from RP3 and RP4. This allowed for the comparison between physical testing properties of the material and microscopic properties such as grain boundaries and interconnectedness.

METHODS

Standards are in place to ensure aggregate quality and prior-to-use representative samples must be collected to obtain meaningful test results verifying aggregate quality. The most important part of aggregate testing is to secure a representative sample. If the aggregate sample is not representative of the rock being mined then the testing and evaluation may be rendered useless by an improper sampling technique. It is important to use a random sampling technique in order to represent all of the material being used or produced.

Sampling

There are many different sampling techniques; hence a sampling protocol is required to maintain repetitiveness and quality. Samples may be collected randomly to be used for quality control or may be selected to represent a group of material. For this study, representative samples were collected from eight locations within the Vulcan Materials Inc. quarry in Notasulga, Alabama and are described in this section. These samples were collected via hand grab sampling from material present as float or shot rock representing the material seen in the high walls around the quarry at specific locations. The quarry face was inspected to determine visual variations in different rock layers including differences in color, texture, and structures. Separate samples of float rock were collected for each rock unit observed within the highwall. Since these samples were collected at specific sites, the grab sample is only representative of the rock lithology of that specific location. Since the lithology is consistent throughout the rock unit sampled, the grab sample can be considered to be random and reasonably representative of that lithology. As a result of specific rock units being targeted for testing, a grab sample was

the best method for obtaining an adequate sample size of that specific lithology for aggregate testing. Hand samples were collected at the grab sample location and labeled. The outcrop was described in a field notebook to register descriptions of lithologies and structures and to record measurements of the various fabric elements. The GPS coordinates for each site were recorded and plotted on a map showing the locations of each sample (Figure 4).

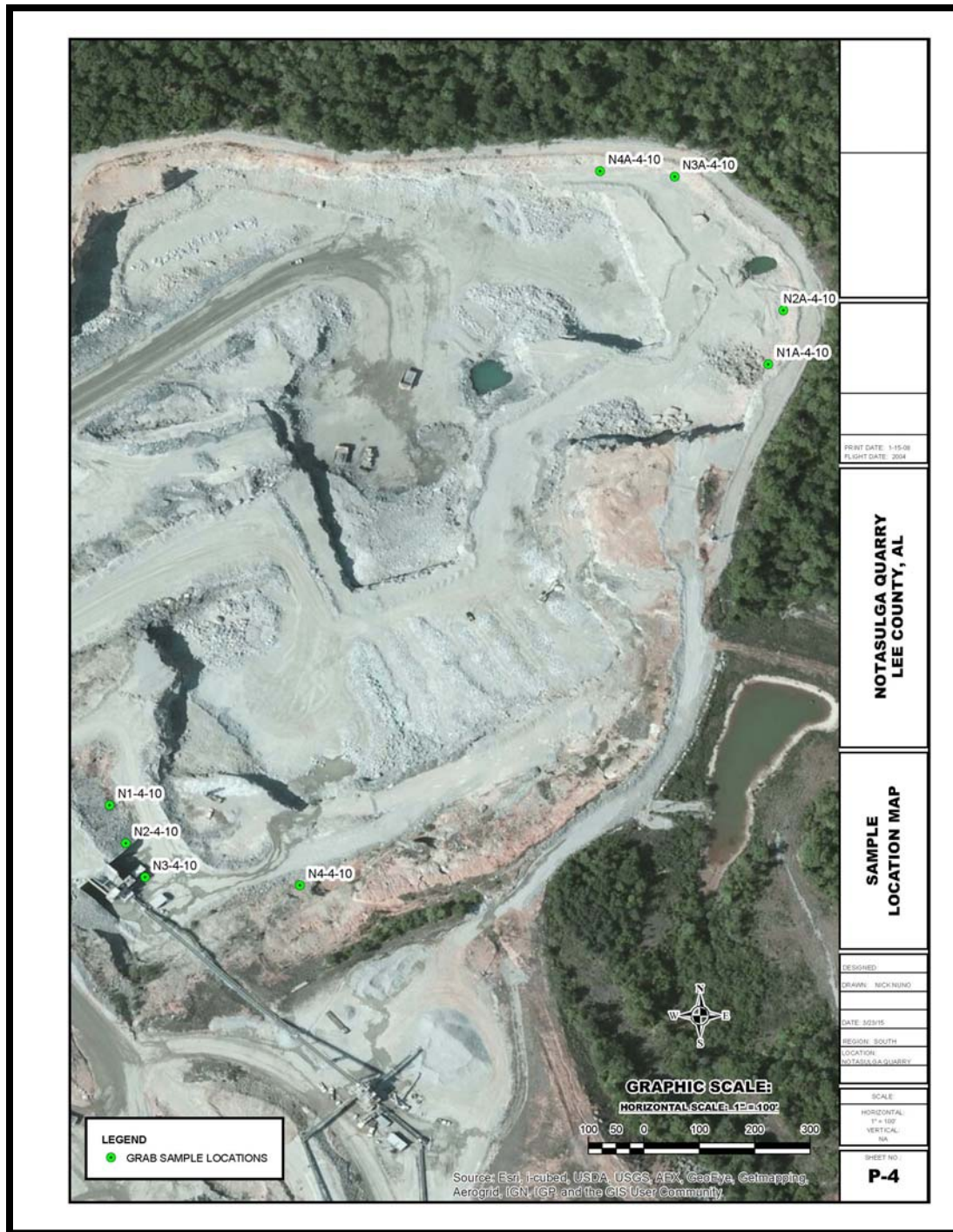


Figure 4. Location of hand samples collected within the Notasulga quarry on April 10, 2010.

N1-4-10

Sample N1-4-10 was collected on the upper bench of the quarry in the west highwall under the crusher (N 32.60852°, W 85.63969°) from the Farmville metagranite rock unit (unit 3 of Bogdan, 2009). This sample is a granitic gneiss with rare small garnets within the foliation and chalcopyrite coating some fracture surfaces. Approximately 50 pounds of material was collected in the form of a large boulder to ensure there was enough material for testing. Foliation in these outcrops dip to the northwest but sample N1-4-10 was collected as a float block that was not in place but clearly was derived from the highwall at this location.

N2-4-10

N2-4-10 was collected on the upper bench of the quarry about fifty feet to the south-southeast of N1-4-10. The rock is a granite gneiss that contains some pink microcline and some strained quartz as seen in hand sample by cloudy quartz ribbons. There appears to be a weak foliation in the rock. The location of this sample could not be determined accurately using a handheld GPS device due to the quarry highwall blocking satellite position. Approximately 50 pounds of material was collected in the form of a large boulder to ensure there was enough material for testing. The material had been shot from the highwall and the location is assumed to be approximate. An orientated sample with a strike of N15E and a dip of 69° west was also collected at this site.

N3-4-10

Sample N3-4-10 was collected on the upper bench of the quarry about seventy-five feet from sample N1-4-10 farther southeast following the highwall. The rock is an alkali feldspar metagranite with a pegmatite dike cross cutting the sample. The sample contains quartz, plagioclase, and some biotite as seen in hand sample. Pink microcline looks dirty and has probably undergone alteration. The location of this sample could not be determined accurately using a handheld GPS device. Approximately 50 pounds of material from a large float block was collected for physical testing. An orientated sample was not collected at this site.

N4-4-10

N4-4-10 sample was collected on the upper bench of the quarry about 300 feet east of N3-4-10. This sample is a mixture of metagranite and pegmatite containing plagioclase, quartz, and biotite as observed in hand sample. The rock appears to be somewhat weathered as indicated by its brittleness and open grain boundaries. The location of this sample could not be determined accurately using a handheld GPS device. Approximately 50 pounds of material was collected and no orientated sample was collected.

N1A-4-10

Sample N1A-4-10 was collected on the lower bench of the quarry in the east highwall (N 32.61026°, W 85.63717°). Although lower in the pit, this sample is stratigraphically above the samples taken on the upper

bench. It was collected from the Farmville metagranite rock unit (unit 4 of Bogdan, 2009). The sample is an augen gneiss and microcline, biotite and quartz are observed in the hand sample. A large float block approximately 50 pounds was collected to ensure enough material was present for analysis. An orientated sample with a strike of N12W and a dip of 85° E was collected at this site.

N2A-4-10

This sample was collected on the lower bench of the quarry approximately one-hundred feet to the north-northwest of N1A-4-10 stratigraphically above the samples taken on the upper bench. This rock is a metagranite containing muscovite and quartz as identified in the hand sample. It is dark gray in color and contains a xenolith of what appears to be metagraywacke of the Auburn Gneiss. The location of this sample could not be determined accurately using a handheld GPS device. A float block of this sample weighing approximately 50 pounds was collected to ensure enough material was present for analysis.

N3A-4-10

Sample N3A-4-10 was collected on the lower bench of the quarry approximately three-hundred feet to the northwest of N2A-4-10 (N 32.36661°, W 85.38236°). Although lower in the pit, this sample is stratigraphically above the samples taken on the upper bench. The rock is from a microcline-quartz pegmatite and contains microcline, plagioclase, biotite, and quartz. A large boulder of this sample weighing

approximately 50 pounds, as was an orientated sample with a strike of N12W and a dip of 85° E.

N4A-4-10

This sample also was collected on the lower bench of the quarry, approximately one-hundred-fifty feet to the west of N3A-4-10, stratigraphically above the samples taken on the upper bench. This augen gneiss sample contains potassium feldspar, biotite and quartz. The location of this sample could not be determined accurately using a handheld GPS device. An approximately 50 pound float block was collected for testing.

Preparation

Prior to performing laboratory tests on a sample it is necessary to process it into the requisite sizes for testing. This is accomplished by crushing the sample. The boulder size samples were first broken with a sledge hammer into smaller more manageable pieces approximately 4 to 6 inches across. These samples were broken in a clean area free from other rock fragments to avoid contamination of the sample. The broken pieces were collected and placed in a five gallon bucket labeled with the sample identification. The samples were then taken to the Alabama Department of Transportation (ALDOT) laboratory in Montgomery, Alabama, where they were crushed using a force fed portable crusher with a 12 inch opening. The material was crushed to sizes ranging from 1 inch to a -#200 sieve size. The samples were run through the crusher (Figure 5), collected in a bin at the bottom of the crusher and placed into the labeled five gallon sample bucket. The crusher was cleaned after each sample was crushed to prevent contamination.



Figure 5. Sample crusher at the Alabama Department of Transportation (ALDOT), Montgomery, Alabama where samples were crushed by the author.

Gradation

Following crushing, the material was taken to the National Center for Asphalt Technology (NCAT) where each sample was passed through a Gilson shaker (Figure 6) to obtain the necessary sieve sizes required for aggregate testing. Each sieve size was weighed and recorded to determine if there was enough material for the required testing. Each sieve size sample was placed into plastic sample bags labeled with the sample name and the individual sieve size. The complete gradations are in Appendix A, “Aggregate Gradation Summary”.



Figure 6. Gilson Shakers at the Alabama DOT in Montgomery, AL.

Testing

ASTM C88 – Standard Test Method for Soundness of Aggregates by Use of Sodium Sulfate or Magnesium Sulfate

This test helps determine how an aggregate will react in certain weather conditions and if it is sound when there is not adequate information available based on service records. This test is performed by repeatedly immersing the sample into a saturated solution of sodium or magnesium sulfate (Figures 7-10) followed by drying the sample to dehydrate the salt in the pore spaces. The expansive force caused by the rehydration of the salt upon re-immersion simulates water freezing within the aggregate pore space.

- **Preparation and Testing Procedures**

The samples were washed and dried at 230 ± 9 °F to obtain a constant weight and separated into the different size fractions required for testing (Figure 7). The size fractions are shown in the chart below:

Size	Mass (grams)
3/4"	500 \pm 30 g
1/2"	670 \pm 10 g
3/8"	330 \pm 5g
#4	300 \pm 5g

After the sample has been weighed and dried, the different size fractions are labeled and placed into mesh cloth. They are then submerged into the sodium or magnesium solution (sodium sulfate solution in this case) for 16 to 18 hours (Figure 8). The samples are then dried at 230 ± 9 °F to obtain a constant mass. Once a constant mass is achieved, the samples must be cooled to room

temperature at which time the process begins again. The repetition of immersing and drying continue for five cycles (Figure 9). Once the last cycle is complete, the sample is washed to clean the sodium or magnesium sulfate from the sample. The sample is dried to a constant weight and sieved over the same size fraction on which it was retained. The sample is then weighed and the weight recorded. The difference between the tested sample and initial weight is the loss in the test and is expressed as the percent loss. The complete sulfate soundness testing results are in Appendix B, “Sulfate Soundness Testing Summary”.



Figure 7. Preparing each sample interval size for submersion into the sodium sulfate solution.



Figure 8. Sample sizes soaking in sodium sulfate solution.



Figure 9. Samples sitting in bath of sodium sulfate solution.

ASTM C127 – Standard Test Method for Density (Specific Gravity), and Absorption of Coarse Aggregate

This test determines the average density of a sample of coarse aggregate particles (not including the volume of voids between the particles), the relative density of that material (specific gravity), and the absorption of the coarse aggregate. This test method is used to determine the density of the solid portion of a large number of aggregate particles and provides an average value that represents the sampled material.

- Preparation and Testing Procedures

The samples are thoroughly mixed and reduced to an approximate weight of 4000 grams. The sample is dried in an oven to a constant mass at a temperature of 230 ± 9 °F. Once the sample is at a constant mass it is cooled to room temperature for about 1 to 3 hours. The aggregate sample is submerged in water at room temperature for 24 ± 4 hours. Once the soaking is complete, remove the sample from the water and roll it in a large absorbent cloth until all visible films of water are removed, weigh the mass of the sample and record it to the nearest 0.5 grams. After determining the mass in air, place the saturated-surface-dry (SSD) sample in the sample container and determine the apparent mass in water at 73 ± 2 °F (Figure 10). Then dry the sample in the oven to a constant mass at a temperature of 230 ± 9 °F and let cool to room temperature. Determine the mass of the sample and calculate the apparent specific gravity, bulk specific gravity, SSD specific gravity, and absorption. The complete density and absorption values are in Appendix C, “Density and Absorption Summary”.



Figure 10. Testing apparatus used to weigh sample in water. The scale has a bucket which hangs in the water to determine weight of the sample under water.

ASTM C131 – Standard Test Method for Resistance to Degradation of Small-Size Coarse Aggregate by Abrasion and Impact in the Los Angeles Machine (Figures 11 & 12).

This test helps determine the quality or competence of aggregate material when compared to aggregate material with a performance history. The test measures the degradation of mineral aggregates resulting from a mixture of actions including abrasion, impact, and grinding in a rotating steel drum containing a specific number of steel balls (Figures 13 & 14). The gradings and the number of steel spheres added to the sample range from “Grading A to Grading D” with the most common and widely accepted grading of “B”. The “B” grading means that 11 steel balls weighing approximately 4584 ± 25 grams will be added to the drum along with 2,500 grams of material retained on the $\frac{1}{2}$ ” sieve and 2,500 grams of material retained on the $\frac{3}{8}$ ” sieve (Figure 13 & 14). The drum rotates and a shelf picks up the sample and steel balls and drops them from the opposite side of the drum which simulates a crushing effect. The drum is rotated for 500 revolutions at a constant specified speed.



Figure 11. The Los Angeles Machine used to determine wear and tear of an aggregate source material.



Figure 12. The Los Angeles Machine with the doors open. The sample material is placed into the feed along with steel balls and locked in place.



Figure 13. One steel ball weighing 390-445 grams. The appropriate numbers of balls are placed into the Los Angeles Machine with the sample and the balls are used to pulverize or grind and crush the sample in order to gather information on how the sample may perform in its intended use.



Figure 14. Eleven steel balls used to perform grading “B” of ASTM C131.

- Preparation and Testing Procedures

The samples are thoroughly mixed and reduced to the approximate weight of 2500 ± 10 grams of $\frac{1}{2}$ inch material and 2500 ± 10 grams of $\frac{3}{8}$ material for a total of 5000 grams needed to run the test. The sample is washed and dried in an oven to a constant mass at a temperature of 230 ± 9 °F. The sample is combined and the weight is recorded. The sample and steel balls are placed in the drum and the test started. The drum will rotate at a speed of 30 to 33 revolutions per minute for 500 revolutions. After the test is complete, the material is removed from the LA machine and sieved. The coarse material is washed and oven dried to a constant mass at a temperature of 230 ± 9 °F. The material remaining is weighed to the nearest 1.0 gram. The loss (difference between the original mass and the final mass of the test sample) is calculated as a percentage of the original mass of the test sample. The complete Los Angeles abrasion loss results are in Appendix D, “Los Angeles Abrasion Losses Summary”.

ASTM C 295 – Standard Guide for Petrographic Examination of Aggregates for Concrete

This guide outlines the techniques which should be used, the selection of properties that should be looked for, and the manner in which such techniques should be employed in the examination of samples of aggregate material. The Standard states what should be included in the end report and should only be used as a guide since there are many ways to perform a petrographic report. Specific procedures employed in the petrographic examination of any sample will depend on the purpose of the examination. ASTM C 295 lists examples of different purposes for petrographic examinations. The purpose of a petrographic examination in this report is to: 1. determine the physical characteristics of the sample; 2. describe and classify the material within the sample; and 3. compare the aggregate material from this source with known test results and determine what the microscopic properties can tell about how an aggregate source will perform in its intended use in cement or asphalt.

- Preparation and Testing Procedures

Eight hand samples were cut for thin section blanks from both orientated and from a selected chunk of float block that was broken by a sledge-hammer. The blanks were shipped to Wagner Petrographic, LLC in Linden, Utah for standard thin section preparation. Two samples, N2-4-10 and N1A-4-10, were oriented which allows for a direct connection of fabrics studied in thin section to those in the outcrop. Sledge-hammer pounding of the float blocks could have induced un-natural or artificial fractures within the sample. In addition, blasting during quarry operations likely induced artificial fractures to the samples. Two of the samples, N4-4-10 and N4-4-10P (P - indicating perpendicular to apparent foliation within the rock), were vacuum impregnated with blue epoxy to keep the rock together and highlight any fractures that were man-made or caused by blasting.

These samples were prepared into standard thin sections. Petrographic examinations of the hand samples were conducted in accordance with ASTM Method C-295, Standard Guide for Petrographic Examination of Aggregates for Concrete on the material. Each thin section was analyzed by the author utilizing a Nikon polarizing microscope with a maximum magnification of 400X. The conditions of rock grains, grain boundaries, and interconnectedness of the grains were noted. The quality or competence of the aggregate material was compared to aggregate physical testing results. This was a controlled study because the material had a performance history. Results of the physical tests and the petrographic analysis for each thin section are presented below.

RESULTS

ASTM Testing

All samples were tested at the National Center for Asphalt Technology (NCAT) located in Auburn, Alabama. Fine and coarse gradations, Los Angeles Abrasion, Sodium sulfate soundness, specific gravity, and absorption tests were performed. Altogether, a total of eight samples were tested: four samples from the upper unit (N1A-N4A) and four from the lower unit (N1-N4). The results of the tests are shown in Table 1.

Table 1. Summary results from the ASTM standard tests run on samples of aggregate material from the Notasulga Quarry.

Sample #	LA Abrasion results (%)	Specific Gravity				Sodium Sulfate Soundness Loss (%)
		Bulk	SSD	Apparent	Absorption (%)	
ALDOT Specs	<50%	>2.550				
VULCAN	41	2.620	2.630	2.650	0.6	
N1A-4-10	34.7	2.596	2.612	2.639	0.6	0.495
N2A-4-10	28.7	2.651	2.667	2.694	0.6	0.023
N3A-4-10	44.4	2.593	2.609	2.636	0.6	0.050
N4A-4-10	37.8	2.625	2.638	2.660	0.5	1.267
N1-4-10	34.4	2.627	2.642	2.667	0.6	0.030
N2-4-10	36.5	2.619	2.635	2.662	0.6	0.025
N3-4-10	42.0	2.606	2.623	2.652	0.7	0.030
N4-4-10	42.7	2.611	2.624	2.646	0.5	0.020
Average	37.7	2.616	2.631	2.657	0.6	0.243

The L.A. abrasion values are consistent with Vulcan Material's testing results published by the Alabama Department of Transportation which had a running average of 41.0%. Bulk specific gravity had a running average of 2.616. Absorption averaged 0.6% and soundness loss was roughly 0.2% for Sodium Sulfate.

Upper Unit

L.A. Abrasion within the upper unit (RP4) ranged from 28.7% to 44.4% with an average of 36.4%. Specific gravity (SSD) had a low of 2.609 and a high of 2.667 with an average of 2.632. Absorption averaged 0.6%; Soundness had an average of 0.459% for Sodium Sulfate.

Lower Unit

L.A. Abrasion within the lower unit ranged from 34.4% to 42.7% with an average of 38.9%. Specific gravity (SSD) had a low of 2.623 and a high of 2.642 with an average of 2.631. Absorption averaged 0.6%; Soundness had an average of 0.020% for Sodium Sulfate.

Detailed results are given in Appendixes A-D.

Petrographic Analysis

Sixteen standard covered thin sections were analyzed for this study. During preparation, two samples (N4-4-10 and N4-4-10P) were notably friable and required blue epoxy impregnation. Eight samples were cut parallel to apparent foliation and eight samples were prepared perpendicular to apparent foliation for a total of sixteen thin sections.

Paired thin sections are described below and thin section photographs of notable features are provided. Thin sections are identified with the use of a P suffice to denote those cut perpendicular to foliation. Photographs were taken under both plain polarized light and crossed polars as noted. Noteworthy features have been labeled in each image. The size scale for mineral constituents in igneous rocks (MacKenzie et al., 1987) was used in sample descriptions and is reproduced below as Table 2. Rock names were assigned using the IUGS classification of Plutonic Rocks (Blatt and Tracey, 1996). Each petrographic description below begins with a modal analysis of mineral abundancies based on visual estimation. Microstructural, fabric, and alteration features are then described in detail in order of decreasing volumetric abundance of that particular mineral phase. The last paragraph in each description is a short discussion of how, based on the petrographic results, the author would predict the material to behave during physical testing, and how this prediction either verifies or conflicts with the actual testing results for this sample reported in Table 1.

Table 2. Terminology used to describe grain sizes in this petrographic report (from Mackenzie et al., 1987).

DESCRIPTIVE TERM	GRAIN/CRYSTAL SIZE RANGE
Coarse-Grained	> 5 mm
Medium Grained	1 to 5 mm
Fine Grained	<1 mm
Very Fine Grained	<0.5 mm

N1-4-10P and N1-4-10

This granitic gneiss sample was collected from the quarry highwall directly below the primary crusher in an area Bogdan (2009) designated as rock package 3 (RP3). It is medium gray to black with some pink grains of microcline, medium grained, alkali feldspar metagranite composed of quartz (40-45%), microcline (30-35%), biotite (8-10%), muscovite (5-8%), plagioclase (3-5%), opaque minerals (2-3%), and trace amounts of clay, sericite, albite, garnet, chlorite, epidote, apatite, and zircon (Figure 15). A weak foliation is present and is defined by alignment of biotite and muscovite.

Quartz occurs as anhedral grains 0.1 mm to 2.5 mm across with flat to undulose extinction (Figures 16 & 17). Numerous hairline fractures healed with opaque minerals occur with most fractures contained within individual quartz grains. A few fractures extend into adjacent quartz grains. Fluid inclusions are common along with inclusions of biotite, muscovite, opaque minerals, and apatite. The quartz grains form generally embayed, interlocking boundaries with adjacent grains (Figures 16 & 17).

Microcline is present as subhedral grains 0.25 mm to 2.5 mm across with most grains exhibiting characteristic tartan twinning (Figures 20 & 21). Some alteration to sericite, clay, muscovite, and opaque minerals has occurred. Albite exsolution has formed microperthitic textures. Inclusions of quartz, muscovite, biotite, opaque minerals, apatite, and clay are present. The microcline forms embayed and interlocking grain boundaries with adjacent grains of quartz, microcline, and plagioclase, and generally straight boundaries with biotite and muscovite (Figure 18 and 19).

Biotite occurs as subhedral to euhedral grains 0.125 mm to 0.75 mm long with brown to light green pleochroism and exhibits the classic bird's eye texture under crossed

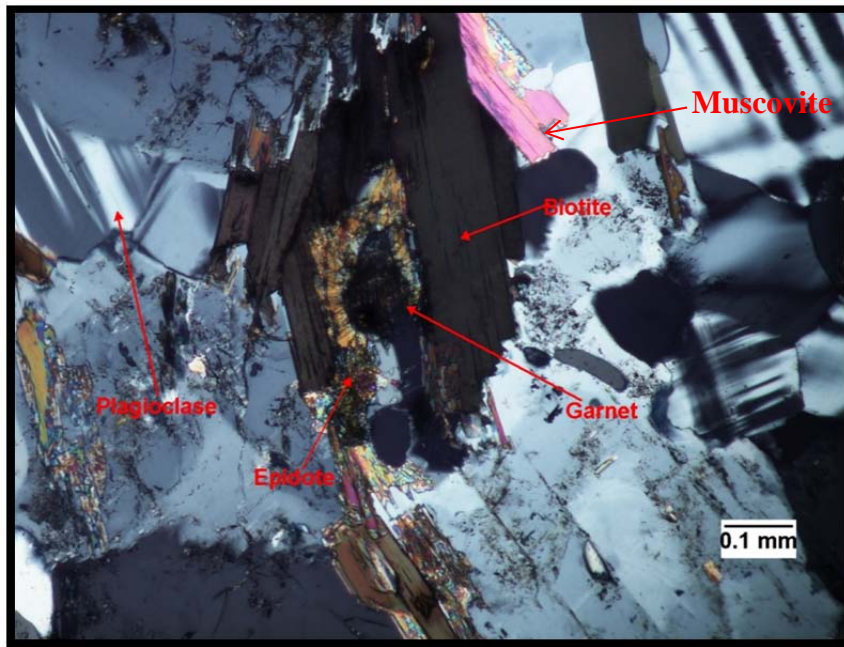


Figure 15. N1-4-10P, Typical view of sample. Photographed with crossed polars at 100X magnification.

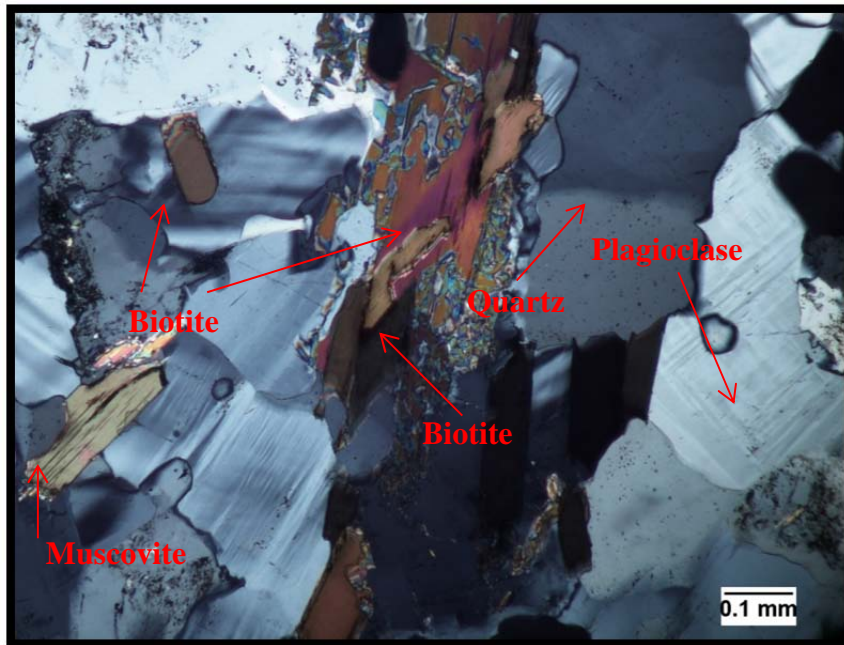


Figure 16. N1-4-10P, Typical view of sample showing interlocking grain boundaries. Photographed under crossed polars at 100X magnification.

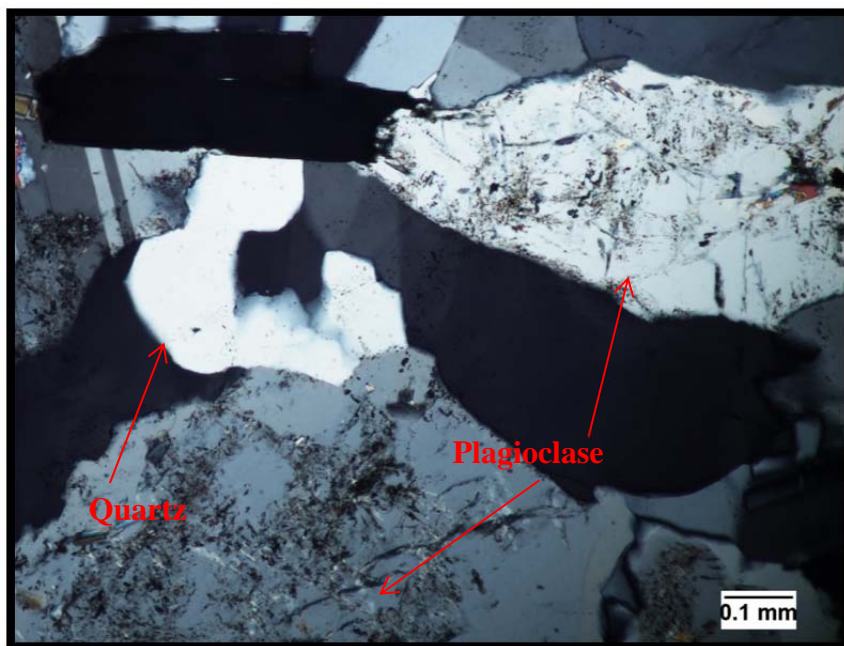


Figure 17. N1-4-10P, Large medium grained quartz grain showing undulatory extinction. Plagioclase is altered to sericite and clay. Photographed under crossed polars at 100X magnification.

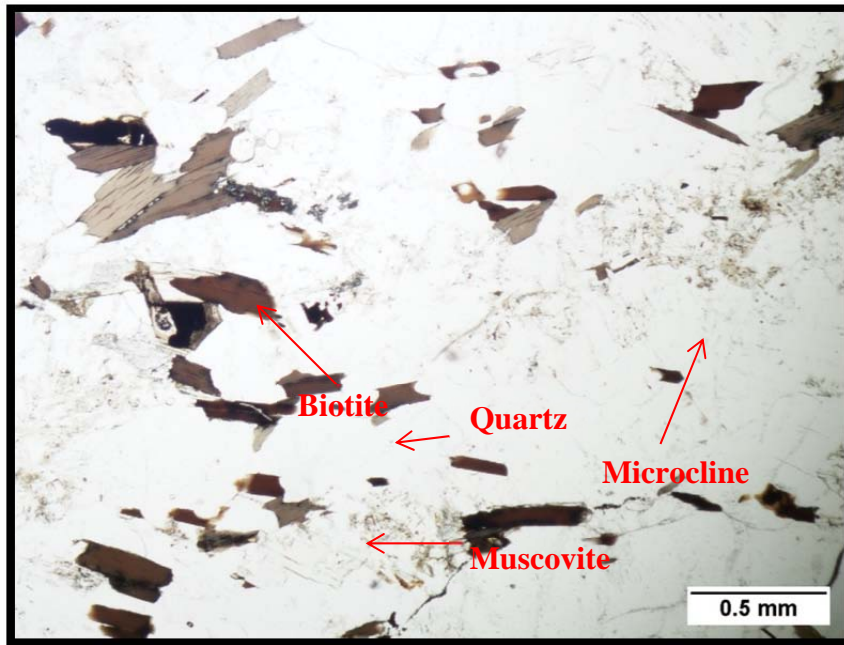


Figure 18. N1-4-10P, Muscovite intergrown with biotite. Photographed under plane polarized light polarized light polarized light light at 40X magnification.

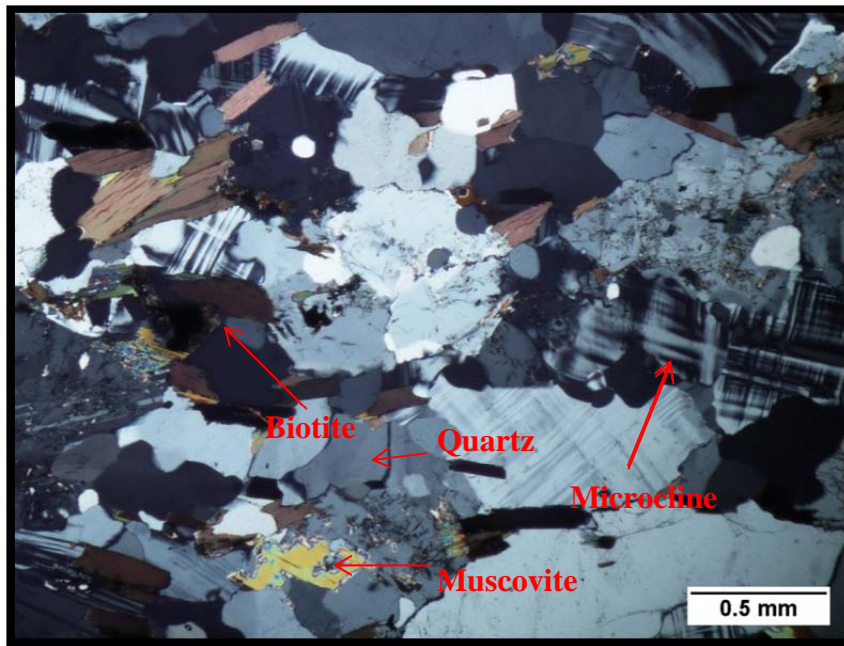


Figure 19. N1-4-10P, Same view as above in Figure 18 but photographed under crossed polars at 40X magnification.

polars. It has good cleavage and forms straight boundaries with adjacent grains along the long axis and embayed boundaries along the short axis (Figure 16). Intergrowths with muscovite are common (Figures 18 & 19). Biotite occurs as discrete flakes locked into the matrix with no clots or bands that could present problems with excess free mica in aggregate (Figures 18 & 19). A few grains have undergone alteration to chlorite. Inclusions of opaque minerals and zircon up to 20 μm across with dark brown pleochroic halos are present.

Muscovite occurs as subhedral to euhedral grains 0.25 mm to 1.0 mm long as a primary mineral and as a product of plagioclase alteration. Symplectic growths (Figures 20 & 21) and intergrowths with biotite are common. The muscovite occurs as individual flakes locked into the matrix with no clots or bands (Figures 20 & 21).

Plagioclase occurs as subhedral grains 0.25 mm to 1.0 mm long with faint to well-developed albite twinning. Saussuritization has produced sericite, clay, muscovite, opaque minerals, albite, and some grungy epidote (Figures 22 & 23). Plagioclase has inclusions of quartz and apatite as well as the alteration products mentioned above. Plagioclase grains form straight to slightly embayed boundaries with adjacent mineral grains (Figure 17).

Opaque minerals occur as anhedral to subhedral grains 0.25 mm to 0.5 mm across. Some pyrite was noted in hand samples and a major portion of the opaque minerals within all the samples discussed in this report are believed to be pyrite.

The following minerals are all found in trace quantities within this thin section. Clay occurs as very fine grains in plagioclase and microcline as a result of alteration. Sericite occurs as very fine anhedral grains in altered plagioclase and microcline. Albite

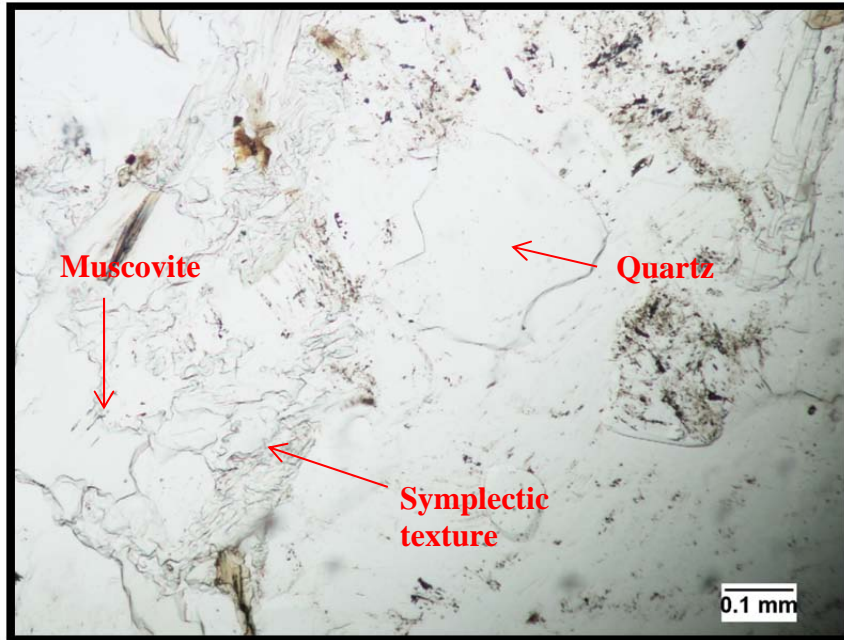


Figure 20. N1-4-10P, Muscovite with symplectic texture. Photographed under plane polarized light polarized light light at 100X magnification.

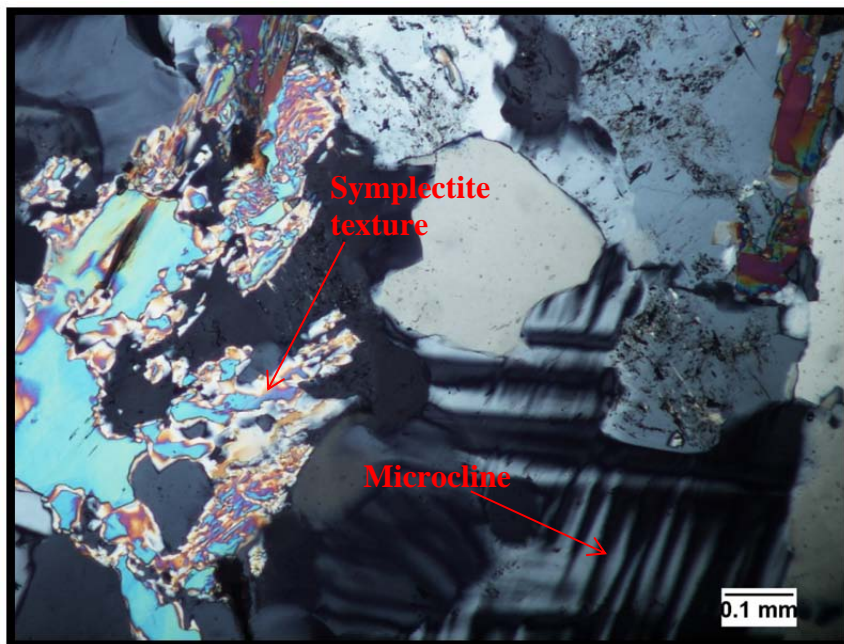


Figure 21. N1-4-10P, Same view as above in Figure 20 but photographed under crossed polars at 100X magnification.

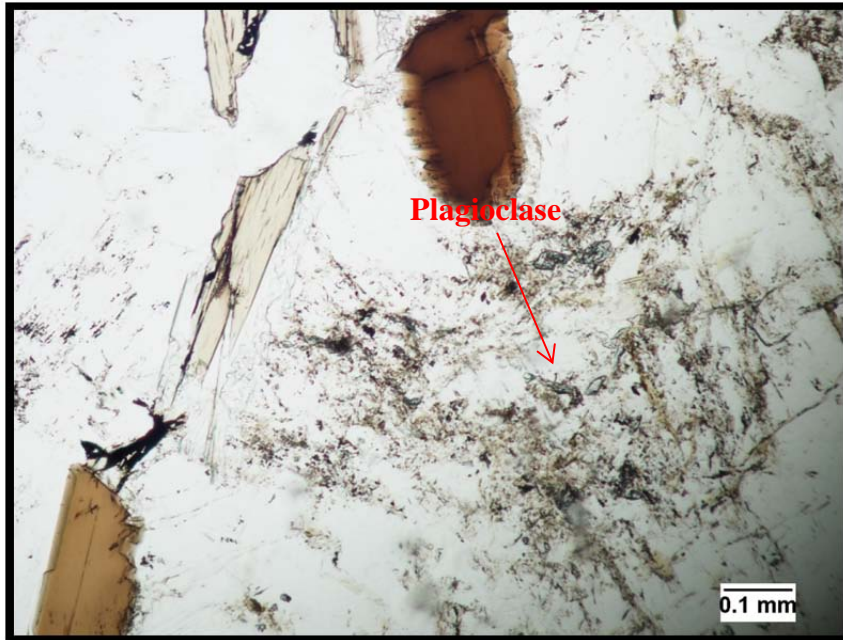


Figure 22. N1-4-10P, Plagioclase undergoing saussuritization producing fine grained sericite, albite, and clay. Photographed under plane polarized light at 100X magnification.

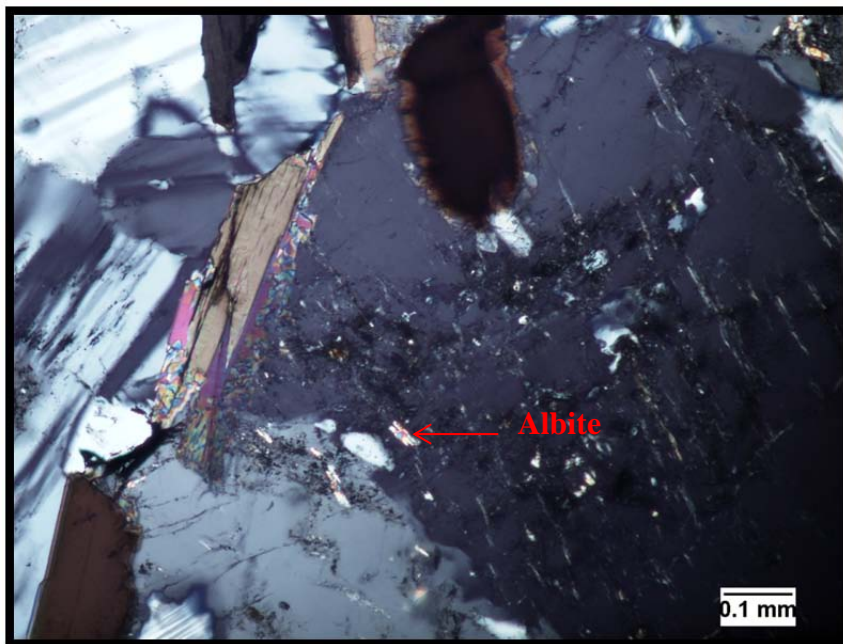


Figure 23. N1-4-10P, Same view as above in Figure 22 but photographed under crossed polars at 100X magnification. The bright interference colors of the stand out in contrast to the plagioclase.

occurs as a product of alteration of plagioclase and as exsolution grains in microcline forming perthitic textures. Garnet occurs as subhedral to euhedral grains 0.25 mm to 2.5 mm in diameter with inclusions of opaque minerals and numerous fractures healed with opaque minerals. Epidote occurs as euhedral to subhedral grains from alteration of plagioclase. The epidote contains very abundant inclusions of opaque minerals and has a very grungy appearance. Apatite occurs as a few scattered euhedral grains 0.25 mm to 0.5 mm. Zircon occurs as euhedral grains up to 20 μm in the biotite flakes.

The prevalent interlocking grain boundaries and relatively small grain sizes produced an aggregate with Los Angeles abrasion loss of 34.4% which is well below Alabama and surrounding state DOT's maximum allowable loss of 50.0%. The small quantity of clay and chlorite present in the sample did not affect sulfate soundness losses and the sample met all Alabama and surrounding state DOT's specifications. Sodium sulfate soundness loss of this material was 0.03%. The lack of ferro-magnesium minerals (hornblende), which tend to have a higher specific gravity, along with the dense nature of the sample and the lack of open fractures produced a relatively low bulk specific gravity of 2.627 and absorption of 0.6%. This will meet customer demands and allow the finished aggregate product to be competitive in the market. No alkali-aggregate reactive minerals such as opal, chert, or strained quartz were found. The healed fractures in quartz are of limited length and will not impact quality. The 13-18% biotite and muscovite is high but the majority is locked into the matrix as individual flakes with no clots or bands that could produce excess free mica. Clay, sericite, and opaque minerals are present in such small quantities that they will not influence test results or quality. Microcline has a well-developed cleavage that breaks readily during crushing. The 30-

35% microcline is a cause for concern but the relatively small grain size, 0.25-2.5 mm will limit the breakage along cleavage and the microcline has had no effect on Los Angeles abrasion loss. The alkali feldspar metagranite represented by these two thin sections will produce a quality aggregate that has met all physical testing specifications.

N2-4-10P and N2-4-10

These samples are granite gneiss and are medium gray to dark gray with some creamy white to pink grains of microcline, medium-grained to coarse-grained, and composed of quartz (45-50%), microcline (20-25%), plagioclase (10-15%), biotite (8-10%), muscovite (5-8%), opaque minerals (1-2%), and trace amounts of clay, sericite, albite, garnet, epidote, chlorite, apatite, and zircon. A slight foliation is can be seen and is defined by alignment of biotite and muscovite.

Quartz occurs as anhedral grains 0.125 mm to 4.5 mm in diameter with flat to undulose extinction (Figure 24 C). Hairline fractures are healed with possible quartz and some opaque minerals within the fracture can be observed but most fractures are contained within individual quartz grains. A few fractures extend into adjacent quartz grains. Fluid inclusion trails are well aligned and are common along with inclusions of biotite, muscovite, opaque minerals, and apatite. The quartz forms embayed interlocking boundaries with surrounding grains (Figures 25 & 26).

Microcline occurs mainly as subhedral grains 0.25 mm to 1.0 mm. One microcline grain was up to 5.25 mm across, with most grains exhibiting tartan twinning and a few grains exhibiting twinning in only one direction. Most microcline is pristine with minimal alteration. Some albite exsolution is present forming faint perthitic textures. Inclusions of quartz, muscovite, biotite, opaque minerals, and clay are present. The microcline forms embayed and interlocking grain boundaries with adjacent grains of quartz, microcline, and plagioclase, and generally straight boundaries with biotite and muscovite.

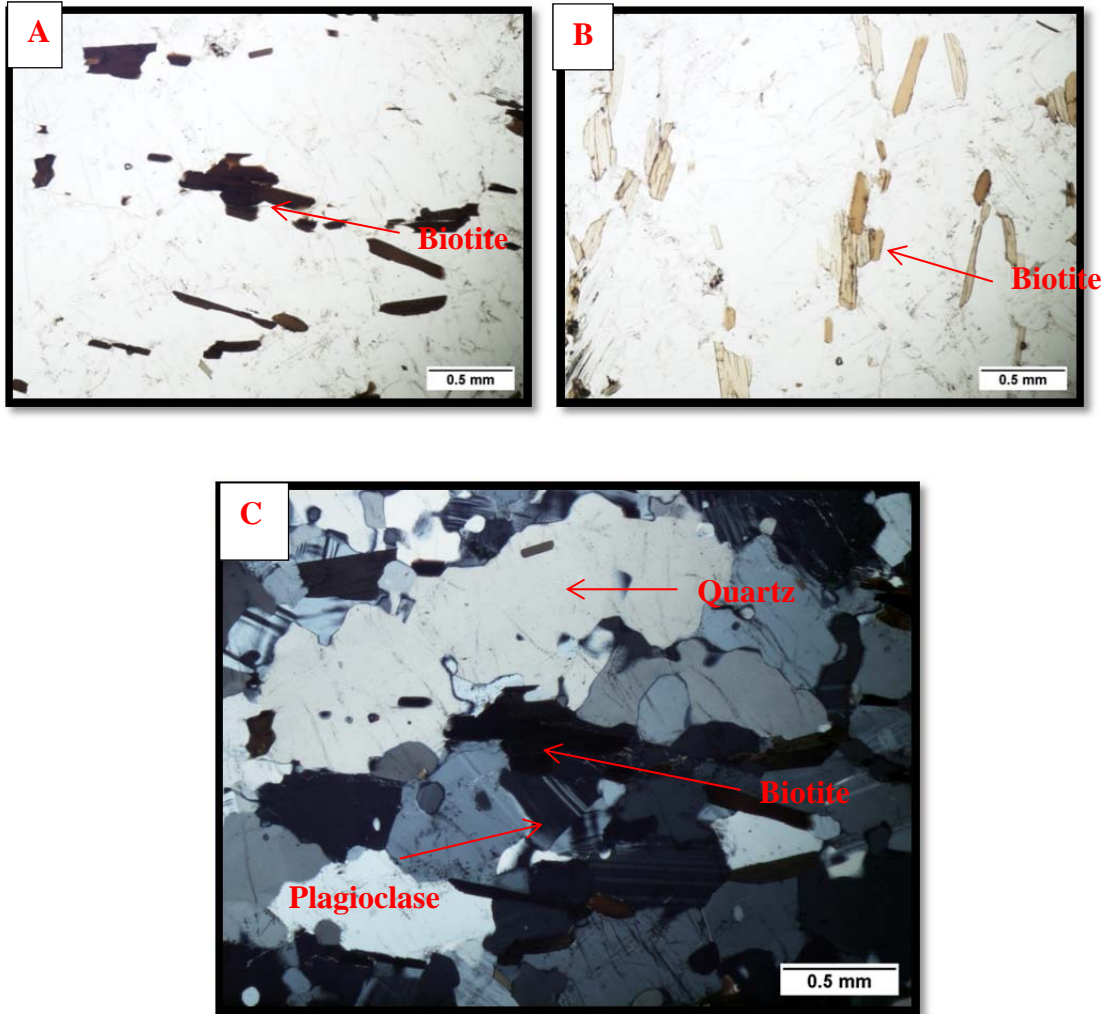


Figure 24. N2-4-10P, A.) Biotite under plane polarized light showing dark brown pleochroism. B.) Same view as A. but rotated 90° to show the light brown pleochroism. C.) Typical view of sample showing minerals present. The quartz within this thin section has slightly undulatory extinction. Same view as A. but photographed under crossed polars at 40X magnification.

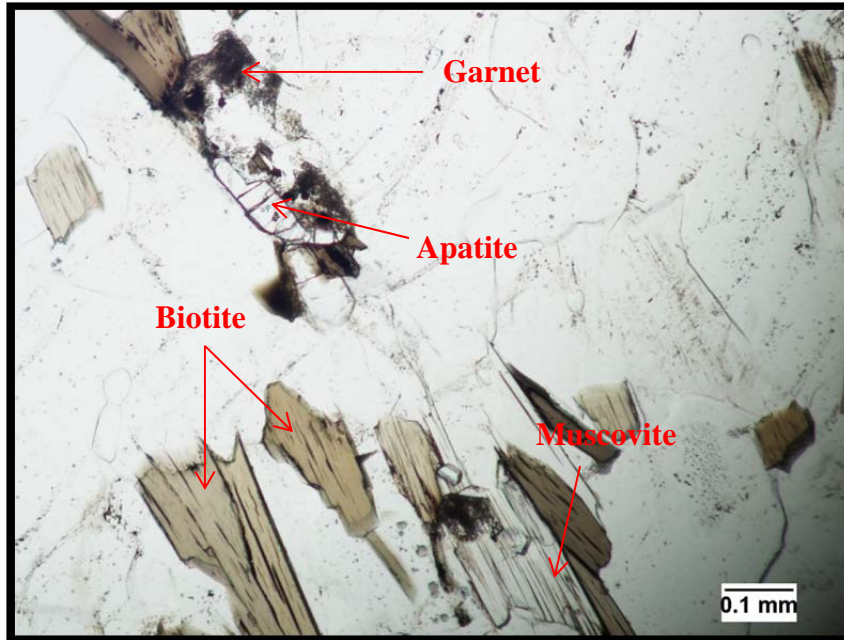


Figure 25. N2-4-10P, Biotite interlocked with quartz grains. Apatite is present. Remnants of garnet can be seen within this slide. Photographed under plane polarized light at 100X magnification.



Figure 26. N2-4-10P, Same view as above in Figure 25 but photographed under crossed polars at 100X magnification. Quartz shows slightly undulatory extinction.

Plagioclase occurs as subhedral grains 0.25 mm to 1.5 mm across with faint to well-developed albite twinning. The plagioclase grains are pristine to slightly altered. Minor alteration is present as saussuritization producing sericite, clay, muscovite, opaque minerals, epidote, and albite (Figures 27 & 28). The plagioclase grains form slightly embayed boundaries with adjacent mineral grains. Poorly-developed myrmekite is present as blebs and vermicular growths of quartz in plagioclase are poikilitically enclosed by microcline. In addition to alteration minerals, the plagioclase includes inclusions of quartz and biotite.

Biotite occurs as subhedral to euhedral grains 0.125 mm to 1.0 mm long with brown to light brown pleochroism (Figures 24 A & B) and exhibits the classic bird's eye extinction under crossed polars. It has good cleavage and forms straight boundaries with adjacent grains along the long axis and embayed boundaries along the short axis. Biotite occurs as discrete flakes locked into the matrix with no clots or bands that could present problems with excess free mica in aggregate (Figures 24, 25, & 26). A few biotite grains have undergone chloritic alteration. Inclusions of opaque minerals, muscovite, and zircon up to 20 μm across with dark brown pleochroic halos are present.

Muscovite occurs as subhedral to euhedral grains 0.125 mm to 1.0 mm long. The muscovite occurs as a primary mineral and as a product of plagioclase alterations. Symplectic growths are common (Figures 29 & 30). Muscovite is commonly intergrown with biotite. The muscovite occurs as individual flakes locked into the matrix with no clots or bands.

Opaque minerals occur as anhedral to subhedral grains 0.125 mm to 0.25 mm across.

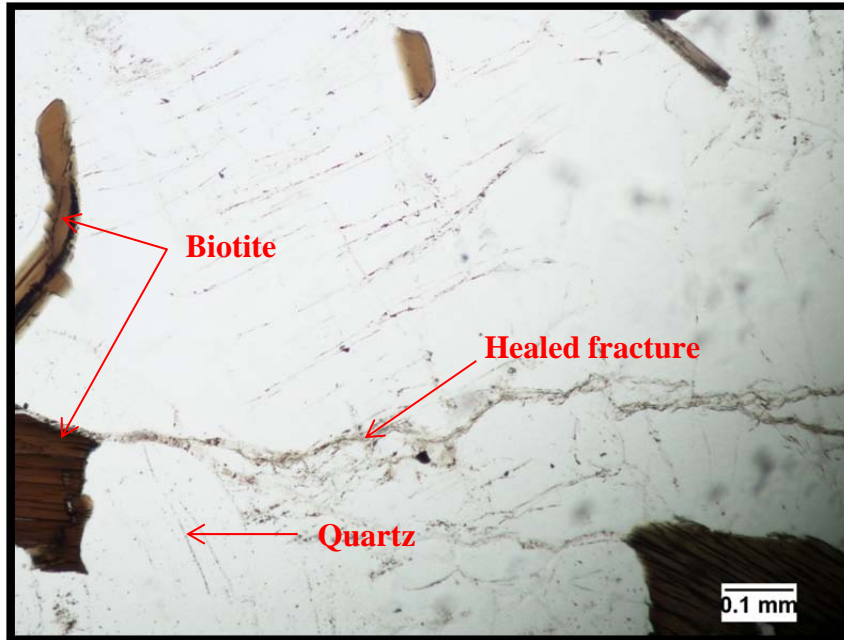


Figure 27. N2-4-10P, Grungy plagioclase grain undergoing saussuritization producing clay and sericite. Healed fractures common in the thin section. Plagioclase grain boundaries interlock with the quartz and biotite grain boundaries. Photographed under plane polarized light at 100X magnification.

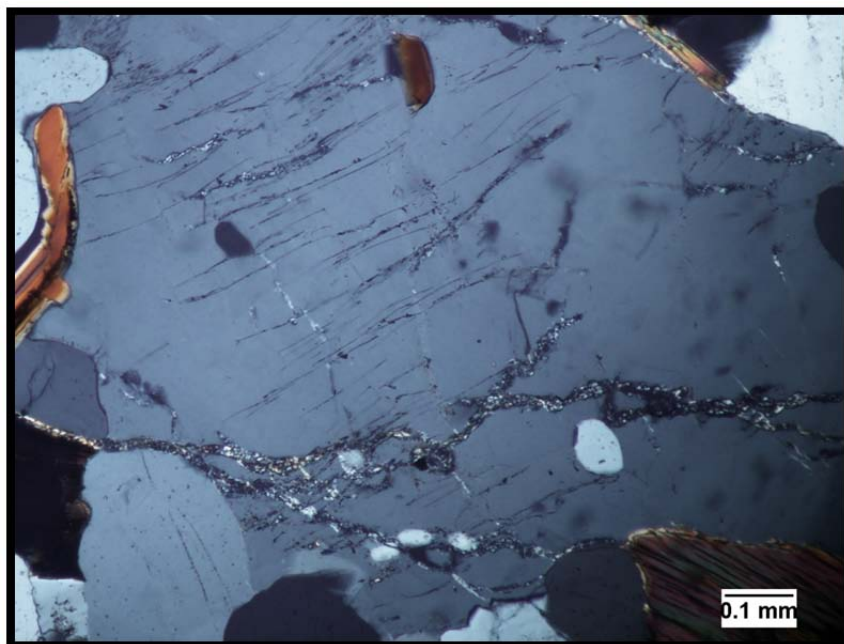


Figure 28. N2-4-10P, Same view as above in Figure 27 but photographed under crossed polars at 100X magnification.

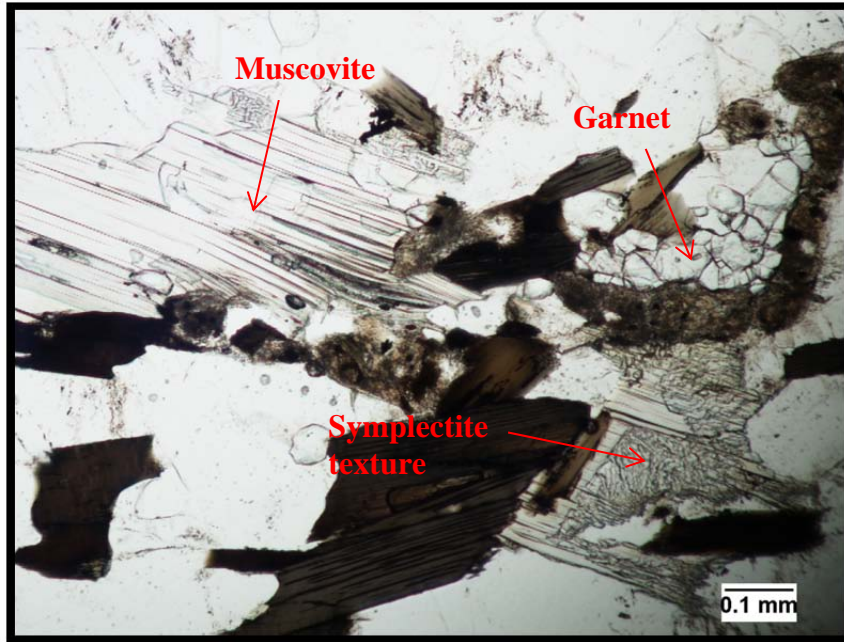


Figure 29. N2-4-10P, Muscovite with some grains exhibiting symplectite texture. Isotropic garnet is present. Photographed under plane polarized light at 100X magnification.

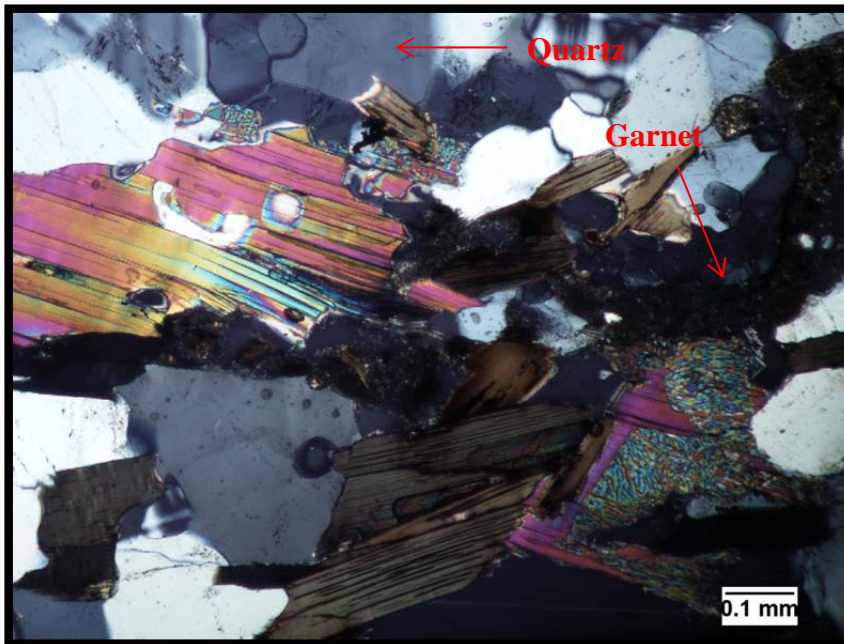


Figure 30. N2-4-10P, Same view as above in Figure 29 but photographed under crossed polars at 100X magnification.

Sericite occurs as very fine anhedral grains in altered plagioclase and microcline. Clay occurs as very fine grains in plagioclase and microcline as a result of alteration. Albite occurs as an alteration product of plagioclase and as exsolution lamellae forming perthitic textures in microcline. Garnet occurs as subhedral to euhedral grains 0.25 mm to 2.5 mm in diameter with inclusions of opaque minerals and numerous fractures healed with opaque minerals. Epidote occurs as euhedral to subhedral grains from alteration of plagioclase. Chlorite occurs as an alteration product of biotite, is pleochroic from light green to dark green and exhibits dark gray interference colors. Apatite occurs as a few scattered euhedral grains 0.20 mm to 0.45 mm in diameter as inclusions in quartz, plagioclase, and microcline. Zircon occurs as euhedral grains up to 20 μm across with dark brown pleochroic halos in the biotite.

The mineral compositions and textures were similar to N1-4-10 and there was relatively no change in testing results between the samples. Bulk specific gravity was 2.619 and Los Angeles abrasion resulted in 36.5% loss. Los Angeles abrasion may have been slightly higher due to the higher percentage of altered plagioclase within the sample. Absorption was exactly the same as N1-4-10 and sodium sulfate loss was 0.025%. The sulfate loss is minor and could have been caused by operator testing error although the author is unaware of any errors that he might have caused while testing this particular sample.

N3-4-10P and N3-4-10

Two lithologies are present in this set of thin sections. Alkali feldspar metagranite has been intruded by a pegmatite with a contact approximately 1.5 mm to 2.0 mm wide. Within this sample the pegmatite has a granophyric texture (Figures 31 & 32). Muscovite can be observed with symplectic intergrowths (Figures 33 & 34). Plagioclase has shown moderate alteration to sericite and clay (Figures 35 & 36). Biotite has undergone partial to complete alteration to chlorite and the biotite adjacent to the granophyric texture has been more highly altered (Figures 37 & 38). A sharp increase in grain size is present in the pegmatitic portion adjacent to the altered band. There is no discernable foliation present within thin sections. The two lithologies are discussed separately below.

ALKALI FELDSPAR METAGRANITE

A portion of this thin section comprises a medium gray to white with some pink grains of microcline, medium-grained, alkali feldspar metagranite composed of quartz (40-45%), microcline (35-40%), biotite (8-10%), muscovite (3-5%), plagioclase (3-5%), and trace amounts of opaque minerals, chlorite, clay, sericite, albite, apatite, and zircon.

Quartz occurs as anhedral grains 0.125 mm to 2.5 mm across with flat to undulose extinction. Fluid inclusion trails are well aligned and are common along with inclusions of biotite, muscovite, and apatite. Numerous hairline fractures are healed with opaque minerals with most fractures limited within individual quartz grains and a few fractures extending into surrounding quartz grains. The quartz forms mostly embayed interlocking boundaries with neighboring grains (Figures 35 & 36).

Microcline occurs as subhedral grains 0.25 mm to 2.5 mm with most grains

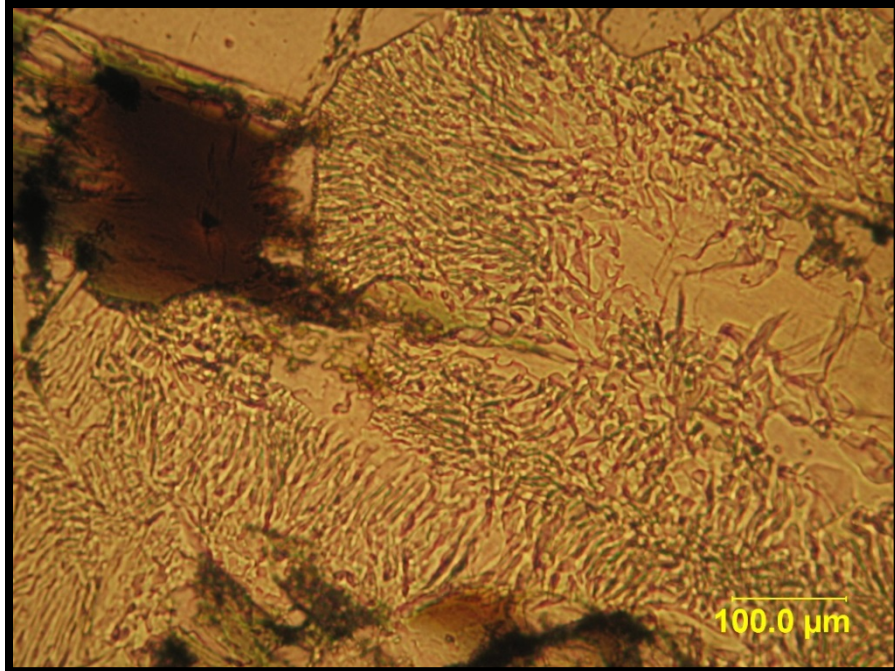


Figure 31. N3-4-10, Granophyric texture in alkali feldspar metagranite. Photographed under plane polarized light at 100X magnification.

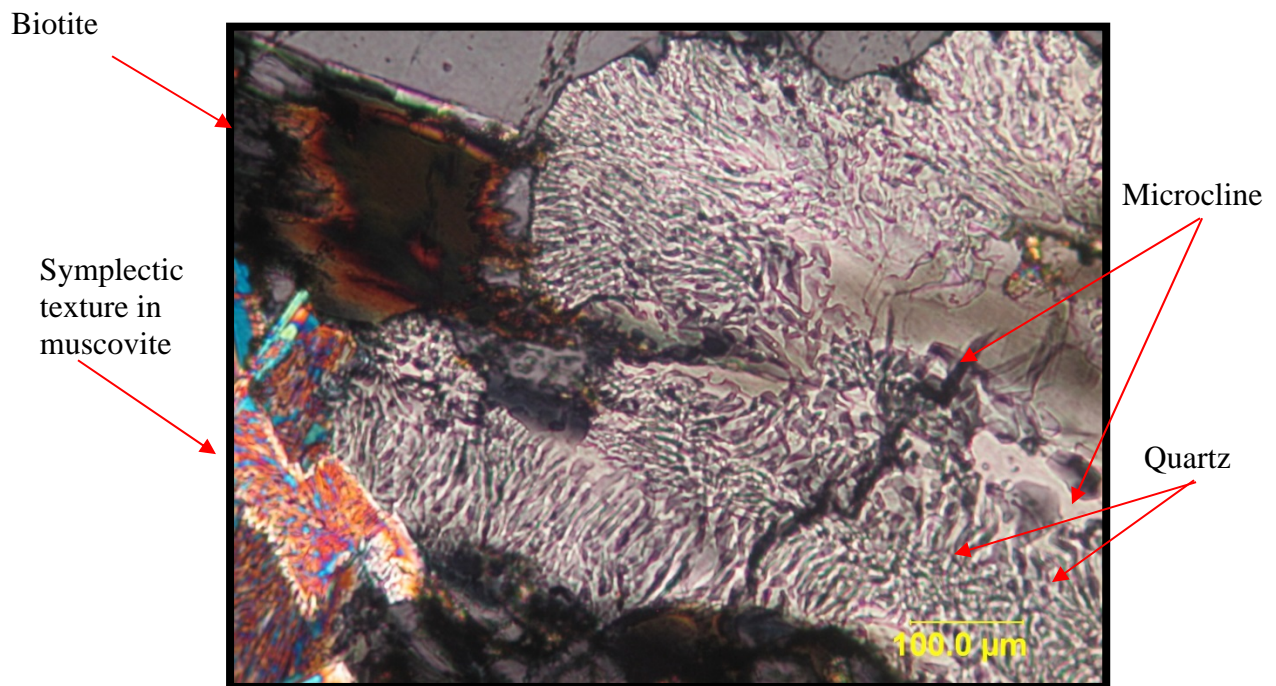


Figure 32. N3-4-10, Same view as above in Figure 31 but photographed under crossed polars at 100X magnification.

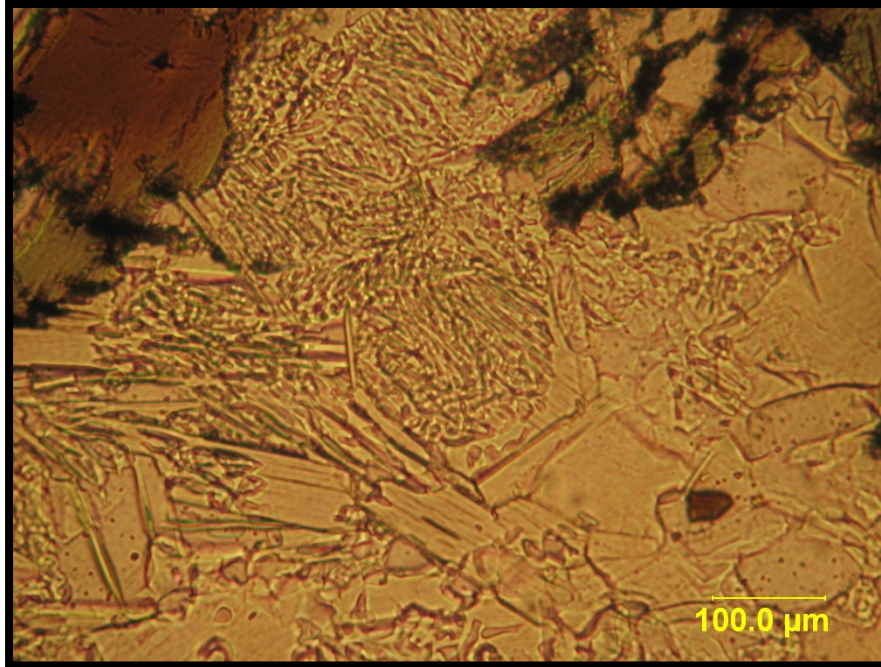


Figure 33. N3-4-10, Symplectic texture in muscovite. Photographed under plane polarized light at 100X magnification.

Granophyric texture

Symplectic texture in muscovite

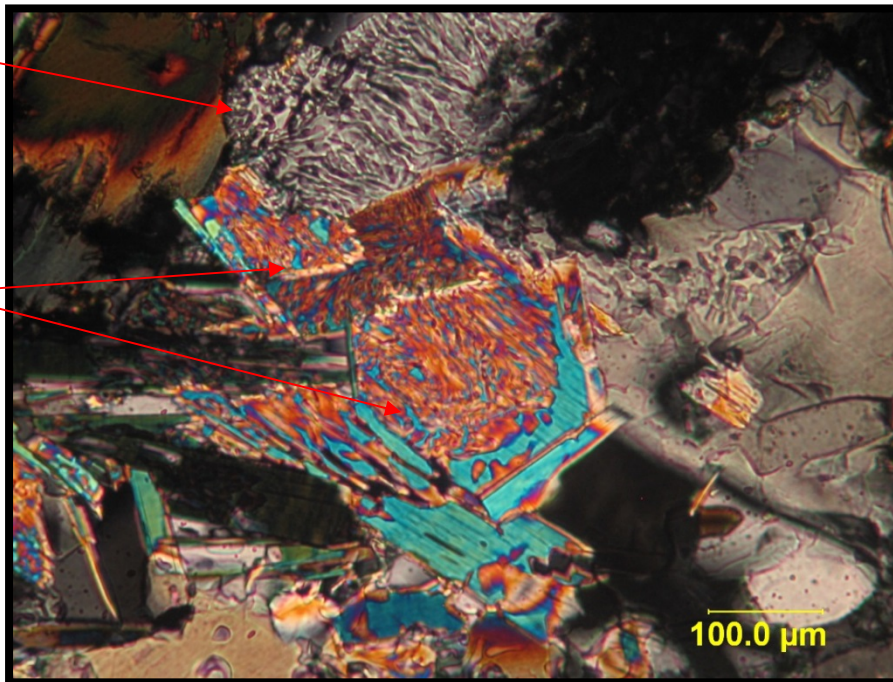


Figure 34. N3-4-10, Same view as above in Figure 33 but photographed under crossed polars at 100X magnification.

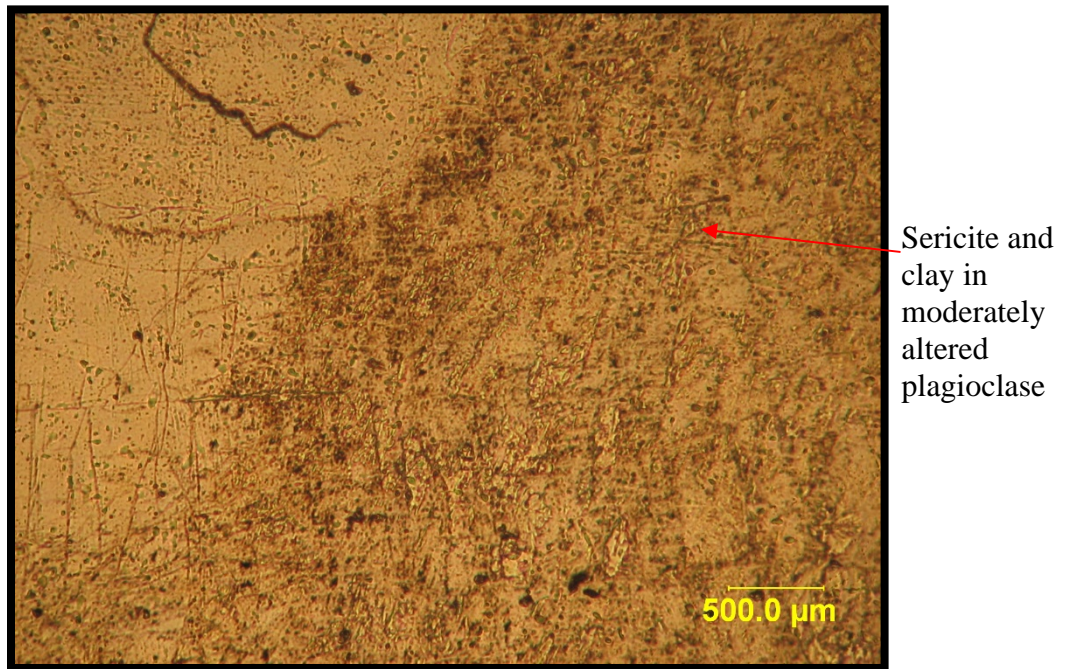


Figure 35. N3-4-10, Plagioclase undergoing saussurization to sericite and clay. Photographed under plane polarized light at 40X magnification.

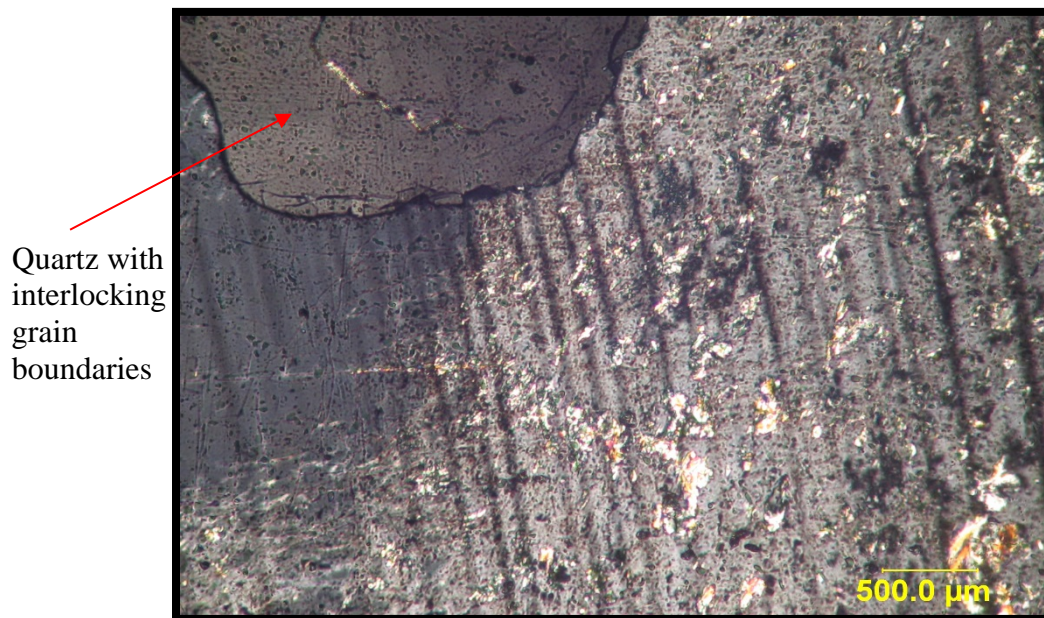


Figure 36. N3-4-10, Same view as above in Figure 35 but photographed under crossed polars at 40X magnification.

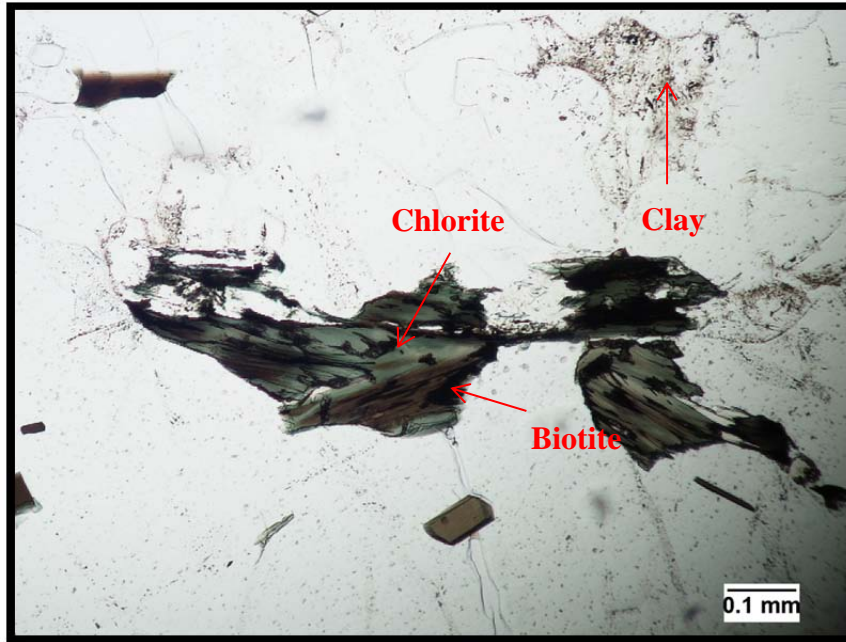


Figure 37. N3-4-10, Biotite that has altered to chlorite and plagioclase saussuritized to produce clay. Photographed under plane polarized light at 100X magnification.

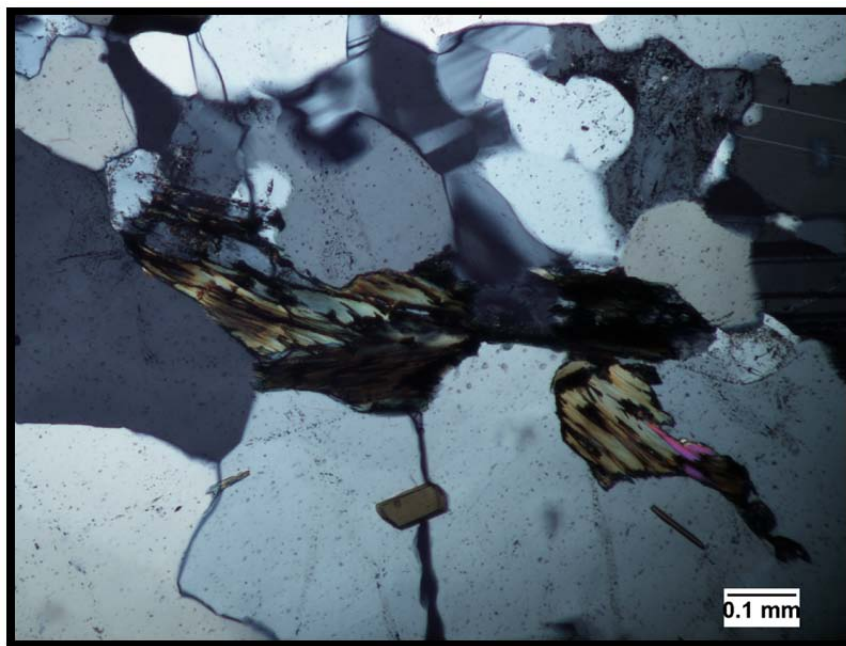


Figure 38. N3-4-10, Same view as above in Figure 37 but photographed under crossed polars at 100X magnification.

exhibiting characteristic tartan twinning and a few grains exhibiting twinning in only one direction (Figures 41 & 42). Most microcline is pristine with minimal alteration. Some minor albite exsolution is present. Inclusions of quartz, albite, and clay are present. The microcline forms embayed and interlocking grain boundaries with surrounding grains of quartz, microcline, and plagioclase, and generally straight boundaries with biotite and muscovite (Figures 41 & 42).

Biotite occurs as subhedral to euhedral grains 0.125 mm to 0.5 mm in diameter with brown to light brown pleochroism and exhibits the classic bird's eye extinction under crossed polars. It has good cleavage and forms straight boundaries with adjacent grains along the long axis and embayed boundaries along the short axis. Biotite occurs as isolated flakes locked into the matrix with no clots or bands that could present problems with excess free mica in aggregate. Some biotite is intergrown with biotite. Some biotite contains small zircon grains which have undergone decay and produced pleochroic halos. Many grains have undergone alteration to chlorite with some grains completely replaced by chlorite (Figures 39 & 40). Inclusions of opaque minerals are present.

Muscovite occurs as subhedral to euhedral grains 0.125 mm to 0.75 mm in diameter. Symplectic growths are common. The muscovite occurs as individual flakes locked into the matrix.

Plagioclase occurs as subhedral grains 0.25 mm to 0.75 mm across with faint to well-developed albite twinning. The plagioclase grains are slightly to moderately altered by saussuritization producing sericite, clay, and albite (Figures 35 & 36). The plagioclase

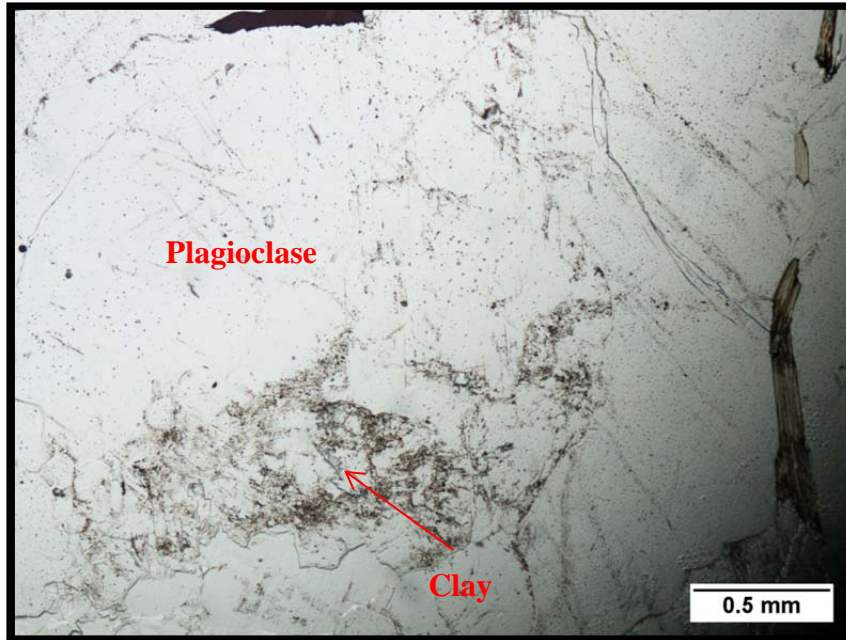


Figure 39. N3-4-10, Plagioclase having undergone saussuritization producing sericite and clay. Photographed under plane polarized light at 40X magnification.

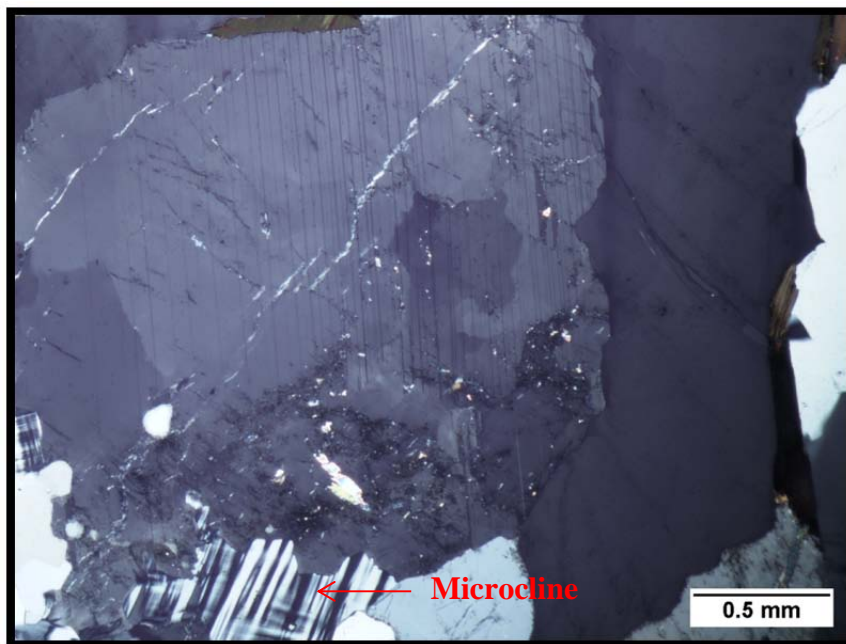


Figure 40. N3-4-10, Same view as above in Figure 39 but photographed under crossed polars at 40X magnification.

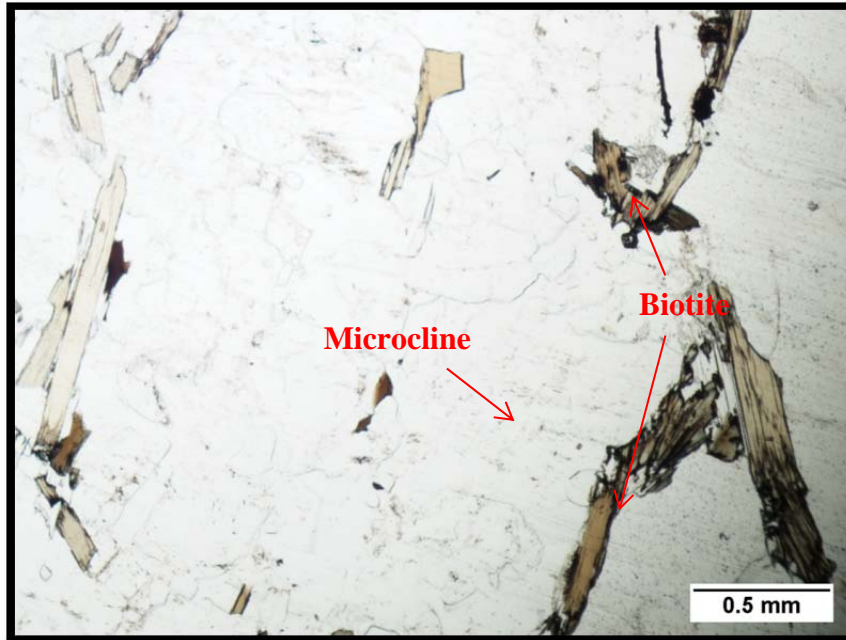


Figure 41. N3-4-10, Biotite is pleochroic light brown to dark brown under plane polarized light at 40X magnification. Typical microcline and quartz interlocking grain boundaries.

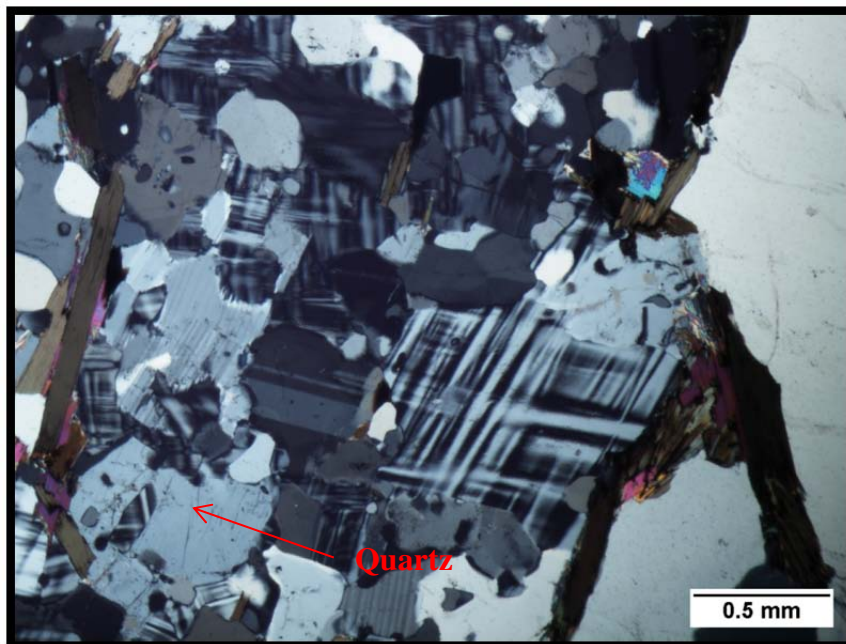


Figure 42. N3-4-10, Same view as above in Figure 41 but photographed under crossed polars at 40X magnification.

grains form slightly embayed boundaries with adjacent mineral grains. Minor amounts of poorly-developed myrmekite is present as vermicular growths of quartz in plagioclase from the breakdown of microcline. In addition to alteration minerals, the plagioclase includes inclusions of quartz and biotite.

Opaque minerals occur as anhedral to subhedral grains 0.125 mm to 0.25 mm across. Some pyrite was noted in hand samples and a major portion of the opaque minerals are believed to be pyrite. Chlorite is present as an alteration product of biotite that has partially to completely replaced grains of biotite. It is pleochroic from light green to dark green with interference colors that range from gray to black. Sericite, clay, and albite occur as alteration products in plagioclase and microcline. Apatite occurs as a few scattered euhedral grains 0.25 mm to 0.5 as inclusions in quartz, plagioclase, and microcline. Small zircon grains are present in biotite undergoing decay and producing pleochroic halos.

PEGMATITE

This portion of the thin section is a medium gray to white with some pink grains of microcline, coarse-grained, pegmatite composed of plagioclase (45-50%), quartz (25-30%), microcline (8-10%), biotite (3-5%), muscovite (3-5%), chlorite (2-3%), clay and sericite (1-3%), and trace amounts of opaque minerals.

Plagioclase occurs as subhedral grains up to 8.5 mm across with faint to well-developed albite twinning. The plagioclase grains show minor to moderate alteration to saussuritization producing sericite, clay, and albite. Plagioclase grains have embayed boundaries with all adjacent mineral grains. There are some myrmekitic textures which

formed near boundaries with microcline. In addition to alteration minerals, the plagioclase has of quartz and microcline.

Quartz occurs as anhedral grains up to 4.5 mm across with flat to undulose extinction. The quartz grains form embayed boundaries with surrounding grains. Numerous hairline fractures have been healed with quartz or opaque minerals occur with most fractures contained within individual quartz grains and a few fractures extending into surrounding quartz grains. There are a few scattered fluid inclusions and inclusions of biotite. Biotite in the quartz has undergone some alteration to chlorite.

Microcline occurs as subhedral grains up to 3.75 mm across with most grains exhibiting characteristic tartan twinning. Some microcline has endured minor alteration to sericite, clay, muscovite, albite, and opaque minerals. Some albite exsolution is present having formed faint perthitic textures. Inclusions of quartz, biotite, sericite, and clay are present. The microcline has formed embayed and interlocking grain boundaries with adjacent grains of quartz, microcline, and plagioclase, and straight boundaries with biotite and muscovite.

Biotite grains are subhedral to euhedral grains up to 1.5 mm long with brown to light green pleochroism and exhibit the classic bird's eye texture under crossed polars. It has good cleavage and form straight boundaries with adjacent grains along the long axis and embayed boundaries along the short axis. Biotite occurs as discrete flakes locked into the matrix with no banding or clots that may present problems with excess free mica in aggregate. Most biotite has undergone alteration to chlorite.

Muscovite occurs as subhedral to euhedral grains up to 1.0 mm long. Symplectic textures are common within the muscovite. The muscovite occurs as individual flakes locked into the matrix with no clots or bands.

Opaque minerals occur as a few scattered anhedral to subhedral grains up to 0.1 mm across. Clay, sericite, and albite occurs as very fine grains in plagioclase and microcline as a result of alteration.

Chlorite is present as an alteration product of biotite. Chlorite has partially to completely replaced grains of biotite. It is pleochroic from light green to dark green and has gray to black interference colors.

The interlocking grain boundaries of the alkali feldspar metagranite and relatively small grain sizes would produce an aggregate with Los Angeles abrasion losses below Alabama and surrounding state DOT's maximum allowable loss but the large grain sizes of pegmatite have cause elevated Los Angeles abrasion losses. This is due to the influence of the cleavage in the plagioclase and microcline and the brittle nature of the large quartz grains. Los Angeles abrasion loss within this sample was 42.0% which was higher than the previous two samples. The clay and chlorite present in the sample have not elevated the sulfate soundness loss. Sulfate loss was 0.03% which was similar to the previous two samples. In the event test results become problematic, blasting patterns can be arranged such that an acceptable blend of alkali feldspar metagranite and pegmatite that meets all test requirements can be achieved. Specific gravity of this sample was 2.606 with an absorption of 0.7% due to the larger grain sizes within the pegmatite and elevated chlorite and high alteration of plagioclase.

N4-4-10P and N4-4-10

The sample is a white with some pink grains of microcline, coarse-grained, metagranite which has been cross cut by a pegmatite as seen by the increase in grain size. The thin section is composed of plagioclase (35-40%), microcline (25-30%), quartz (20-25%), biotite (1-3%), muscovite (1-3%), clay and sericite (3-5%), garnet (1-2%), chlorite (1-2%), and trace amounts of fluorite and opaque minerals. There is no discernable foliation present within the two samples. Several open fractures filled with blue epoxy (Figures 43 & 44) are present and are probable artifacts of sampling (i.e. fractures induced when sample collected and reduced in size using a large hammer).

Plagioclase occurs as subhedral grains up to 11 mm across with faint to well-developed albite twinning. Plagioclase has undergone moderate to nearly complete alteration to sericite and clay (Figures 45 & 46). The plagioclase grains have embayed, interlocking boundaries with all adjacent mineral grains (Figures 43 & 44). Healed fractures commonly occur within plagioclase grains with a few open fractures filled with blue epoxy extending across multiple adjacent grains. A minor amount of poorly-developed myrmekite has formed in plagioclase near boundaries with microcline. In addition to alteration minerals, the plagioclase includes inclusions of muscovite, biotite, quartz and microcline.

Microcline has subhedral habits up to 2.75 mm across and tartan twins. Some microcline has experienced moderate alteration to sericite, clay, muscovite, albite, and unidentified opaque minerals. Some elongate albite exsolution is present forming perthitic textures (Figures 47 & 48). Inclusions of quartz and biotite are also present. Microcline has embayed and interlocking boundaries with adjacent grains of quartz,

microcline, and plagioclase, and generally straight ones with biotite and muscovite (Figures 49 & 50).

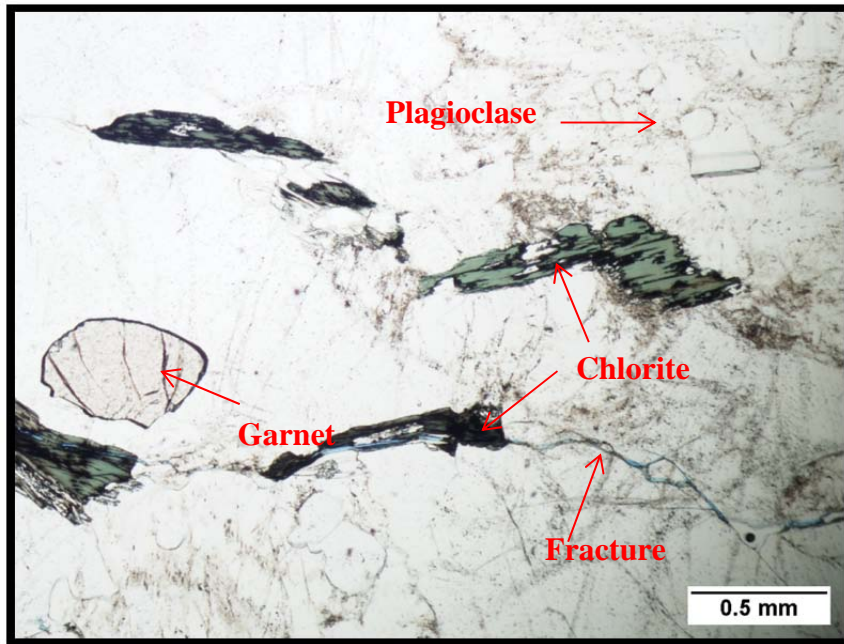


Figure 43. N4-4-10, Biotite completely altered to chlorite and plagioclase undergoing alteration to sericite and clay. Open fracture filled with blue epoxy. Photographed under plane polarized light at 40X magnification.

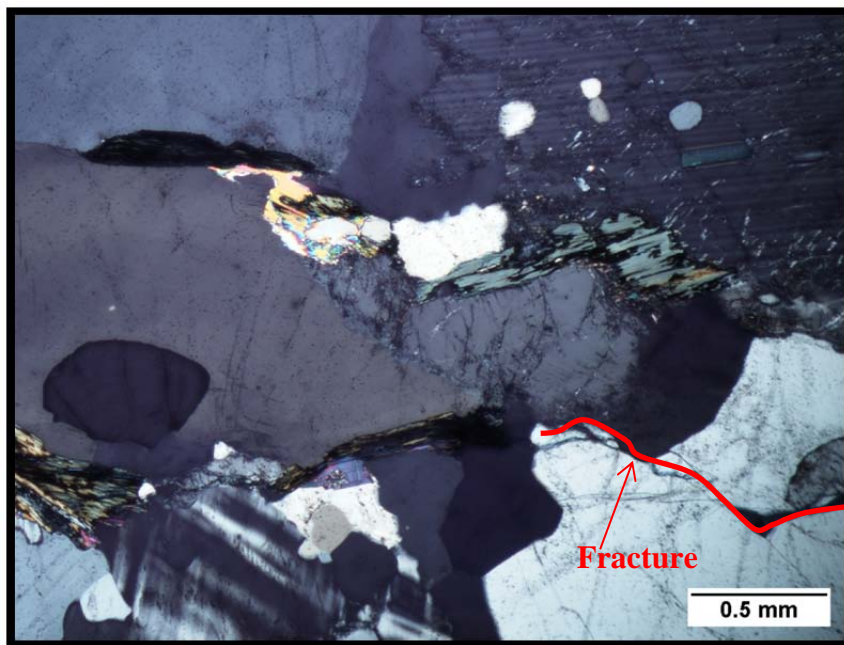


Figure 44. N4-4-10, Same view as above in Figure 43 but photographed under crossed polars at 40X magnification. Note the interlocking, embayed grain boundaries.

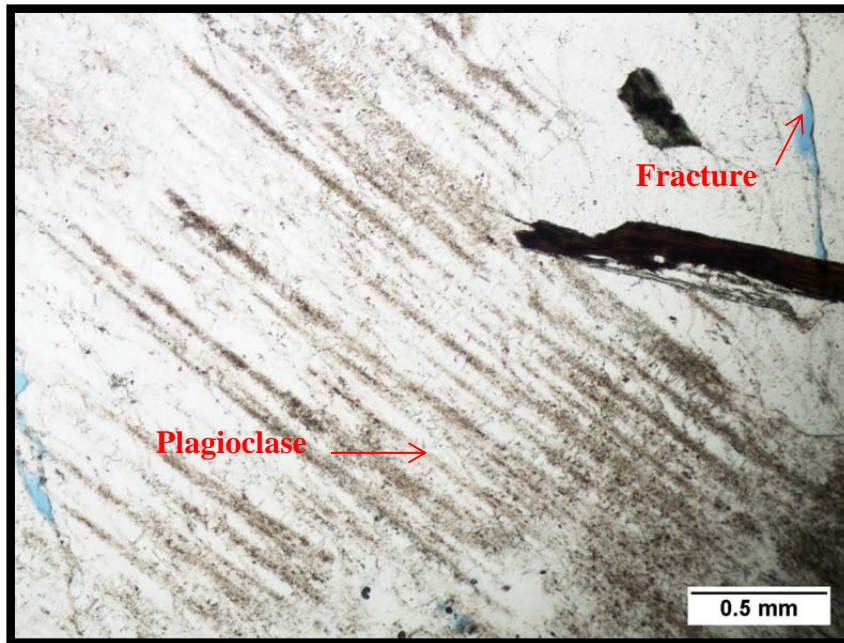


Figure 45. N4-4-10, Plagioclase grain with moderate alteration to sericite and clay. Photographed under plane polarized light at 40X magnification.

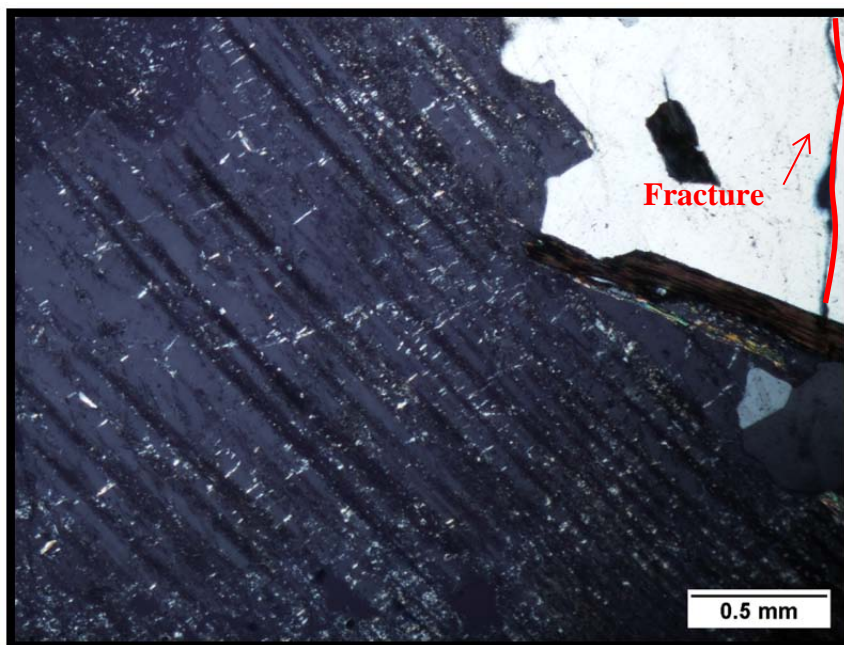


Figure 46. N4-4-10, Same view as above in Figure 45 but photographed under crossed polars at 40X magnification.

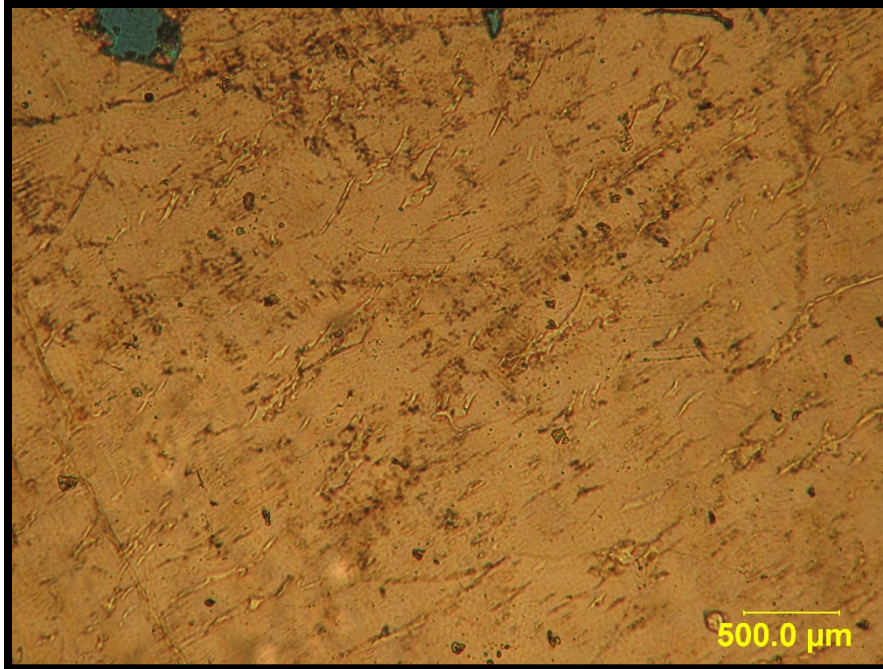


Figure 47. N4-4-10, Albite exsolving in microcline producing perthitic textures. Photographed under plane polarized light at 40X magnification.

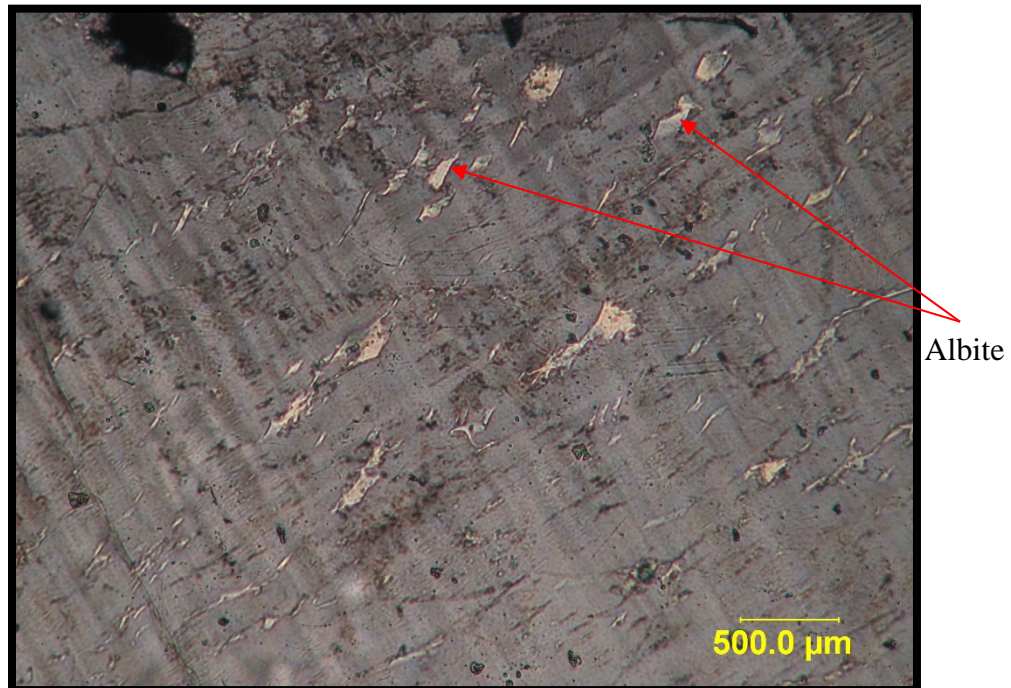


Figure 48. N4-4-10, Same view as above in Figure 47 but photographed under crossed polars at 40X magnification.

Quartz has anhedral shapes and is less than 4.5 mm in diameter and flat field to undulatory extinction. Quartz grains have embayed, interlocking boundaries with surrounding grains (Figures 43 & 44). Hairline fractures healed with opaque minerals are common and may be contained within individual quartz grains but many are filled with epoxy and extend into adjacent grains. The open fractures are interpreted as artifacts of sampling and perhaps blasting during the quarrying process. Scattered fluid inclusions, muscovite inclusions, and inclusions of biotite exist within the quartz and have undergone some alteration to chlorite.

Subhedral to euhedral grains of biotite as less than 1.5 mm long with dark brown to light green pleochroism and exhibit bird's eye texture under crossed polars. Biotite is typically partially to completely altered to chlorite (Figures 49 & 50). Some intergrowths of biotite with muscovite and/or garnet are present (Figures 51 & 52). Inclusions of opaque minerals are common in the biotite. Biotite has good cleavage and forms straight boundaries with adjacent grains along the stretched axis but embayed boundaries on the short axis (Figures 49 & 50). There are clusters of biotite and chlorite observed within this sample.

Subhedral to euhedral grains of muscovite are up to 0.75 mm long and form discrete platelets as intergrown with biotite or occur as inclusions in plagioclase (Figures 53 - 56). Symplectic textures are common. Muscovite occurs as individual grains within the matrix with no significant clots or bands over the entire thin section.

Very fine grains of clay and sericite are found in plagioclase and microcline as an alteration product. Chlorite is alteration product of biotite and is pleochroic from light green to dark green with interference colors ranging from gray to black (Figure 53 & 54).

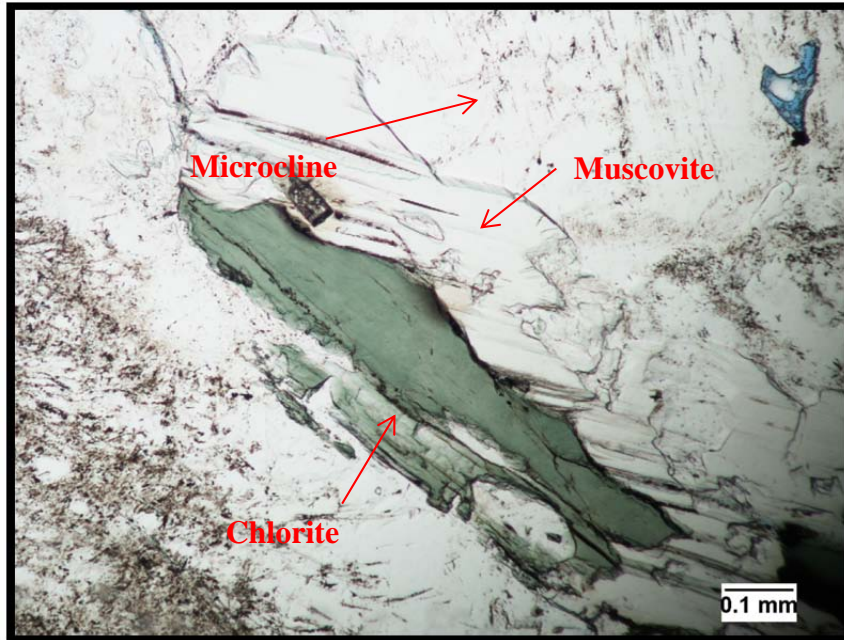


Figure 49. N4-4-10, Biotite completely altered to chlorite intergrown with muscovite. Photographed under plane polarized light at 100X magnification.

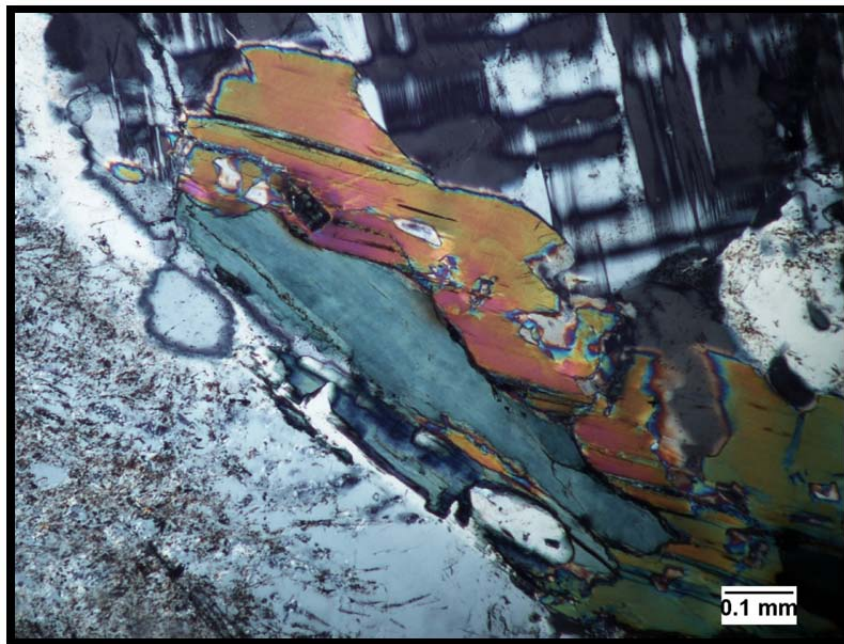


Figure 50. N4-4-10, Same view as above in Figure 49 but photographed under crossed polars at 100X magnification. Here it is clear that microcline has interlocking, embayed boundaries with plagioclase and also with muscovite where the short axis has been exploited.

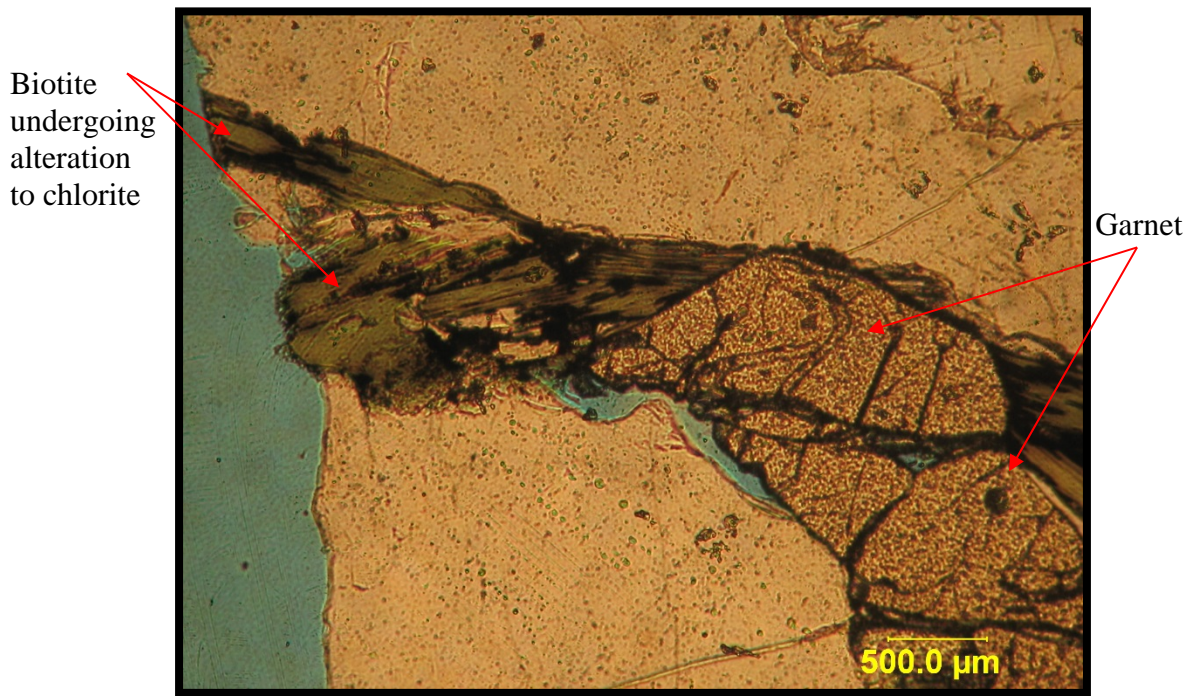


Figure 51. N4-4-10, A clot of garnet with intergrown biotite and muscovite. Biotite has undergone alteration to chlorite. Photographed under plane polarized light at 40X magnification.

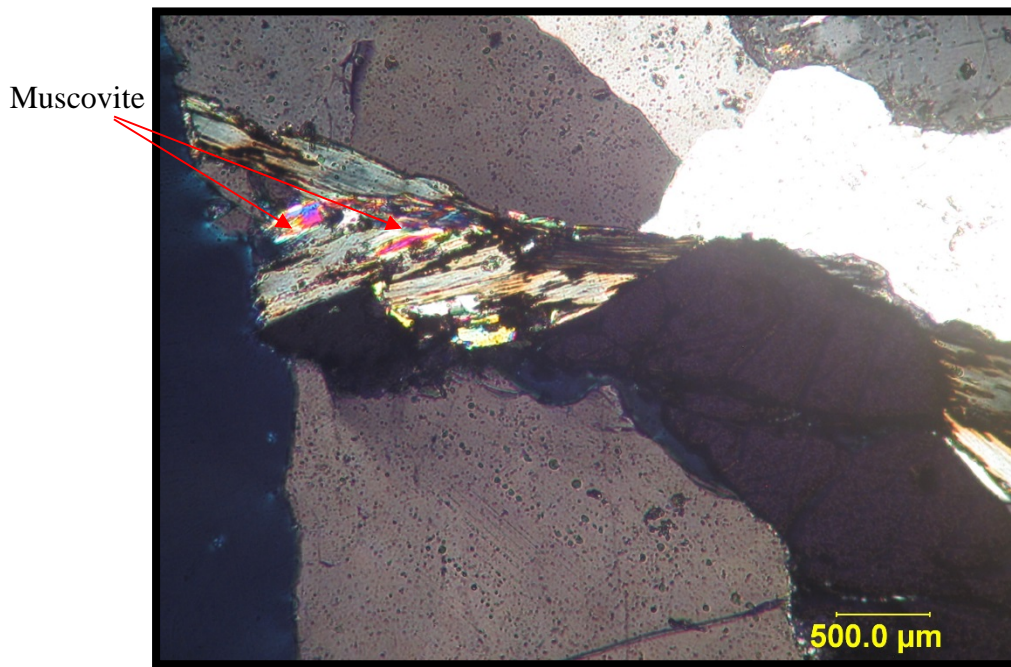


Figure 52. N4-4-10, Same view as above in Figure 51 but photographed under crossed polars at 40X magnification.

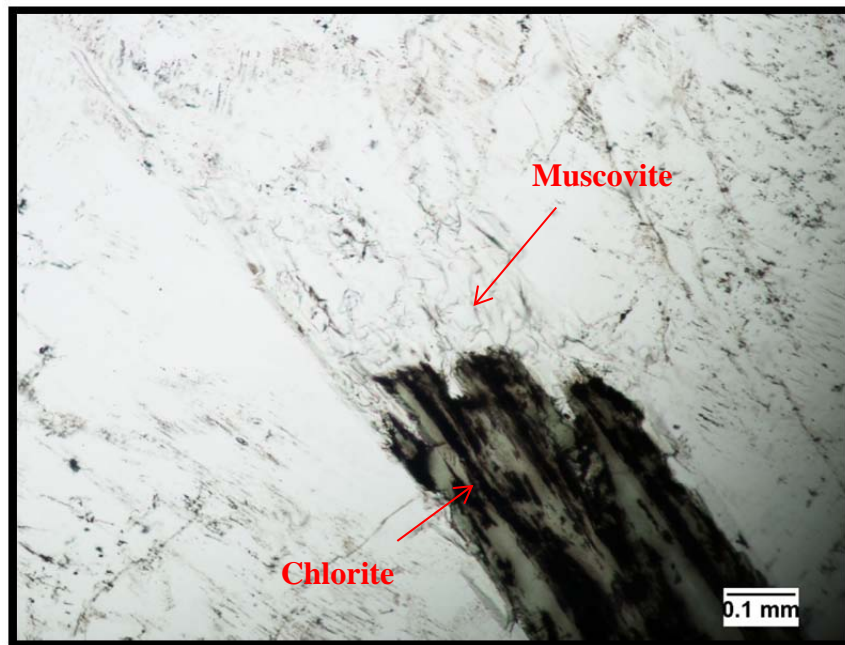


Figure 53. N4-4-10, Chlorite replacing biotite and intergrowths of muscovite within a microcline grain. Photographed under plane polarized light at 100X magnification.

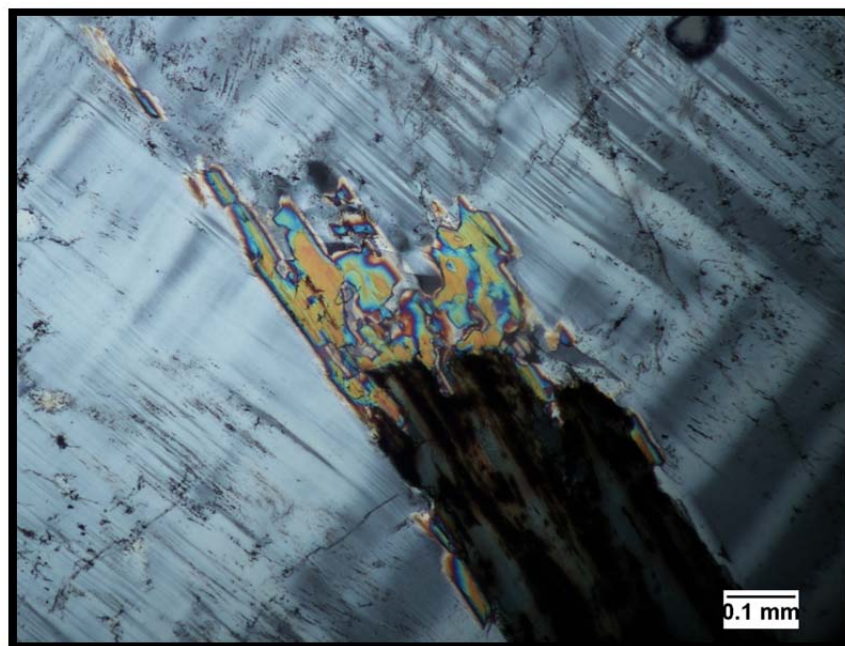


Figure 54. N4-4-10, Same view as above in Figure 53 but photographed under crossed polars at 100X magnification.

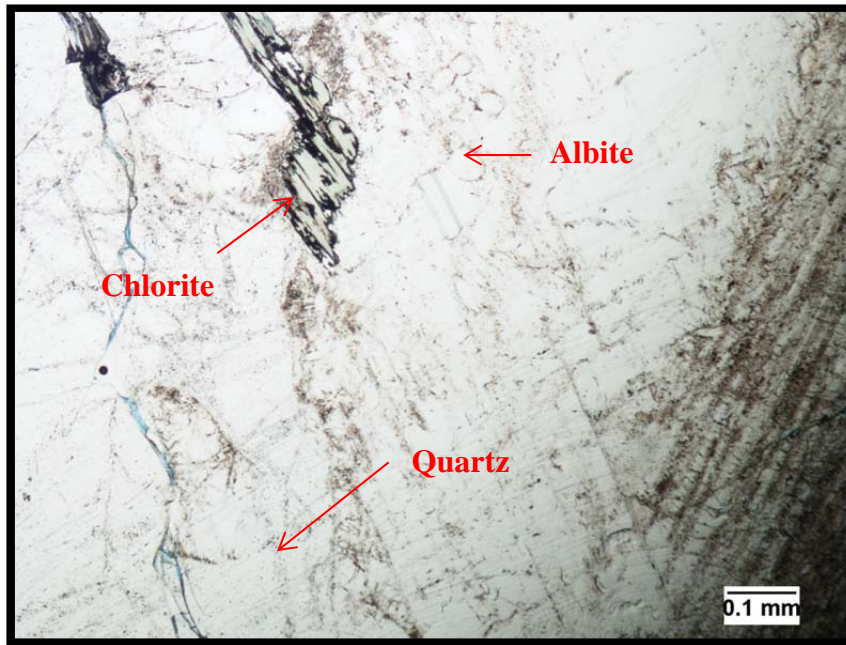


Figure 55. N4-4-10, Chlorite replacing biotite and intergrowths of muscovite. Plagioclase undergoing alteration to sericite. Albite poikilitically enclosed in plagioclase. Photographed under plane polarized light at 100X magnification.

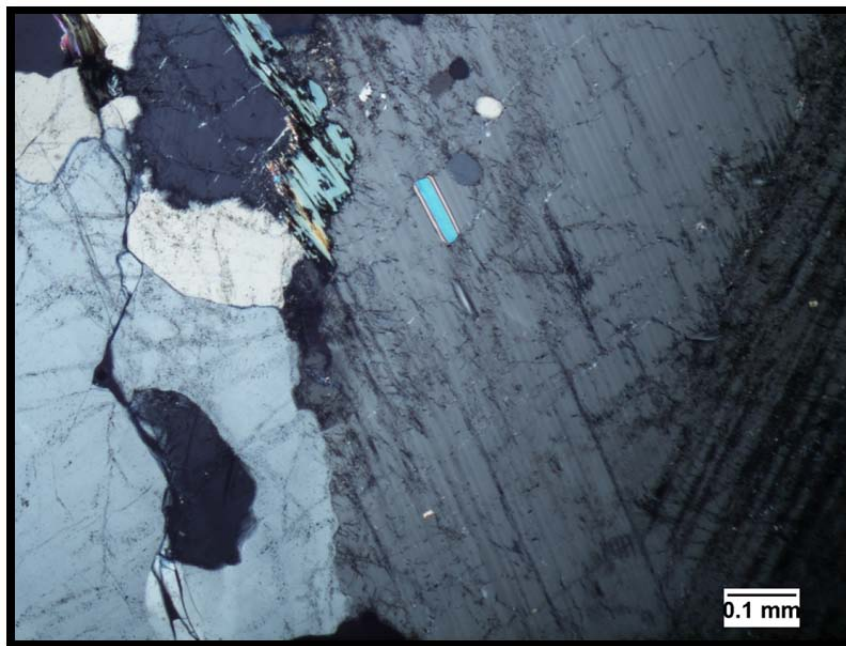


Figure 56. N4-4-10, Same view as above in Figure 55 but photographed under crossed polars at 100X magnification.

Subhedral to euhedral garnet grains are 0.25 mm to 1.75 mm in diameter. Garnet contains inclusions of opaque minerals and has abundant fractures filled with opaque minerals.

Subhedral to euhedral fluorite grains are less than 2.5 mm across and have characteristic octahedral cleavage. A few fractures observed within fluorite grains are filled with opaque minerals. A few scattered anhedral to subhedral opaque mineral grains up to 0.1 mm across occur in the matrix and as inclusions in biotite, microcline, and garnet.

Sample N4-4-10 has relatively large grains of microcline, plagioclase, and quartz that have caused elevated Los Angeles abrasion losses of 42.7% due to the influence of clots of biotite and chlorite, the well-developed cleavages in the feldspars, and the brittle behavior of quartz under these test conditions. Absorption may be slightly higher due to the fractures within individual grains but also should not affect the production product. The absorption of N4-4-10 was the lowest of all the samples at 0.5%. Open fractures which cut across multiple grain boundaries within the thin section are probable artifacts of sample collection and reduction to testing size. Sulfate soundness losses in the sample might be predicted to be elevated due to the open fractures, alteration of plagioclase grains to sericite and clay, and the presence of chlorite produced by alteration of biotite. However, this was not the case, sulfate soundness results remained low having a loss of 0.020%.

N1A-4-10P and N1A-4-10

Sample N1A-4-10 is a medium gray to black with some pink grains of microcline, medium-grained augen gneiss (Figure 57 & 58) composed of microcline (30-35%), quartz (30-35%), plagioclase (20-25%), biotite (5-7%), muscovite (3-5%), clay and sericite (2-3%), chlorite (1-2%), and trace amounts of epidote and opaque minerals. There is a well-developed foliation present within this thin section as defined by the alignment of biotite and muscovite.

Subhedral grains of microcline are up to 4.0 mm in diameter. Poikilitic microcline contains altered plagioclase grains with sericite, clay, muscovite, opaque minerals and vermicular quartz that may be remnants of myrmekitic growth in the plagioclase (Figures 59 & 60). Many grains are tartan twinned. Perthitic intergrowths of albite found through exsolution are faintly developed. Inclusions of quartz and biotite are also present. Microcline has embayed and interlocking grain boundaries with adjacent grains of quartz, microcline, and plagioclase, whereas generally straight boundaries are associated with biotite and muscovite (Figures 59 & 60).

Anhedral grains of quartz are less than 2.5 mm across with flat to undulose extinction. Quartz grains typically have embayed and interlocking grain boundaries with surrounding grains (Figures 61 & 62). Fluid inclusions are commonly linear and occur together with inclusions of biotite, muscovite, microcline, and opaque minerals.

Plagioclase grains are as subhedral, up to 1.25 mm across, and albite twins are faint to well-developed. The plagioclase grains are slightly to heavily altered by saussuritization producing sericite, clay, and opaque minerals (Figures 63 & 64). Plagioclase grains have embayed boundaries with all adjacent mineral grains.

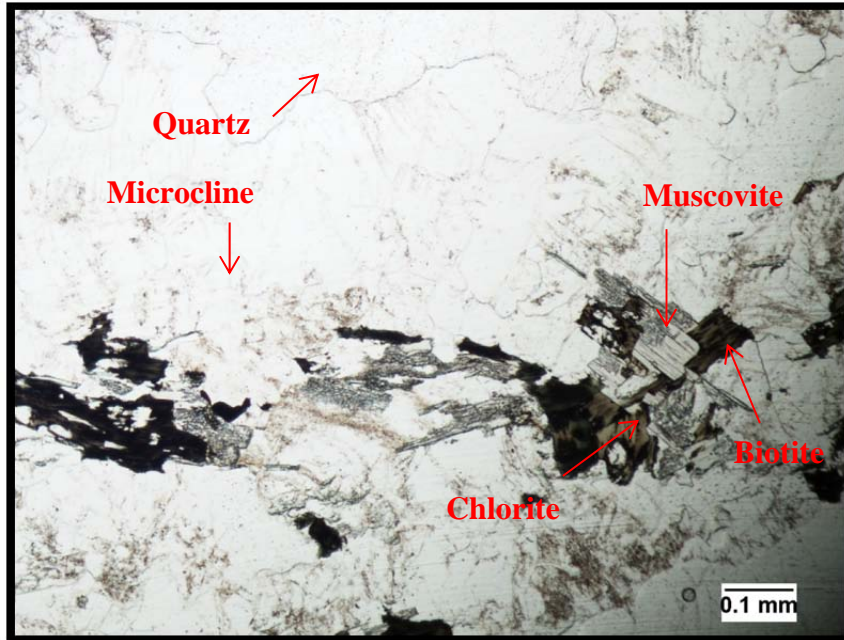


Figure 57. N1A-4-10, Typical view of sample matrix. Photographed under 100X magnification.

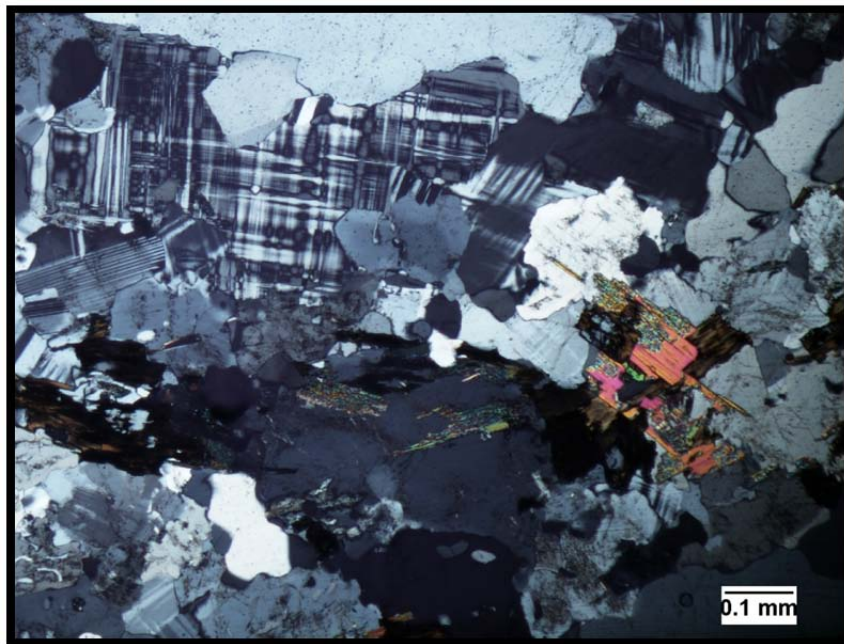


Figure 58. N1A-4-10, Same view as above in Figure 57 but photographed under crossed polars at 100X magnification. Grain boundaries are embayed and interlocking.

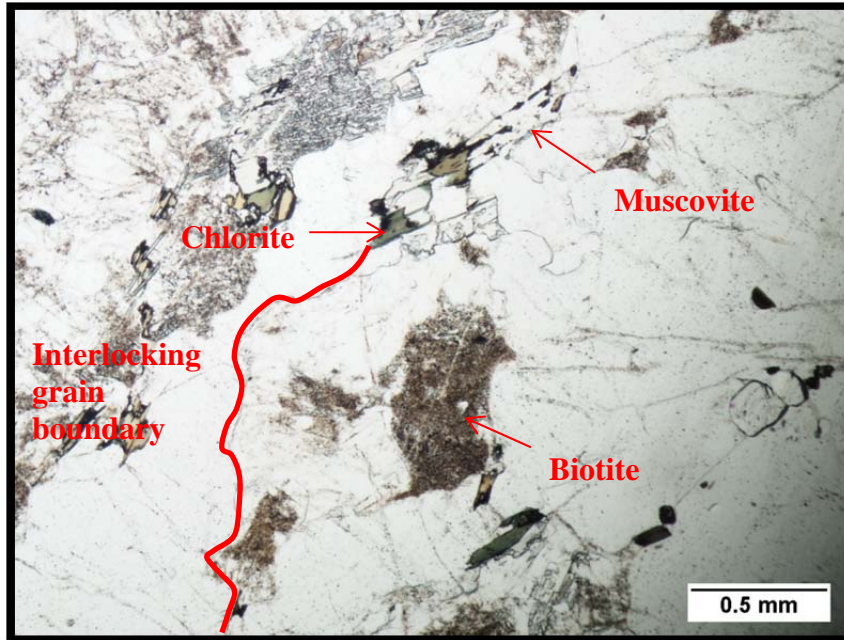


Figure 59. N1A-4-10, Interlocking grain boundaries. Biotite has altered to chlorite and muscovite has symplectic texture. Photographed under 40X magnification.

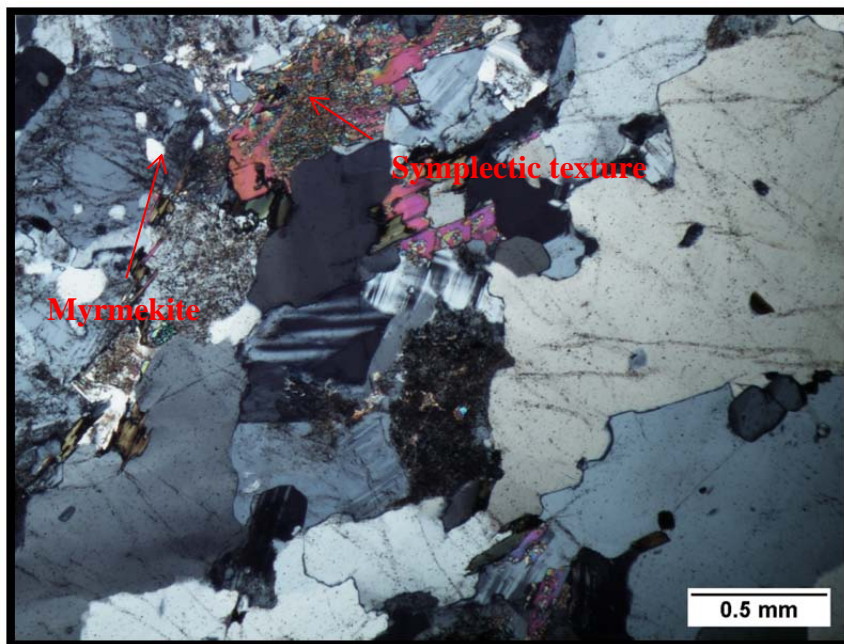


Figure 60. N1A-4-10, Same view as above in Figure 59 but photographed under crossed polars at 40X magnification.

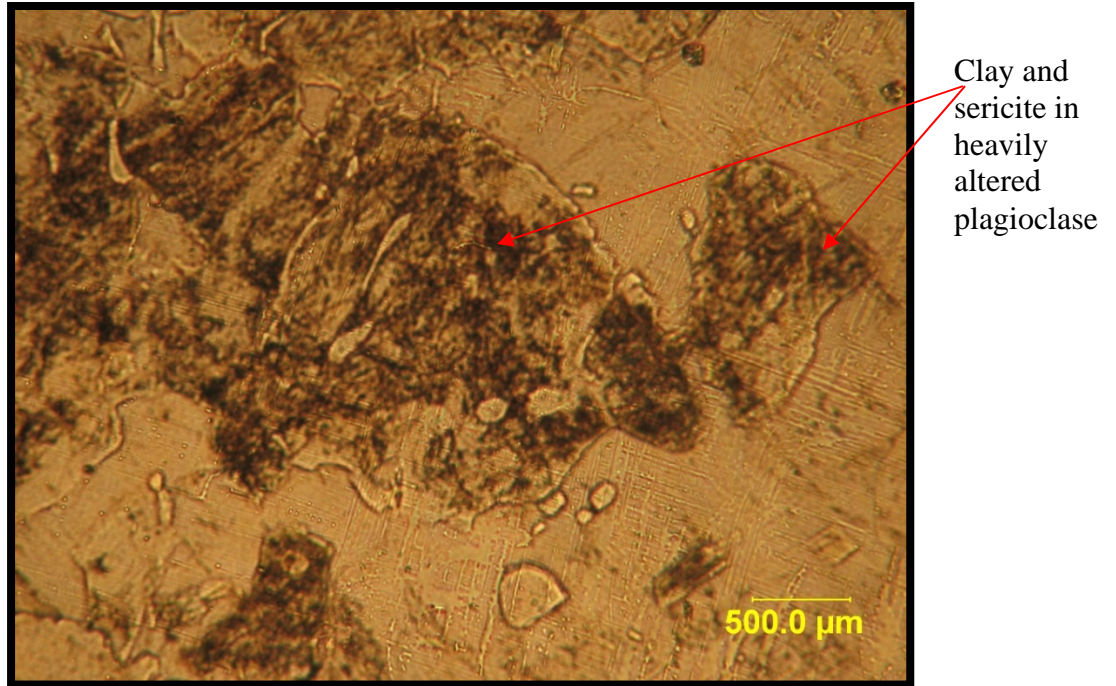


Figure 61. N1A-4-10, Highly altered plagioclase grains poikilitically enclosed in microcline. Photographed under plane polarized light at 40X magnification.

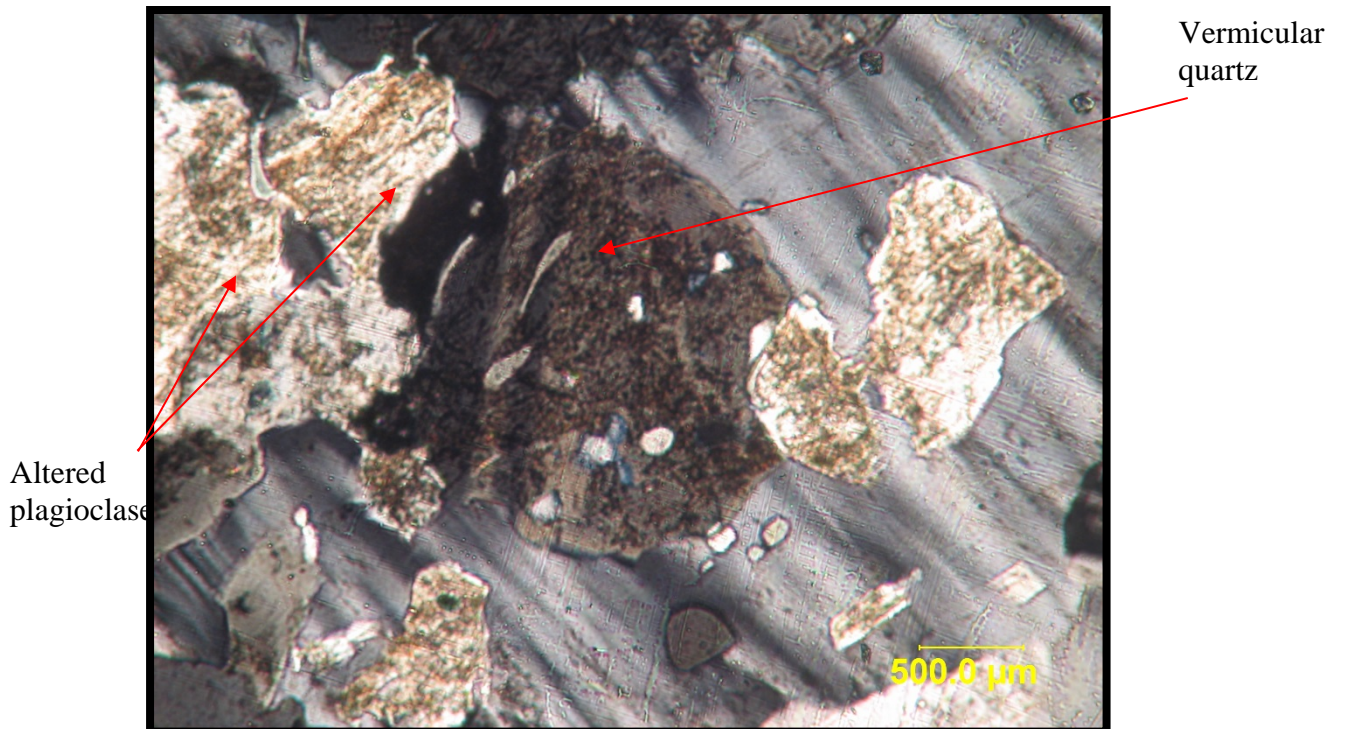


Figure 62. N1A-4-10, Same view as above in Figure 61 but photographed under crossed polars at 40X magnification.

Myrmekitic texture has developed in plagioclase near boundaries with microcline. In addition to alteration minerals, the plagioclase includes fluid inclusions and inclusions of muscovite, biotite, quartz and microcline.

Subhedral to euhedral grains of biotite are up to 1.5 mm in length. Biotite has dark brown to light green pleochroism and bird's eye texture under crossed polars. Many biotite grains are partially to completely altered to chlorite (Figures 63 & 64). Muscovite and epidote are intergrown with biotite (Figures 65 & 66). Inclusions of opaque minerals are observed in biotite. Cleavage is well developed and forms straight boundaries with adjacent grains whereas embayed boundaries formed perpendicular to cleavage (Figures 65 & 66). Biotite is both locked into the matrix minerals and forms clots (Figure 65 & 66).

Muscovite is subhedral to euhedral, up to 1.0 mm long, and displays symplectic texture. Muscovite generally occurs as individual flakes locked into the matrix.

Very fine grains of clay and sericite occur in plagioclase and microcline as an alteration product. Chlorite is the product of altered biotite and it has partially to completely replaced biotite grains. It is pleochroic from light green to dark green with interference colors ranging from gray to black. A few opaque minerals are scattered about the thin section and is anhedral to subhedral (0.1 mm across). Epidote is rare and is intergrown with biotite that has altered to chlorite (Figures 65 & 66).

Testing results of this sample show average results across the board. Prevalent interlocking grain boundaries and moderately small grain sizes of N1A-4-10 have produced an aggregate with Los Angeles abrasion loss of 34.7% which is well below the

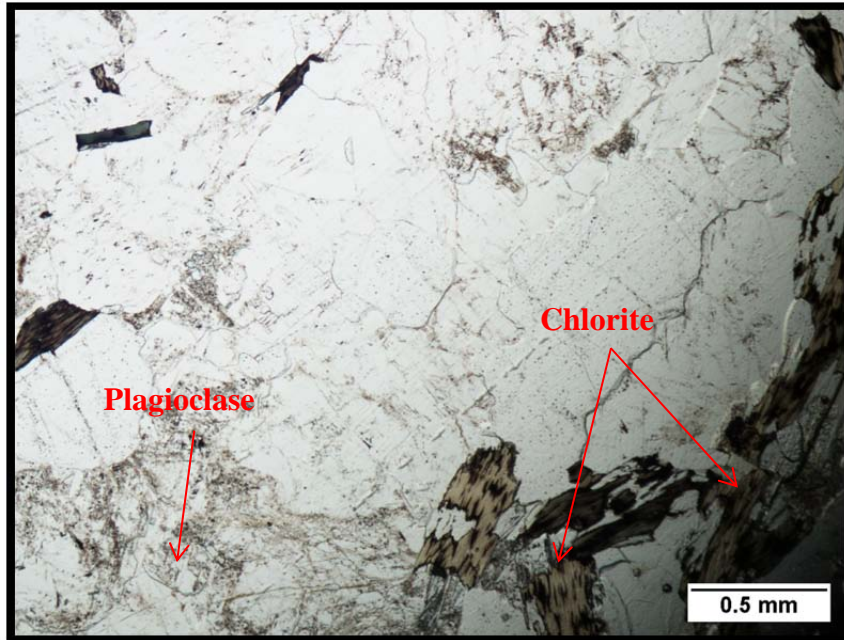


Figure 63. N1A-4-10, Biotite altered to chlorite, the latter having a fibrous texture. Photographed under 40X magnification.

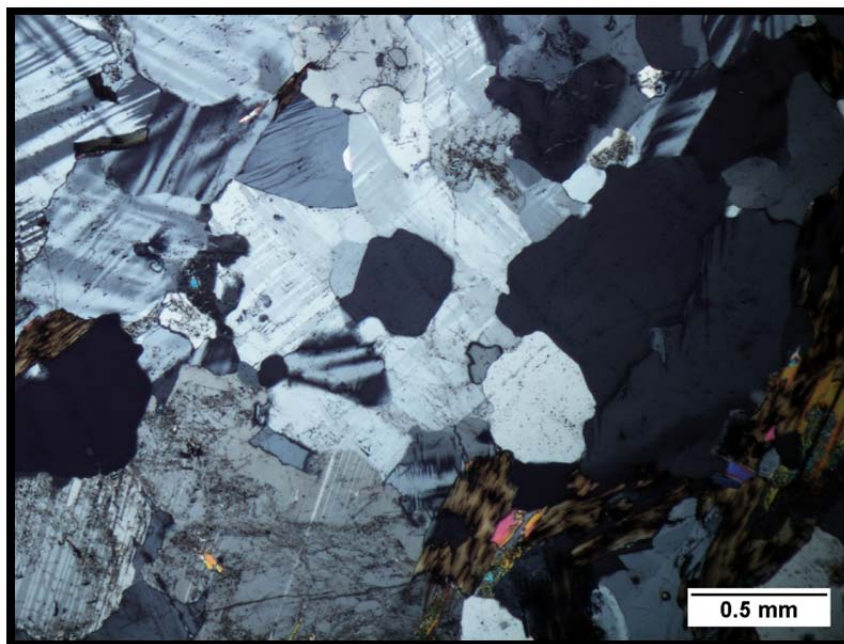


Figure 64. N1A-4-10, Same view as above in Figure 63 but photographed under crossed polars at 40X magnification. Plagioclase undergoing saussuritization to sericite and clay.

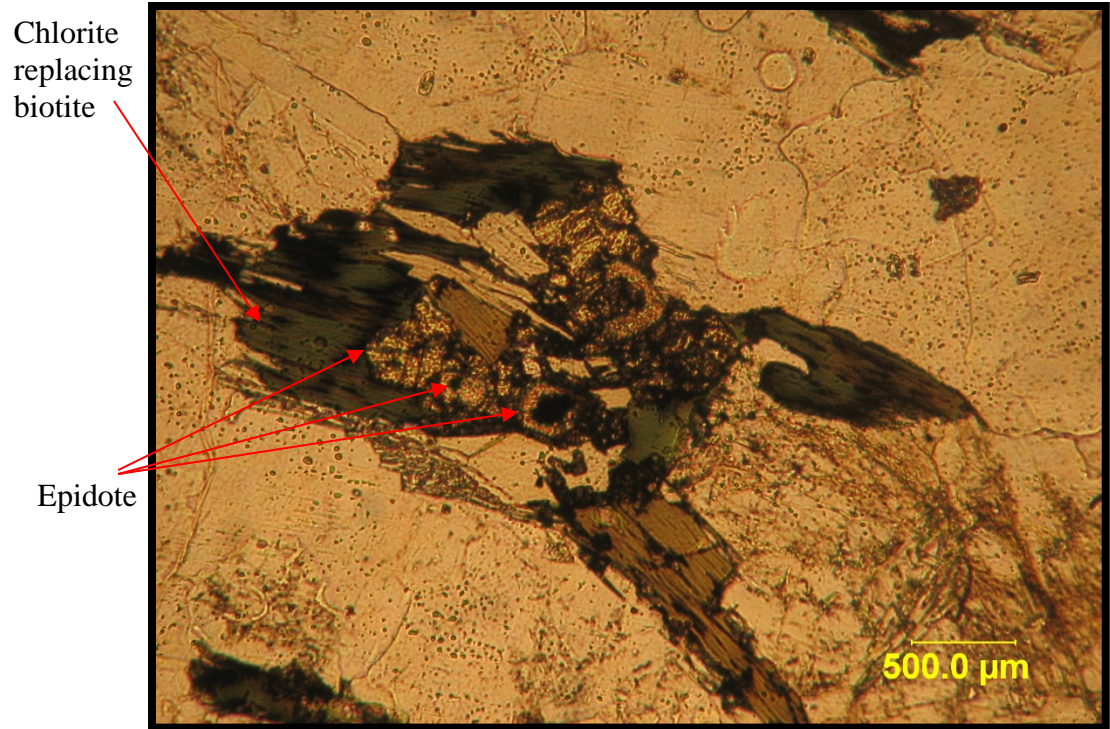


Figure 65. N1A-4-10, Epidote intergrown with biotite forming a clot within the thin section that has undergone alteration to chlorite. Photographed under plane polarized light at 40X magnification.

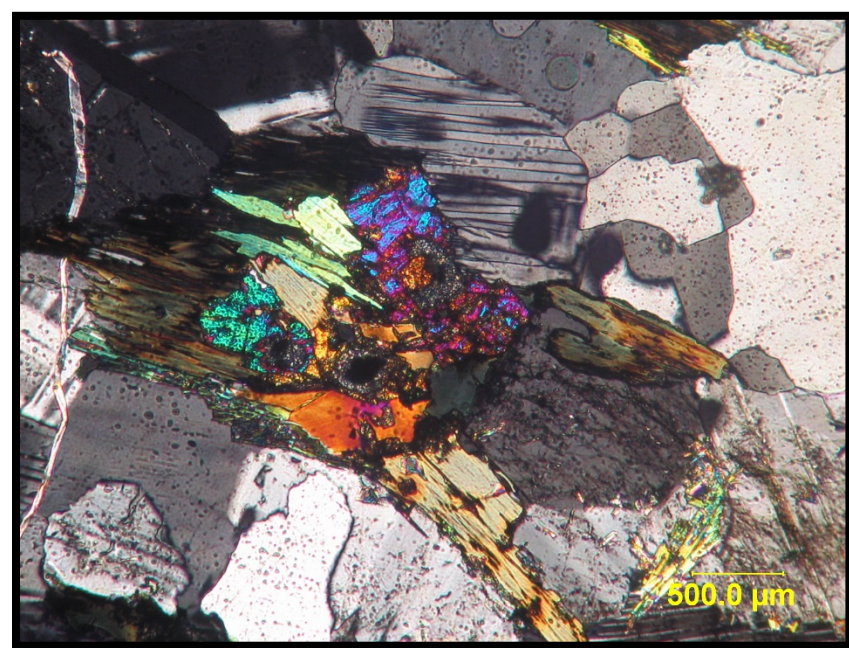


Figure 66. N1A-4-10, Same view as above in Figure 65 but photographed under crossed polars at 40X magnification.

maximum allowable loss. Clay and chlorite in the sample could possibly elevate sulfate soundness losses and as test results show the soundness was 0.495% which is higher than most other samples. The dense nature of the sample and lack of open fractures should result in a relatively low specific gravity and absorption which was seen as the bulk specific gravity was 2.596 and absorption of 0.6%. No alkali-aggregate reactive minerals were observed. Biotite and muscovite content (8-12%) is somewhat high but these phases are mostly locked within the matrix as individual grains with minor clots that may result in excess free mica. Microcline in sample N1A-4-10 has a well-developed cleavage that could break readily during crushing. The 30-35% microcline is cause for concern and the relatively large grain size, up to 4.0 mm could result in breakage along cleavage and elevate the Los Angeles abrasion loss, nonetheless, it should remain below the maximum allowed by the Alabama DOT and surrounding state DOT's because of the predominately interlocking grains.

N2A-4-10P and N2A-4-10

Sample N2A-4-10 is a medium gray, fine- to medium-grained, quartz-rich metagranite composed of quartz (50-55%), biotite (15-20%), plagioclase (10-15%), microcline (8-10%), muscovite (3-5%), and trace amounts of opaque minerals, clay, sericite, albite, garnet, epidote, carbonate, sphene, apatite, and zircon (Figures 67 & 68). A weak foliation is present and is defined by alignment of biotite and muscovite.

Quartz grains are anhedral, 0.1 mm to 1.0 mm in diameter, and have flat to undulose extinction. It generally has embayed boundaries with adjacent grains (Figures 67 & 68). Fluid inclusions are common together with inclusions of biotite, muscovite, opaque minerals, and apatite. Hairline fractures, healed with opaque minerals, mostly cut individual quartz grains but a few extend into adjacent quartz grains.

Subhedral microcline grains are 0.25 mm to 2.5 mm in diameter and exhibit tartan twinning. Some microcline has undergone alteration to sericite, clay, muscovite, and opaque minerals. Albite exsolution has resulted in faint perthitic textures. Inclusions of quartz, muscovite, biotite, opaque minerals, apatite, and clay were also observed. Microcline has embayed and interlocking grain boundaries with adjacent grains of quartz, microcline, and plagioclase, and generally straight boundaries with biotite and muscovite.

Biotite typically defines the foliation and occurs as subhedral to euhedral grains 0.125 mm to 0.75 mm in length with dark brown to light brown pleochroism (Figures 69 - 72). It characteristically has bird's eye extinction. Inclusions of zircon in the biotite are common and have undergone radioactive decay resulting in pleochroic halos. Intergrowths of biotite with muscovite (Figures 69 & 70), garnet and epidote (Figures 75 & 76) are common. Biotite has good cleavage and has straight boundaries along the

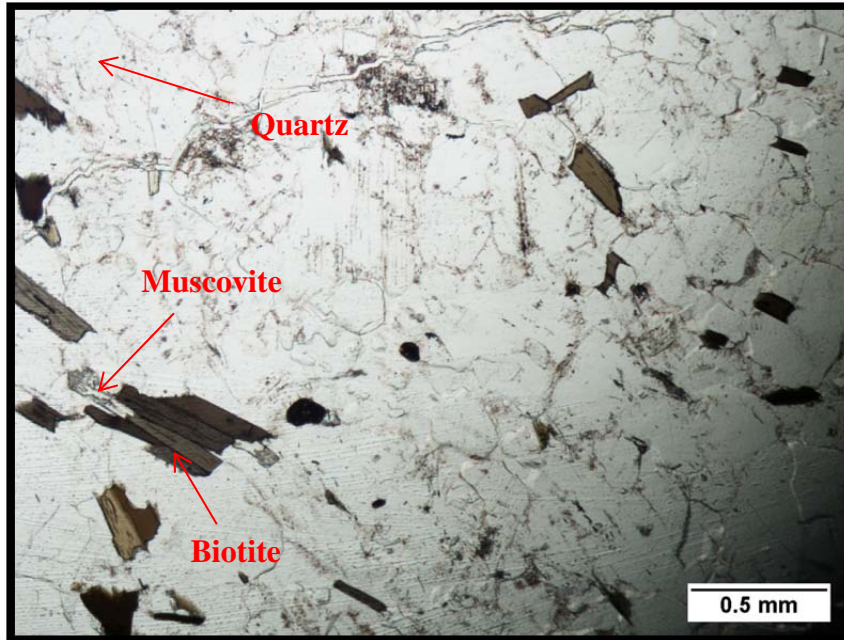


Figure 67. N2A-4-10, Typical view of sample. Photographed under 40X magnification.

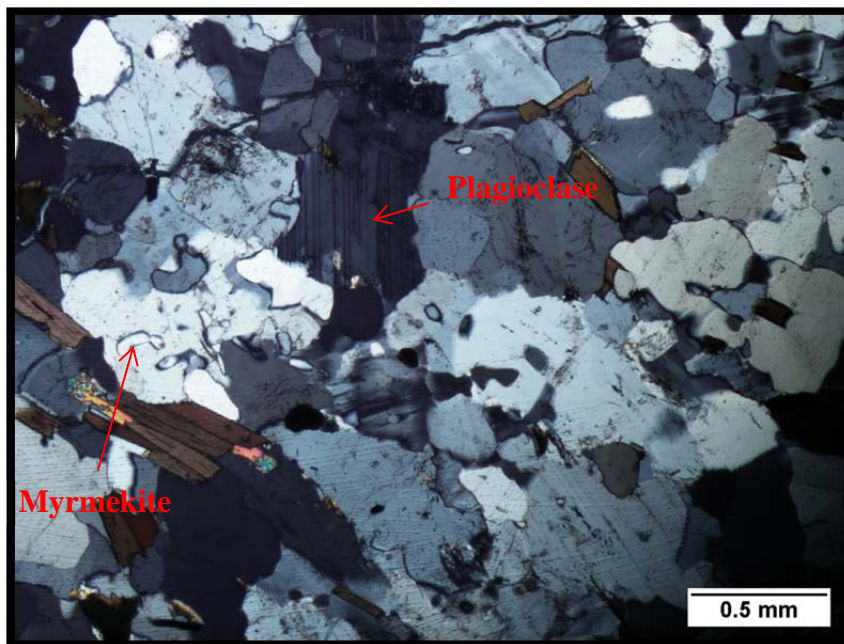


Figure 68. N2A-4-10, Same view as above in Figure 67 but photographed under crossed polars at 40X magnification. Plagioclase grain hosts myrmekitic texture.

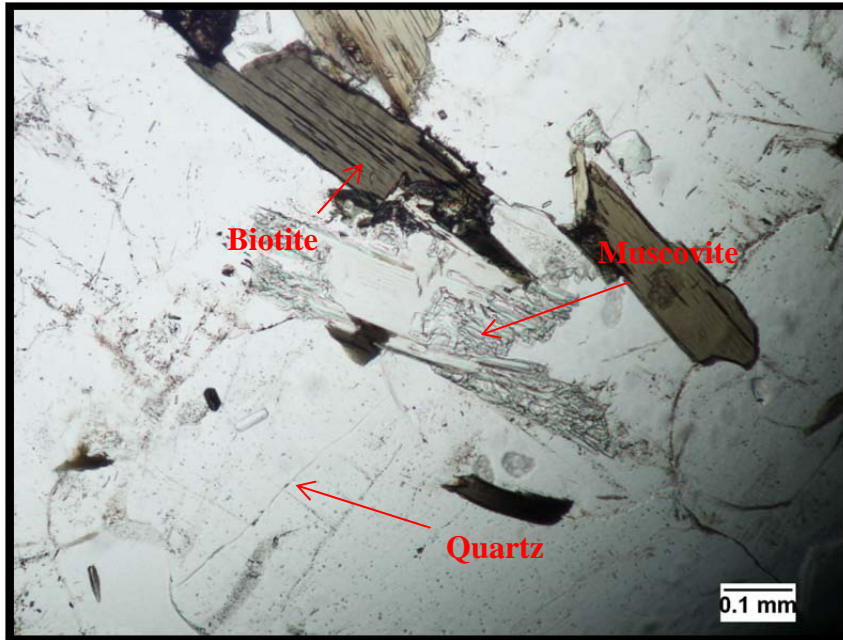


Figure 69. N2A-4-10, Biotite with intergrowths of muscovite with symplectitic texture. Photographed under plane polarized light at 100X magnification.

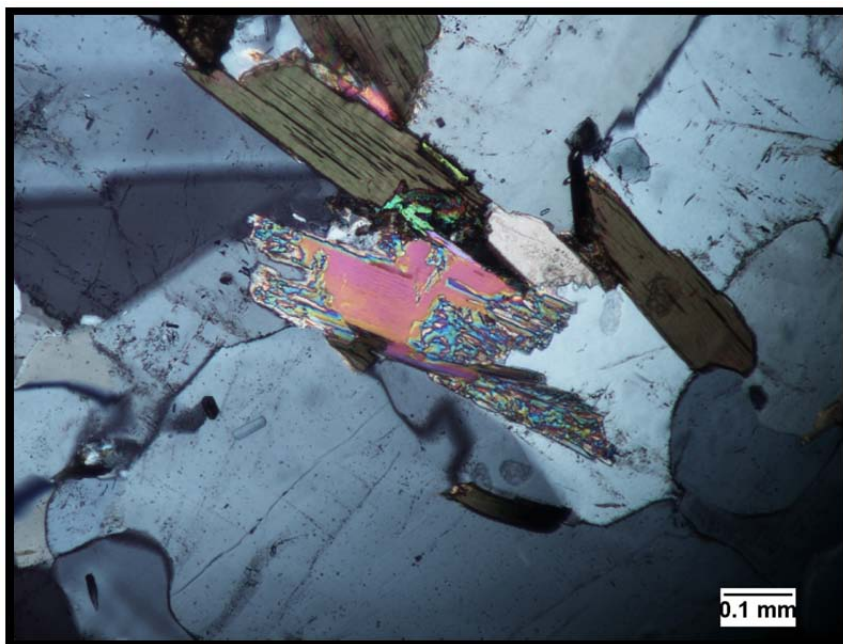


Figure 70. N2A-4-10, Same view as above in Figure 69 but photographed under crossed polars at 100X magnification. Quartz has undulatory extinction with embayed and interlocking grain boundaries.

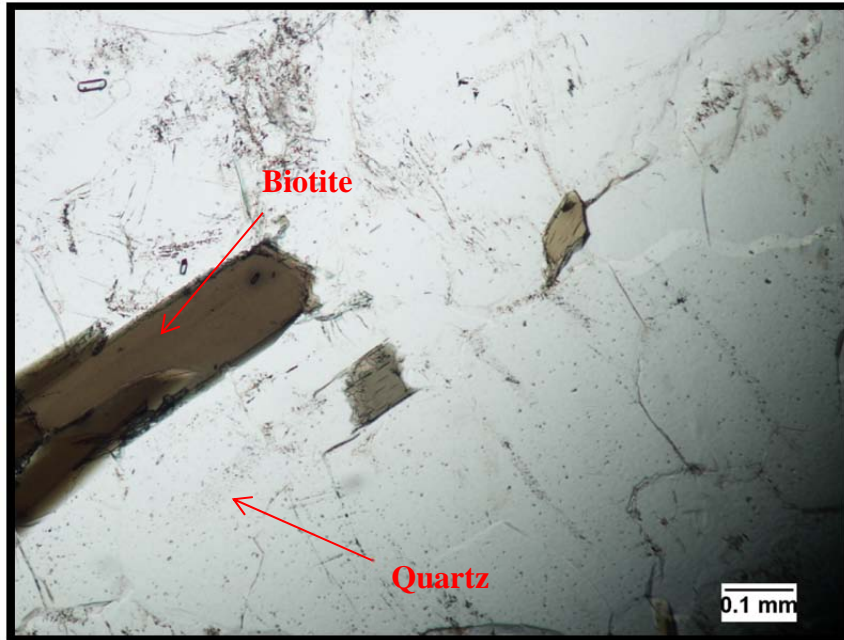


Figure 71. N2A-4-10, Biotite is pleochroic, light brown to dark brown. Photographed under plane polarized light at 100X magnification.

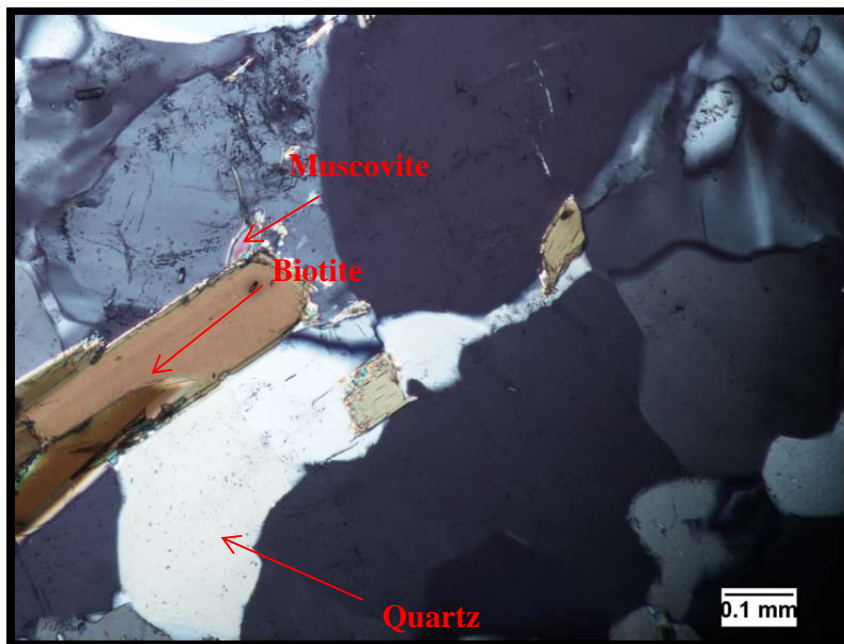


Figure 72. N2A-4-10, Same view as above in Figure 71 but photographed under crossed polars at 100X magnification.

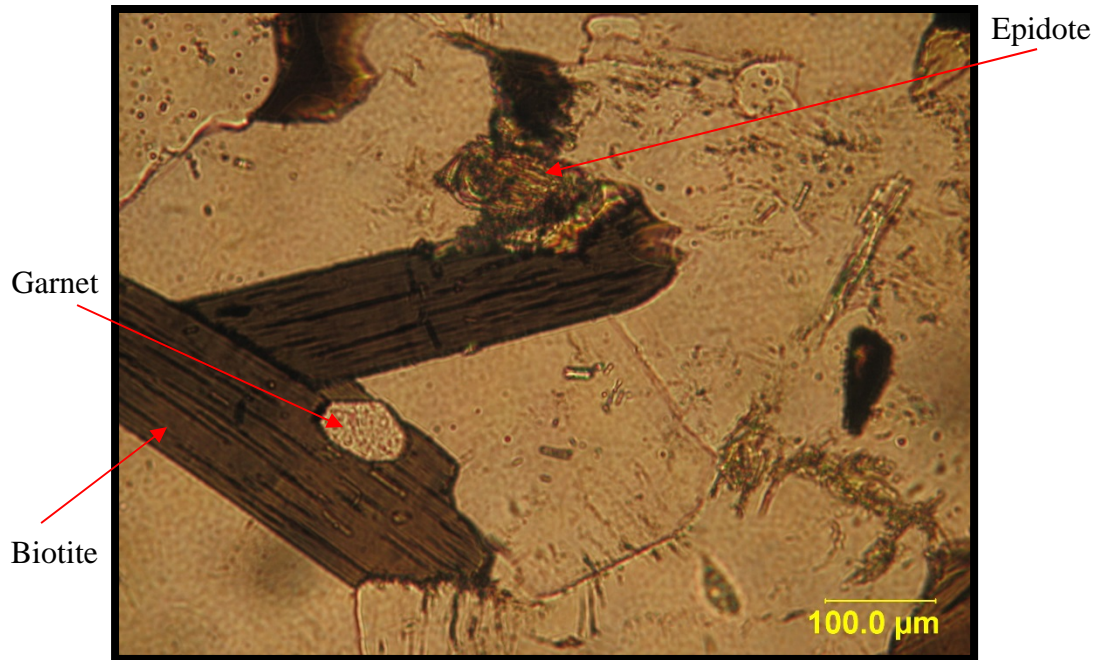


Figure 73. N2A-4-10, Biotite intergrown with garnet and epidote. Photographed under plane polarized light at 100X magnification.

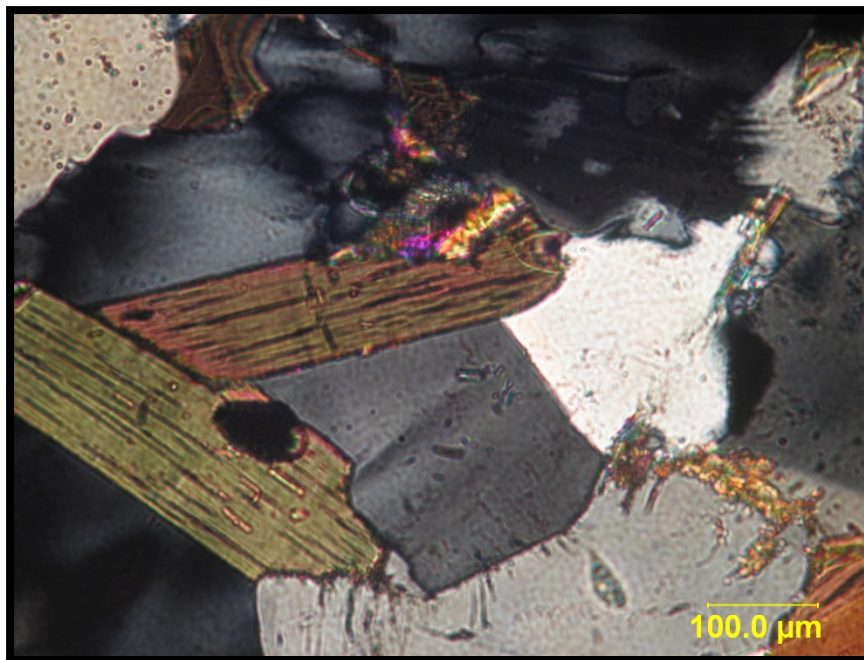


Figure 74. N2A-4-10, Same view as above in Figure 75 but photographed under crossed polars at 100X magnification.

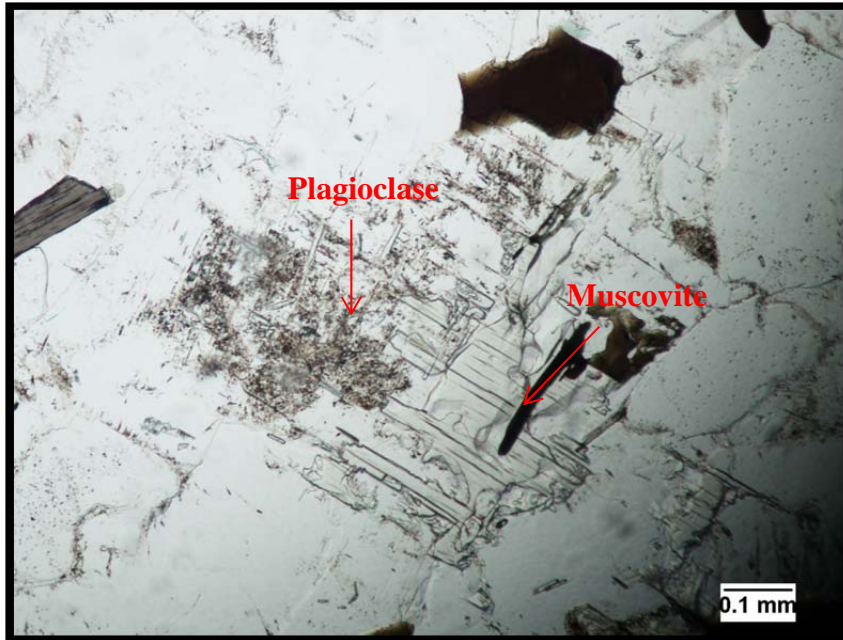


Figure 75. N2A-4-10, Plagioclase with intergrowths of muscovite with symplectic texture. Photographed under plane polarized light at 100X magnification.

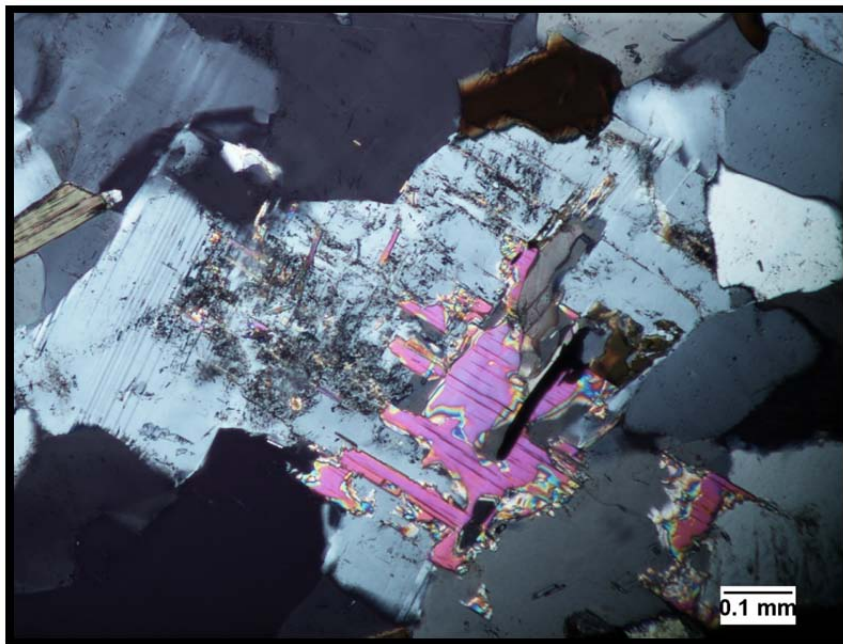


Figure 76. N2A-4-10, Same view as above in Figure 75 but photographed under crossed polars at 100X magnification.

elongated axis and embayed boundaries along the short axis (Figures 77 & 78). Grains are usually solitary and locked into the matrix.

Plagioclase occurs as subhedral grains 0.25 mm to 1.0 mm across. It has faint to well-developed albite twins. Slight to moderate saussuritization produced sericite, clay, muscovite, carbonate, epidote, and opaque minerals (Figures 79 & 80). The plagioclase grains form straight to slightly embayed boundaries with adjacent mineral grains. In addition to alteration minerals, the plagioclase includes inclusions of quartz and biotite.

Muscovite grains are subhedral to euhedral and up to 1.0 mm long. Symplectic growths and intergrowths with biotite are common. The symplectites clearly exploited the long axis as they are observed to follow that crystal direction rather than cut across it (Figures 75 & 76). Muscovite occurs as individual grains within the matrix rather than concentrated in clots or bands. Alignment of muscovite with biotite helps to define the weak foliation present in the sample.

Opaque minerals are anhedral to subhedral and measure 0.125 mm to 0.25 mm across. Very fine grains of clay and sericite occur in plagioclase and microcline as alteration products. Albite is an alteration product of plagioclase and also occurs as exsolution blebs (perthite) in microcline. Garnet grains are subhedral to euhedral, 0.125 mm to 1.0 mm in diameter, and has inclusions of opaque minerals. Numerous fractures are found healed with opaque minerals. Epidote is an alteration product of plagioclase and also occurs as intergrowths with biotite (Figures 73 & 74), two epidote group minerals are observed, epidote and zoisite. Small grains of carbonate are present as an alteration product in plagioclase (Figures 79 & 80). Sphene is present in trace amounts occurring as subhedral to euhedral wedges up to 0.3 mm long. Many sphene grains have

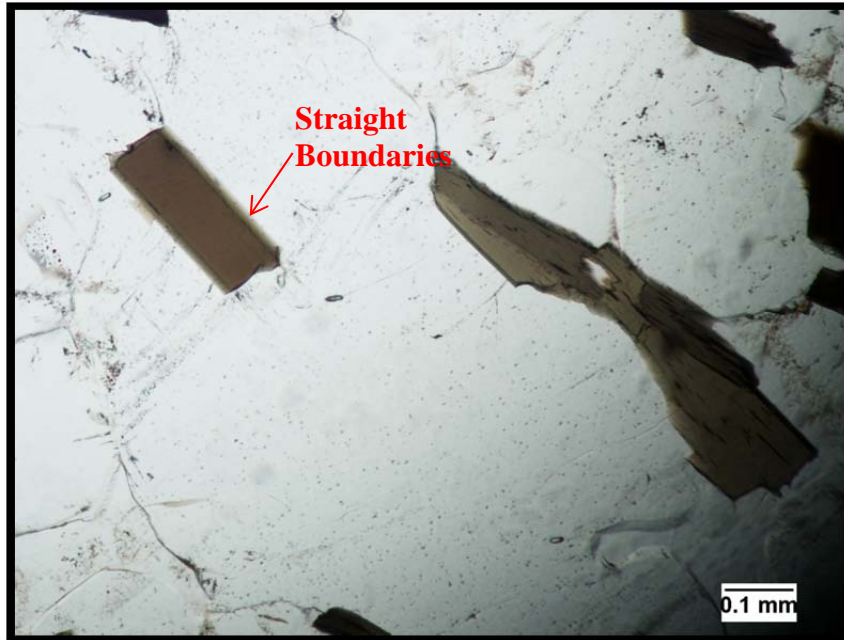


Figure 77. N2A-4-10, Biotite has straight grain boundaries. Most other grain boundaries in the thin section are embayed and interlocking. Photographed under plane polarized light at 100X magnification.



Figure 78. N2A-4-10, Same view as above in Figure 77 but photographed under crossed polars at 100X magnification.



Figure 79. N2A-4-10, Plagioclase with moderate alteration to sericite, clay and carbonate. Photographed under plane polarized light at 100X magnification.

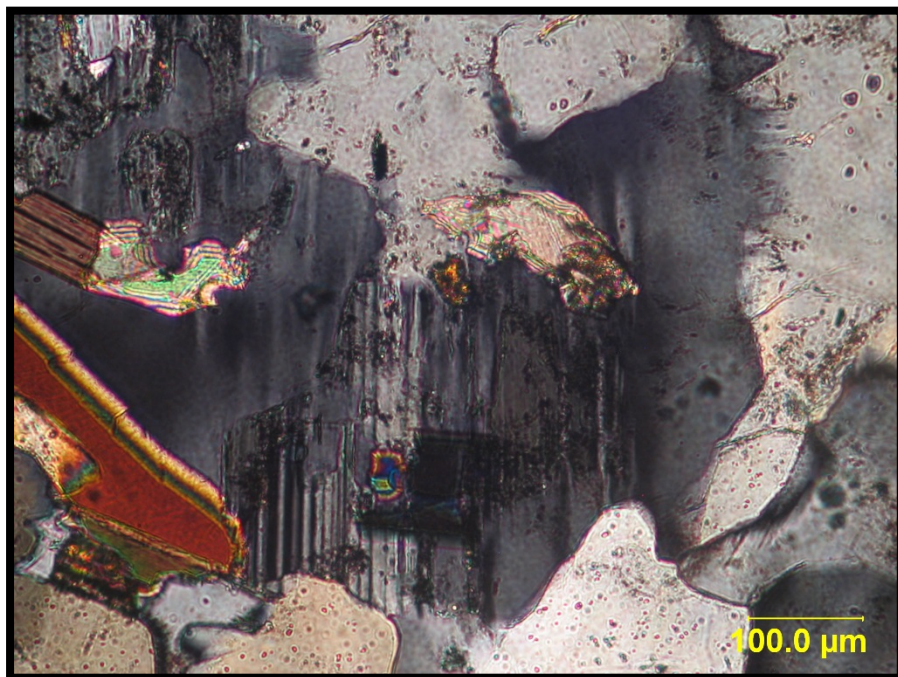


Figure 80. N2A-4-10, Same view as above in Figure 79 but photographed under crossed polars at 100X magnification.

been altered to opaque minerals (Figures 81 & 82). Apatite is present as slender prisms up to 0.2 mm long and as hexagonal plates up to 0.1 mm thick. Zircon occurs as inclusions of zircon in biotite have undergone radioactive decay producing pleochroic halos.

The interlocking grain boundaries and moderately small grain sizes of quartz, biotite, plagioclase, and microcline seen in sample N2A-4-10 have produced an aggregate with Los Angeles abrasion loss of 28.7%. The small quantity of clay and chlorite present and the lack of significant fractures in the bulk sample kept the sulfate soundness loss value low with a loss of 0.023%, far below state acceptable maximum loss limit of 10%. The compact nature of the sample and the lack of open fractures and pore space have produced a bulk specific gravity of 2.651 and an average absorption of 0.6. No alkali-aggregate reactive minerals such as chert or opal are present. This material tested the best because of the lack of weak or soft particles which may break down and weather. The abundant interlocking grains and lack of fractures in sample N2A-4-10 have reduced pore space which otherwise would allow water to penetrate into the sample. The healed fractures in quartz are of limited length within the thin section and did not affect testing results of the material. As in the other thin section samples, the 23-30% biotite and muscovite is high but is locked into the matrix with no need for concern. Microcline has a well-developed cleavage that breaks readily during crushing but the small amounts present (8-10%) and the relatively small grain size, 0.25-2.5 mm along with the interconnectedness with other grains have limited the breakage along cleavage and the microcline did not have any effect on Los Angeles abrasion loss. The metagranite

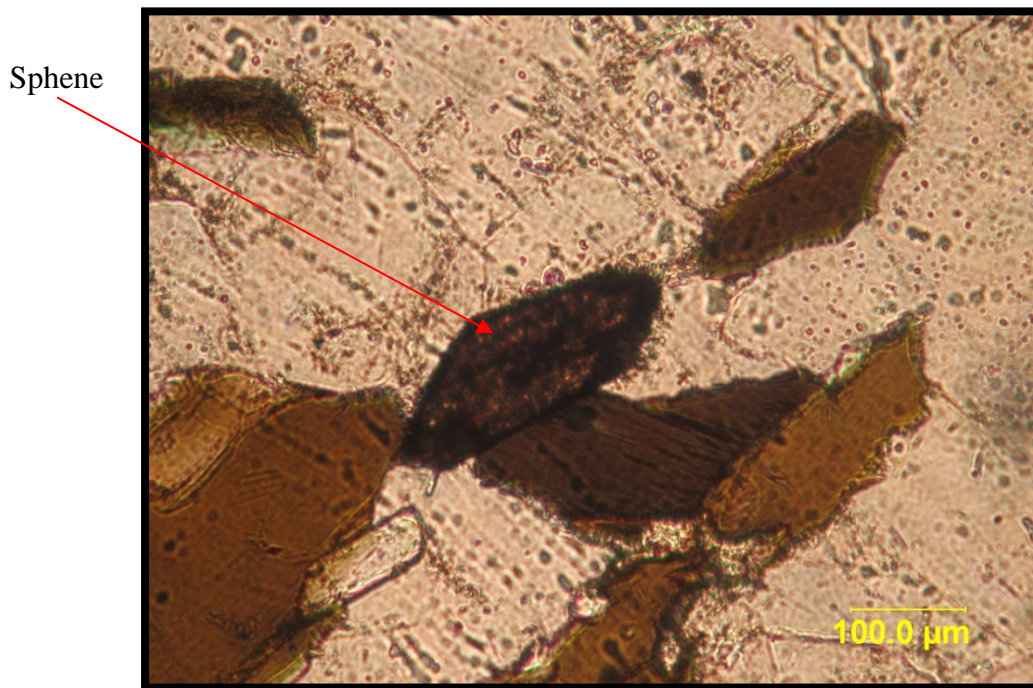


Figure 81. N2A-4-10, Euhedral sphene that has been altered to opaque minerals. Photographed under plane polarized light at 100X magnification.

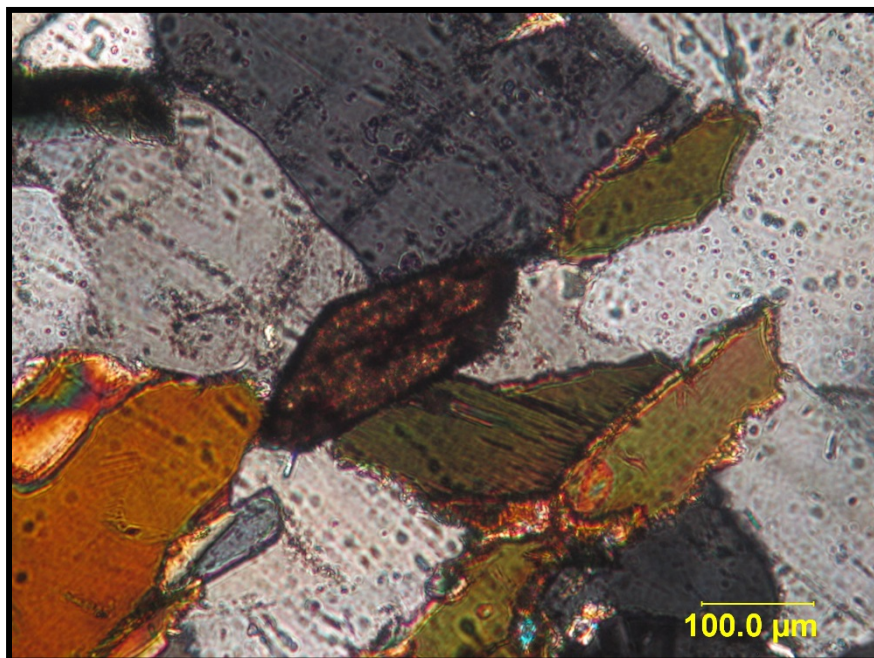


Figure 82. N2A-4-10, Same view as above in Figure 81 but photographed under crossed polars at 100X magnification.

represented by these two thin sections will produce a quality aggregate that have met all physical testing specifications.

N3A-4-10P and N3A-4-10

The sample is a pink, coarse grained microcline-quartz pegmatite composed of microcline (65-70%), quartz (20-25%), plagioclase (5-8%), and trace amounts of biotite, muscovite, clay, sericite, chlorite, opaque minerals, albite, and carbonate.

Microcline is observed to have large subhedral grains up to 12.5 mm in diameter with most grains showing distinctive tartan twinning (Figures 83 & 84). Abundant hairline fractures are healed with carbonate, quartz, and opaque minerals with some fractures confined within individual grains and some healed fractures extending across multiple adjacent grains within the thin section (Figures 85 & 86). Albite exsolution has formed perthitic textures within the microcline grains (Figures 87 & 88). Inclusions of quartz, biotite, and muscovite are also present. The microcline forms embayed and interlocking grain boundaries with neighboring grains (Figures 89 & 90).

The quartz grains within sample N3A-4-10 appear as anhedral grains less than 2.5 mm across with flat to undulose extinction. Hairline fractures have been healed with opaque minerals, quartz, and carbonate. Most fractures are contained within individual quartz grains and a few fractures extending into adjacent quartz and microcline grains (Figures 85 & 86). Fluid inclusions as well as inclusions of muscovite and opaque minerals are common within the quartz grains. The quartz forms generally embayed boundaries with adjacent grains (Figures 89 & 90).

Subhedral grains of plagioclase are observed up to 0.75 mm in diameter with weak to well-developed albite twins. The plagioclase grains are faintly to moderately altered by saussuritization producing sericite and clay (Figures 85 & 86). Plagioclase grains have interlocking boundaries with all adjacent mineral grains. There is some well-

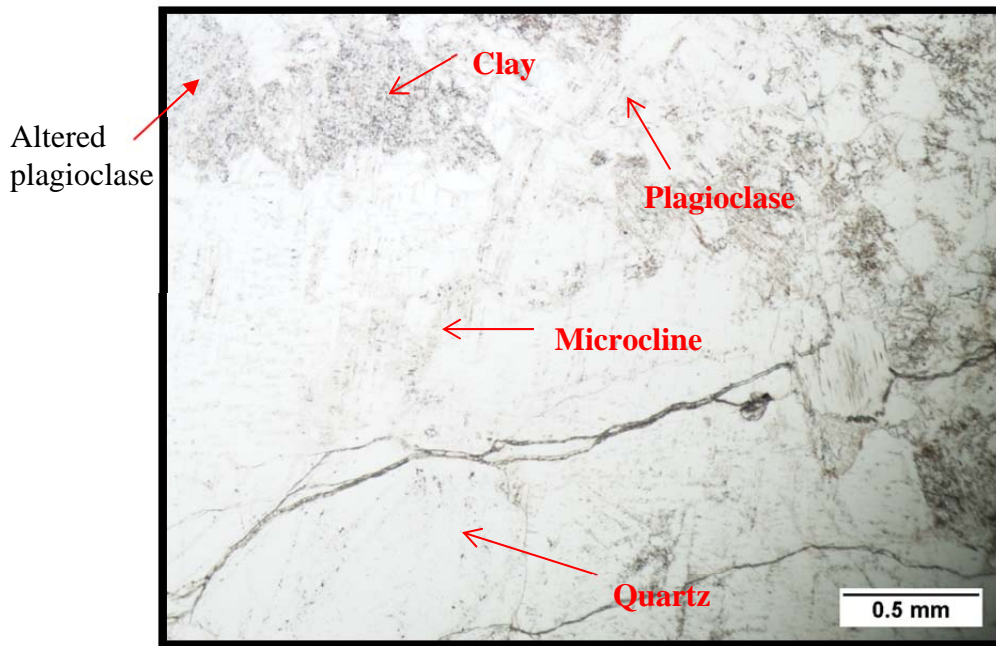


Figure 83. N3A-4-10, Typical view of sample illustrating an abundance of fractures present. Photographed under 40X magnification.

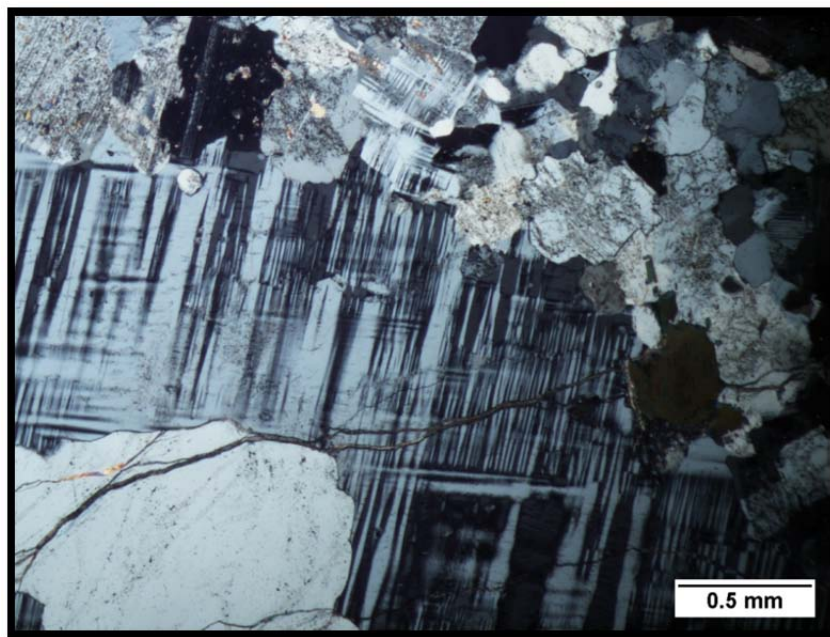


Figure 84. N3A-4-10, Same view as above in Figure 83 showing fractures cutting across multiple grains photographed under crossed polars at 40X magnification.

Fractures
healed with
carbonate,
quartz, and
opaque
minerals

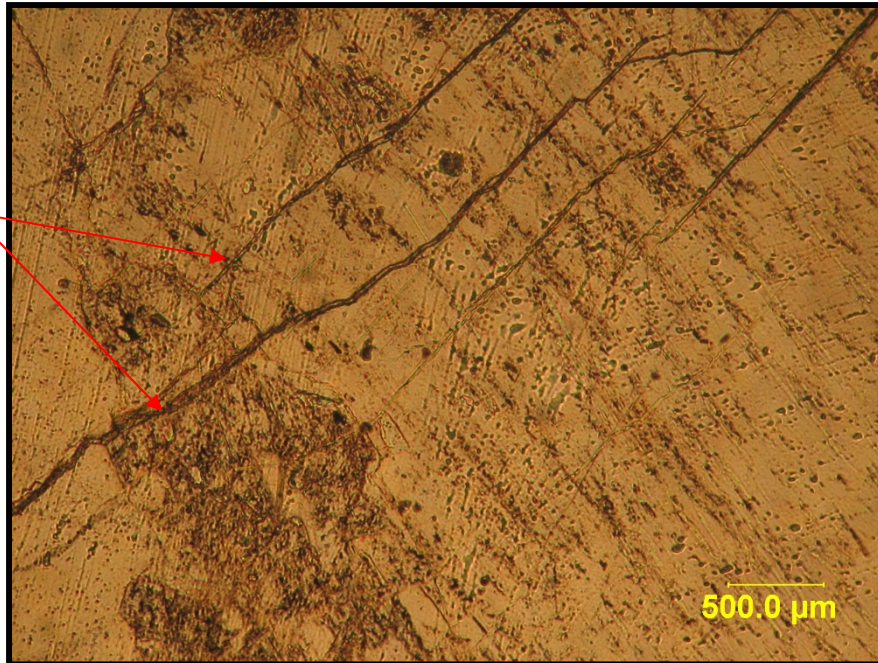


Figure 85. N3A-4-10, Fractures healed with carbonate, quartz, and opaque minerals traversing microcline and plagioclase. Photographed at 40X magnification.

Sericite and
clay in
altered
plagioclase



Microcline

Figure 86. N3A-4-10, Same view as above in Figure 85 but photographed under crossed polars at 40X magnification.

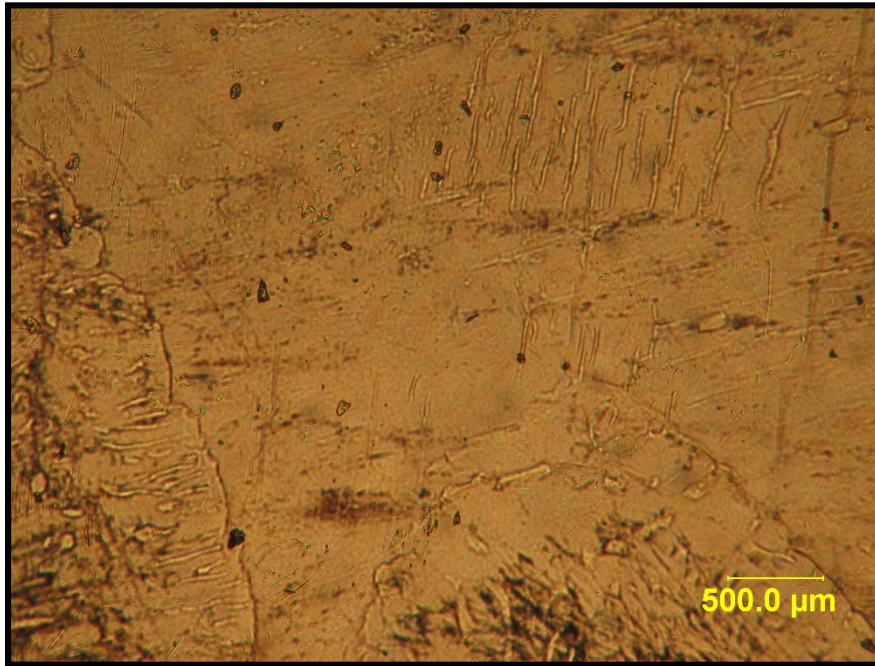


Figure 87. N3A-4-10, Albite exsolution resulting in perthitic texture within microcline. Photographed under plane polarized light at 40X magnification.

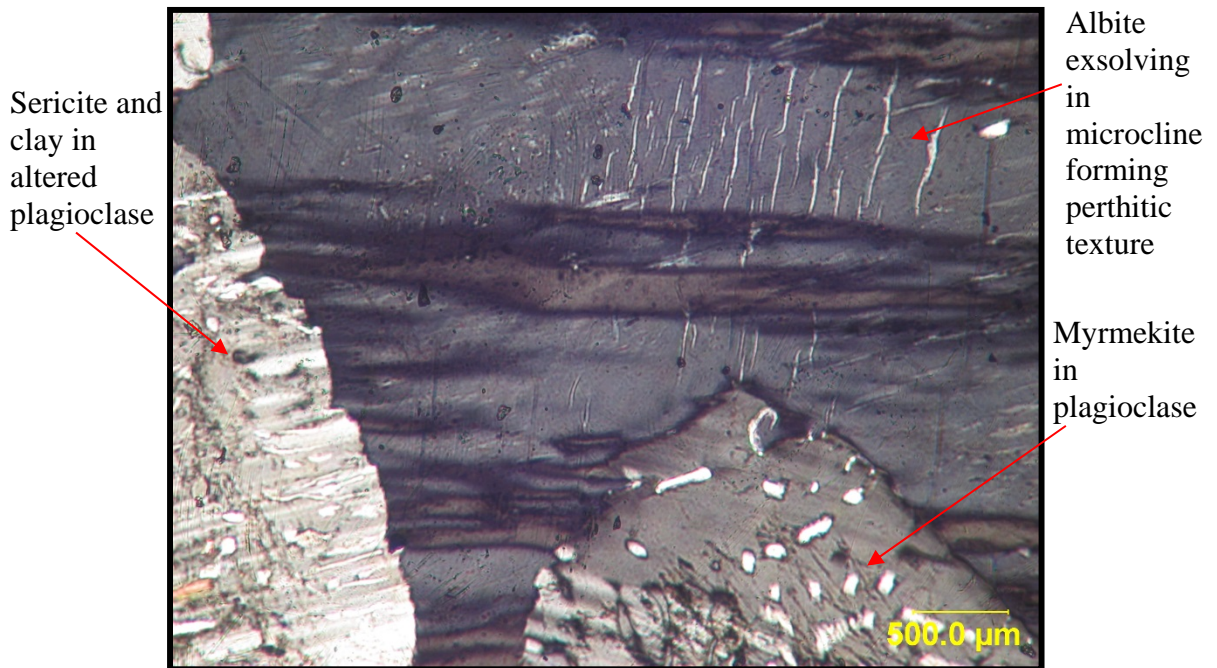


Figure 88. N3A-4-10, Same view as above in Figure 87 but photographed under crossed polars at 40X magnifications. Note the myrmekite in plagioclase.

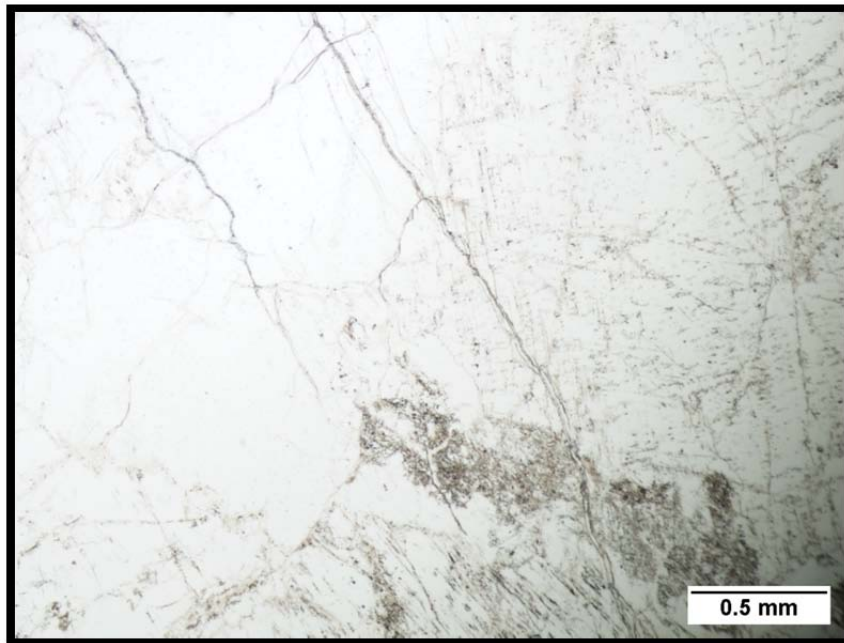


Figure 89. N3A-4-10, Healed fractures extending through quartz and microcline. Photographed under 40X magnification.

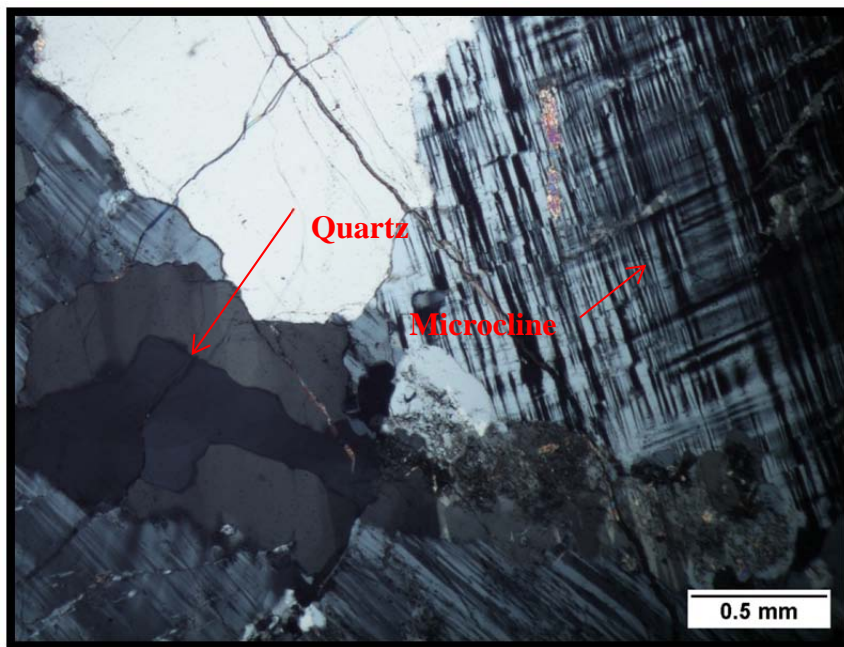


Figure 90. N3A-4-10, Same view as above in Figure 89 but photographed under crossed polars at 40X magnification. Note the interlocking and embayed boundaries between the quartz and microcline grains.

developed myrmekitic texture forming in plagioclase near boundaries with microcline (Figures 87 & 88).

Biotite is observed as subhedral to euhedral grains up to 0.75 mm in length with light brown to dark brown pleochroism and shows bird's eye texture under crossed polars. It has good cleavage and forms straight boundaries with adjacent grains along the long axis and embayed boundaries along the small axis. Biotite is locked into the matrix with no excessive clots or bands. Most biotite has undergone alteration to chlorite which may cause a problem when tested (Figures 91 & 92).

Subhedral to euhedral muscovite grains up to 1.0 mm long are observed within thin section N3A-4-10. Symplectic textures are common in the muscovite (Figures 91 & 92). Individual flakes of muscovite are locked into the matrix.

Very fine grains of clay and sericite are observed and are products of altered plagioclase and microcline. Alteration of biotite has produced chlorite as seen in Figures 93 & 94. Chlorite has completely replaced some grains of biotite. Chlorite is pleochroic from light green to dark green with interference colors ranging from gray to black. Small opaque minerals (<0.2 mm) are observed throughout the matrix, within healed fractures, as inclusions in quartz, and within plagioclase and microcline as an alteration product. Albite occurs as exsolution blebs forming perthitic textures in microcline (Figures 87 & 88). Carbonate is present in healed fractures (Figures 85 & 86).

The elevated Los Angeles abrasion loss of 44.4% was the largest loss of all the samples. The large grain sizes of the microcline and quartz in the sample have been

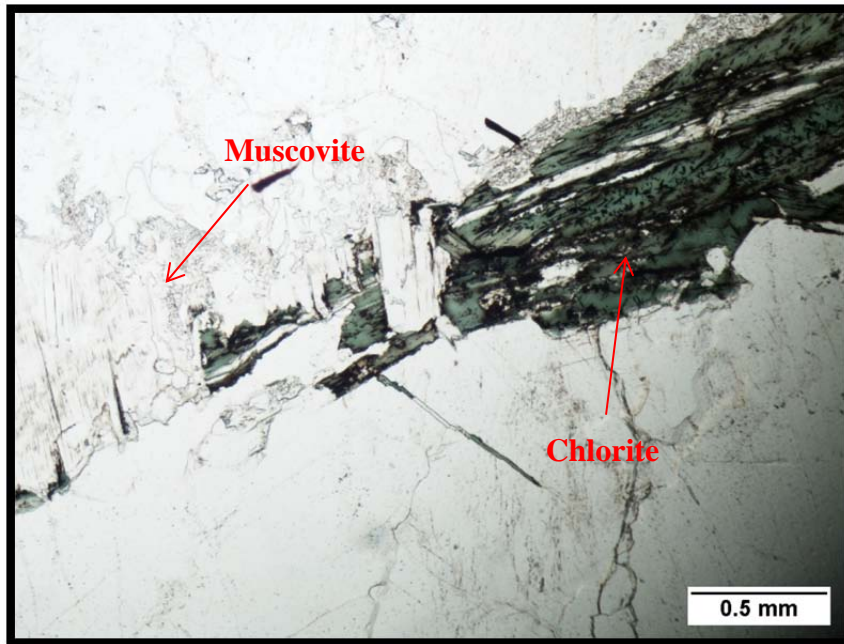


Figure 91. N3A-4-10, Biotite altered to chlorite. Muscovite with symplectic textures. Photographed under 40X magnification.

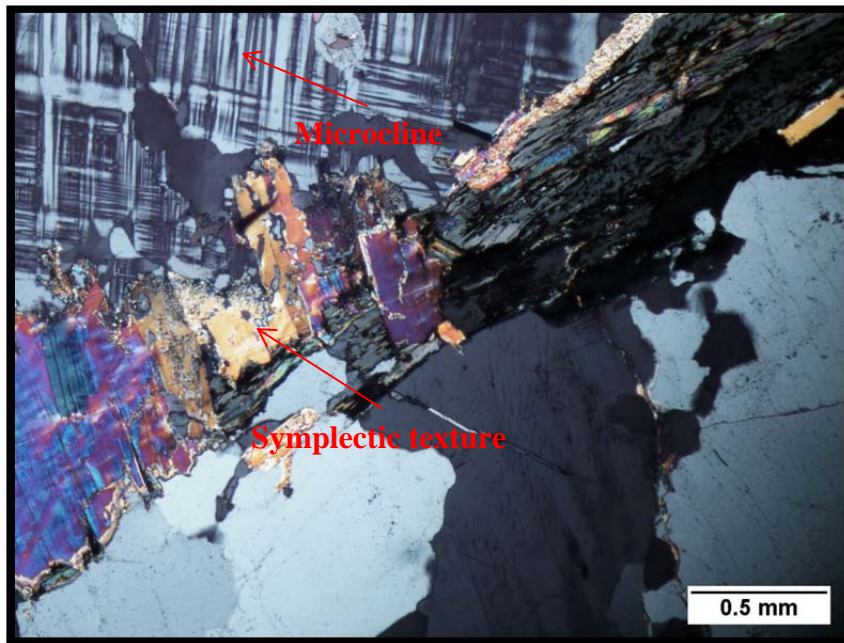


Figure 92. N3A-4-10, Same view as above in Figure 91 but photographed under crossed polars at 40X magnification. Note the symplectic texture within the muscovite.

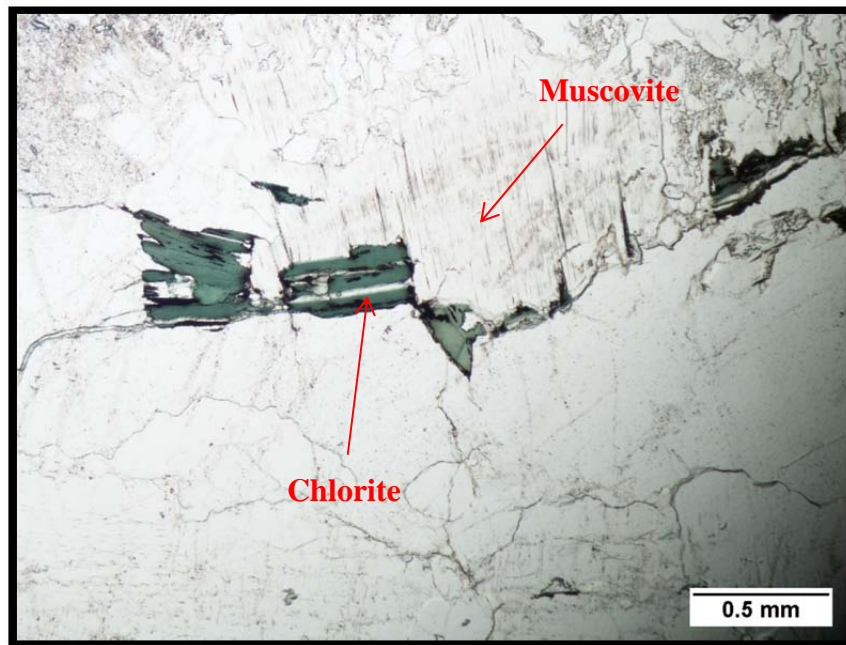


Figure 93. N3A-4-10, Chlorite showing light green to dark green pleochroism. Photographed under 40X magnification.

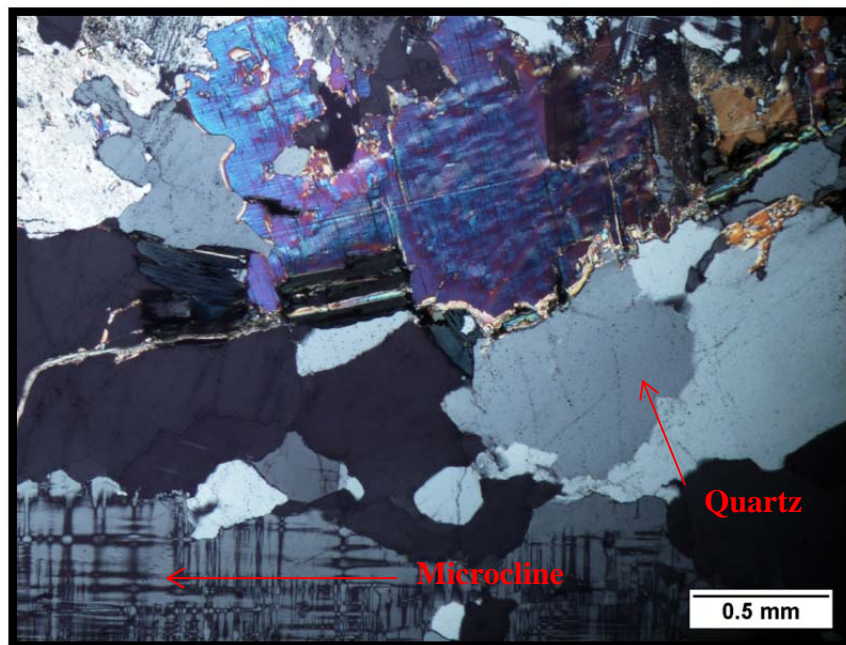


Figure 94. N3A-4-10, Same view as above in Figure 93 but photographed under crossed polars at 40X magnification. Quartz has undulose extinction.

credited for this increase due to the influence of the well-developed cleavages in the microcline and plagioclase. The loss is also attributed to the abundant fractures within sample N3A-4-10. Although the loss does not exceed maximum losses allowed by the Alabama and surrounding state DOT's, it should be closely monitored or blended with more dense material to mitigate the loss and bring it down. Trace amounts of biotite and muscovite are locked into the matrix and have not produced excess free mica within the sample. The sulfate soundness percent loss remains low (0.050%) despite the highly fractured nature of this sample, perhaps owing to their high degree of healing. The bulk specific gravity was 2.593 and was the lowest of all the samples tested within this report. This is probably accredited to the abundant fractures within the pegmatite. Although the fractures have been filled, they may still allow for additional pore space creating a less dense material. Clay, sericite, and opaque minerals are present in such small quantities that they did not affect the absorption. Absorption remained average for this sample with an absorption value of 0.6%. There was grit left on the thin section from slide preparation.

N4A-4-10P and N4A-4-10

Sample N4A-4-10 is a pink, medium-grained augen gneiss composed of quartz (35-40%), microcline (30-35%), plagioclase (25-30%), biotite (3-5%), muscovite (1-2%), and trace amounts of chlorite, opaque minerals, clay, sericite, fluorite, epidote, apatite, and zircon. A poorly-developed foliation is observed within the thin section and defined by the arrangement of biotite and muscovite.

Anhedral grains of quartz are observed up to 2.25 mm in diameter with flat to undulose extinction (Figures 95 & 96). Some hairline fractures healed with opaque minerals are visible with most fractures confined within individual quartz. Fluid inclusions are common along with inclusions of muscovite and opaque minerals. The quartz forms generally embayed boundaries with adjacent grains (Figures 95 & 96).

Subhedral grains of microcline range from 0.75 to 2.5 with some grains up to 4.0 mm across and most grains exhibiting tartan twinning. Some microcline has undergone alteration to sericite, clay, muscovite, albite, and opaque minerals. Some albite exsolution is observed to have formed perthitic textures (Figures 97 & 98). There is a well-developed myrmekitic texture within some plagioclase grains adjacent to microcline grains (Figures 99 & 100). Inclusions of quartz, biotite, and muscovite are also seen within individual microcline grains. Microcline forms embayed and interlocking grain boundaries with surrounding grains of quartz, microcline, and plagioclase, and generally straight boundaries with biotite and muscovite (Figures 101 & 102).

Plagioclase occurs as subhedral grains up to 1.75 mm across with faint to well-developed albite twins. The plagioclase grains are pristine to moderately altered by saussuritization that has produced sericite, clay, and epidote. The plagioclase grains form



Figure 95. N4A-4-10, Embayed and interlocking plagioclase and quartz with undulatory extinction. Photographed under 40X magnification.

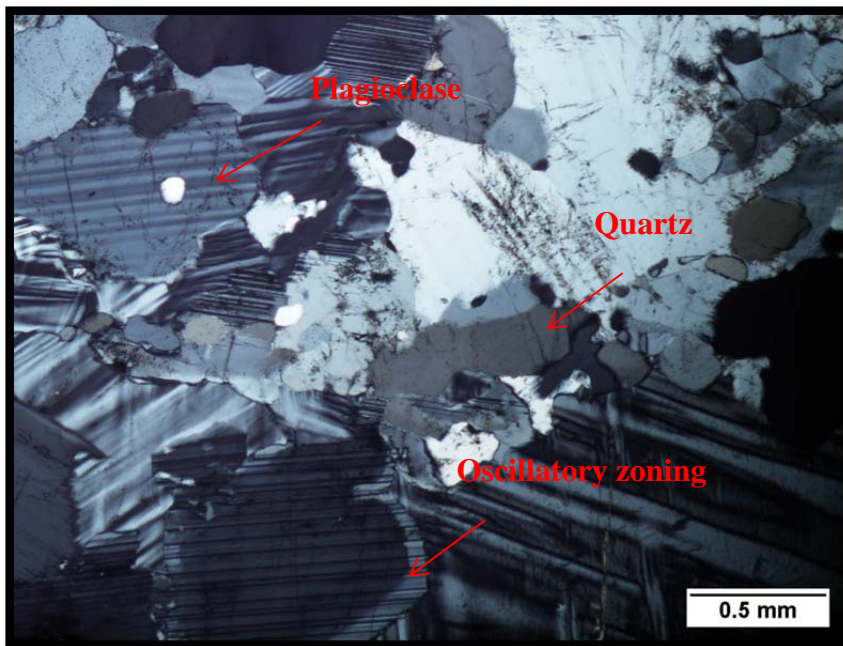


Figure 96. N4A-4-10, Same view as above in Figure 95 but photographed under crossed polars at 40X magnification. Plagioclase shows signs of oscillatory zoning. Note quartz grains with embayed boundaries.

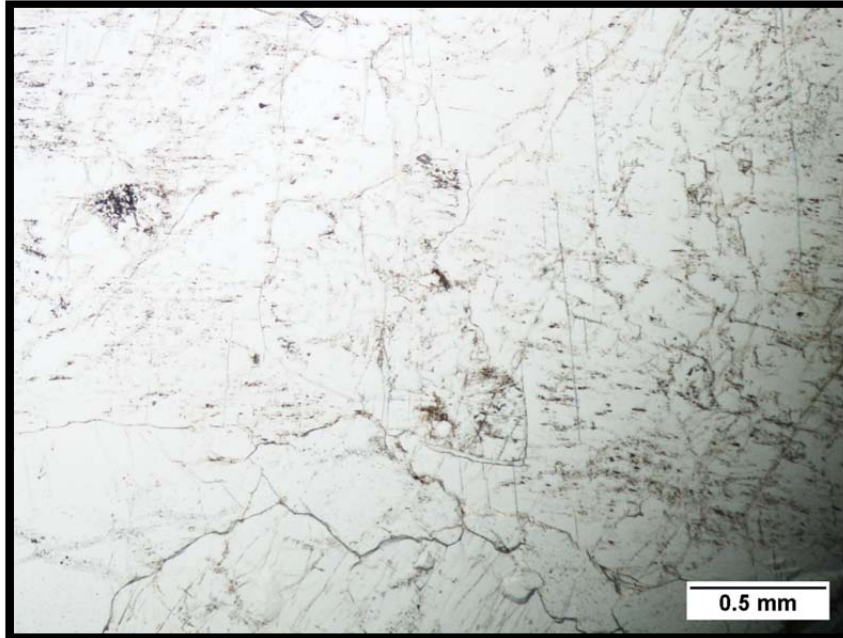


Figure 97. N4A-4-10, Typical view of sample. Microcline has a perthitic texture and myrmekite is present in plagioclase. Photographed under 40X magnification.

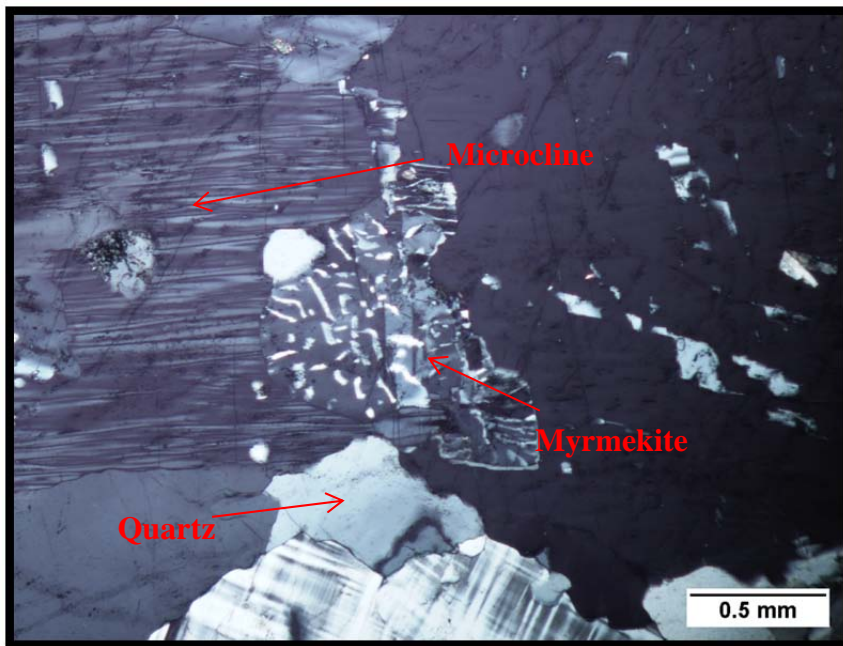


Figure 98. N4A-4-10, Same view as above in Figure 97 but photographed under crossed polars at 40X magnification. Note the perthitic texture within the microcline.

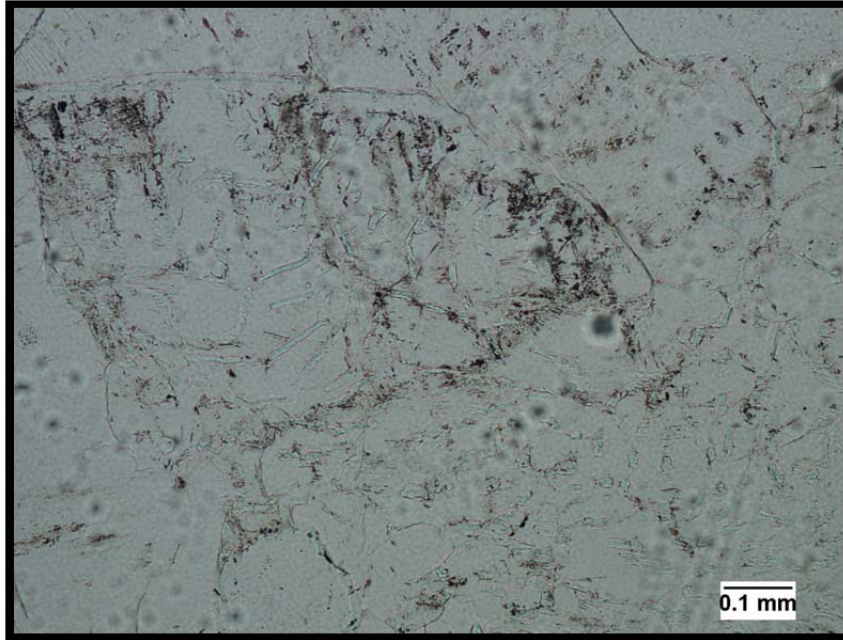


Figure 99. N4A-4-10, Myrmekite in plagioclase adjacent to microcline. Photographed under 100X magnification.

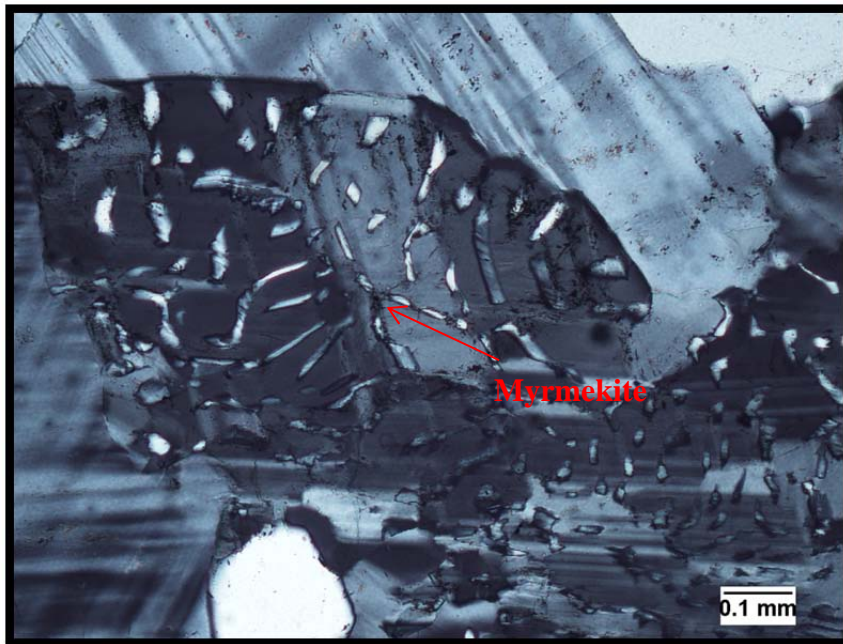


Figure 100. N4A-4-10, Same view as above in Figure 99 but photographed under crossed polars at 100X magnification.

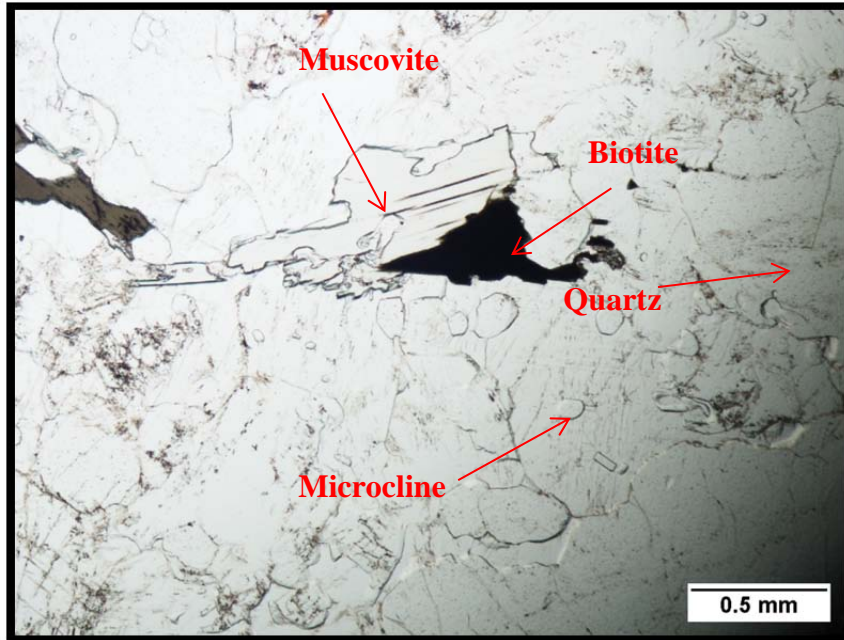


Figure 101. N4A-4-10, Muscovite with symplectic texture and myrmekite in plagioclase. Photographed under 40X magnification.

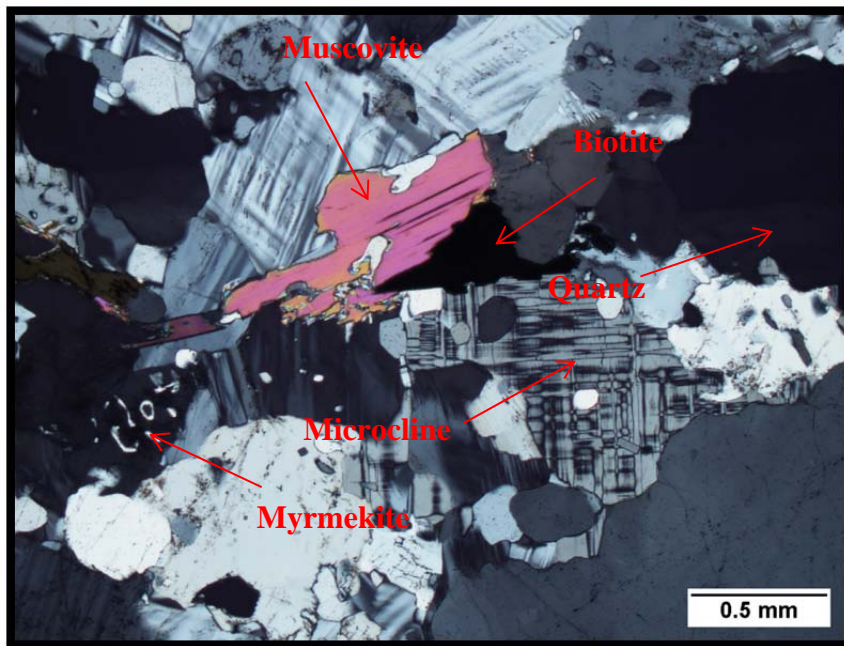


Figure 102. N4A-4-10, Same view as above in Figure 101 but photographed under crossed polars at 40X magnification. Note the embayed boundaries with surrounding grains of quartz and microcline and straight boundaries with muscovite and biotite.

embayed boundaries with all adjacent mineral grains. Myrmekitic textures are common in plagioclase near boundaries with microcline (Figures 97 - 100).

Biotite grains are subhedral to euhedral less than 1.25 mm in diameter, are dark brown to light brown in pleochroism, and exhibit bird's eye extinction under crossed polars. It has good cleavage and forms straight boundaries with adjacent grains along the major axis and rough boundaries along the minor axis. Some biotite has been transformed to chlorite (Figures 103 & 104). Isolated flakes of biotite are locked into the matrix.

Muscovite occurs as subhedral to euhedral grains not exceeding 1.0 mm in length. Symplectic textures are common within the muscovite (Figures 103 & 104). As with the biotite, individual flakes of muscovite are locked into the matrix with no clots or bands.

An alteration product of biotite has created chlorite and has completely replaced some biotite grains (Figures 105 & 106). Chlorite is pleochroic from light green to dark green with interference colors ranging from brown to black in this thin section. Opaque minerals are viewed scattered throughout sample N4A-4-10 and are anhedral to subhedral grains up to 0.5 mm in length. Clay and sericite occur as very fine altered products in plagioclase and microcline. Fluorite is observed as subhedral to euhedral grains up to 2.0 mm in diameter and exhibit octahedral cleavage. A few fractures within the fluorite grains are healed with opaques. Epidote is an alteration product of plagioclase and is viewed as intergrowths within biotite. Euhedral grains of apatite occur as inclusions in quartz, plagioclase, and microcline and apatite grains range from 0.25 mm to 0.5 mm in diameter. Zircon occurs in N4A-4-10 as small grains within biotite and has undergone radioactive decay producing pleochroic halos.

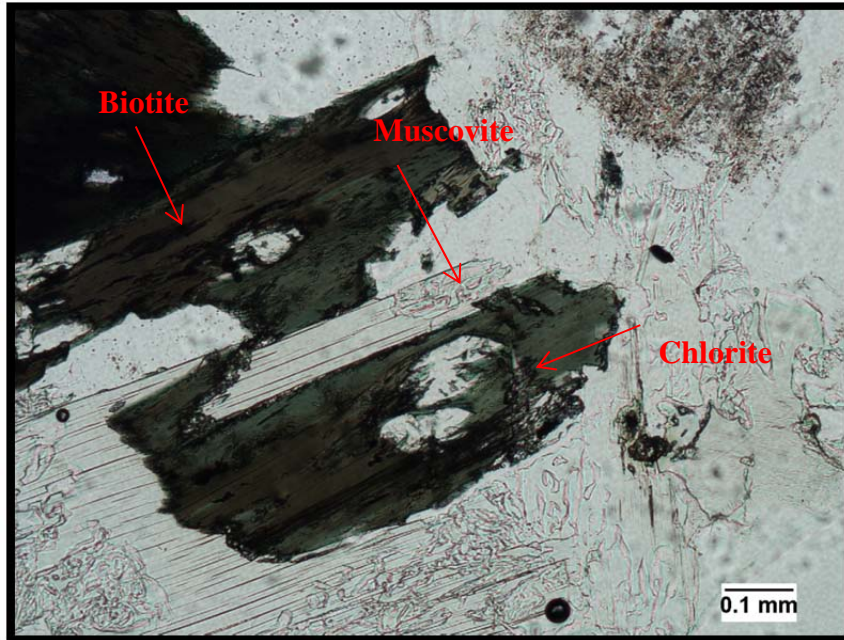


Figure 103. N4A-4-10, Chloritic alteration of biotite with muscovite intergrowths. Photographed under 100X magnification.

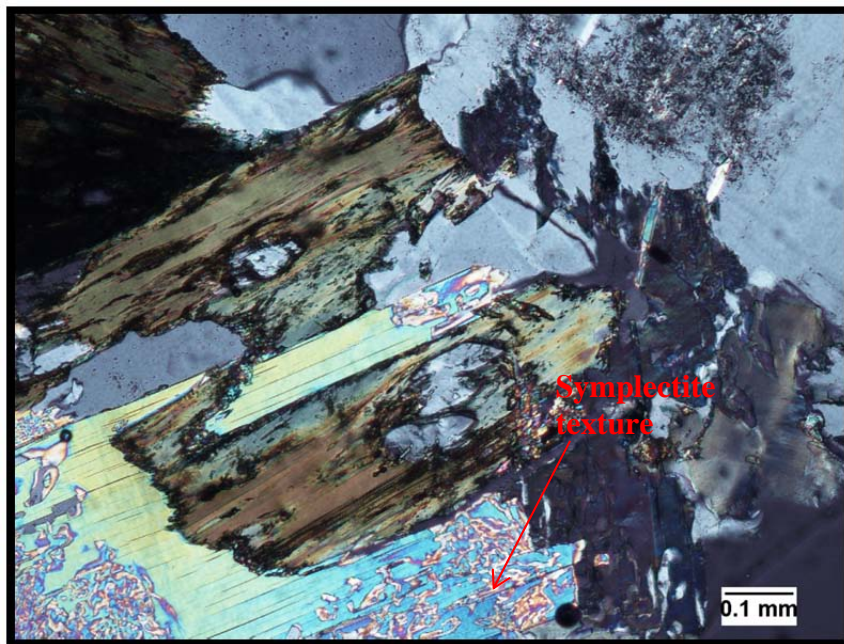


Figure 104. N4A-4-10, Same view as above in Figure 103 but photographed under crossed polars at 100X magnification. Muscovite has symplectite texture.

Interlocking grain boundaries and small grain sizes within the sample have produced testing results with Los Angeles abrasion loss of 37.8% which is consistent with the results obtained by Vulcan Materials. The small nature of the microcline grains (0.75-2.5 mm) will limit the breakage along cleavage and the microcline did not effect Los Angeles abrasion loss. The healed fractures within the thin section are limited in length but the material actually tested for sodium sulfate soundness loss may have been more severely fractured causing the highest loss of all the samples (1.267%). The small quantity of clay and chlorite present in the sample may have also affected sulfate soundness loss. Although this percentage loss is high, from a production viewpoint, it is still well below the maximum allowed by ALDOT (10%). The solid nature of the sample and the lack of open fractures have yielded an average bulk specific gravity and absorption of 2.625 and 0.5% respectively. The metagranite represented by these two thin sections will produce a quality aggregate that will meet all physical testing specifications.

DISCUSSION

Comparison of the physical testing to the findings of the petrographic examination of the samples yields the following observations.

Los Angeles Abrasion Percentage of Loss

The LA abrasion losses ranged from 28.7% to 44.4% with an average loss of 37.7%. The results of the petrographic examination showed that all samples within the study have good interlocking grain boundaries and relatively small grain sizes with the exception of the coarser pegmatite samples. The high LA abrasion losses in samples N3-4-10, N4-4-10, and N3A-4-10 are attributed to them containing pegmatite. The well-developed cleavage of microcline and plagioclase and larger grain size resulted in breakage along cleavage plains creating a higher percentage loss. Quartz by nature is brittle and as grain size increases the quartz has a tendency to fracture in the Los Angeles abrasion machine and when processed at quarries for crushed stone. The metagranite and augen gneiss samples all tested average with LA abrasion percent loss in the mid 30's. The biotite and muscovite present within these thin sections was locked into the matrix allowing little free mica to be produced during testing and had no effect on the percent loss.

All of the samples tested within this report met the maximum allowable Los Angeles abrasion loss allowed by the Alabama Department of Transportation (ALDOT) of 50% for concrete and 48.0% for asphalt. ALDOT reports an average loss of 41.0% for the Notasulga Quarry. As stated above, the tested samples that had above average loss contained pegmatite. If blended with the metagranite, all material will meet specifications.

Sodium Sulfate Soundness Percentage of Loss

Sodium sulfate soundness losses ranged from 0.020% to 1.267% with an average loss of 0.243%. This is well below the maximum of 10% loss allowed by ALDOT specifications. An equigranular rock with interlocking mineral grains and low absorption will not furnish a pathway for solutions to penetrate, freeze and thaw, and fracture the rock. This was the case with the rocks studied within this report. Clay and chlorite in the samples have produced a slightly elevated loss on some samples. Numerous healed fractures observed in the thin sections of samples with elevated sulfate soundness losses may have fractured during crushing allowing sodium sulfate solution to penetrate into the fractures raising the sodium sulfate loss. Sample N4A-4-10 had a high sodium sulfate soundness loss (1.267%) and fractures within the rock were probably responsible for the elevated loss. Although, sample N4-4-10 was fractured and filled with blue epoxy, the soundness loss was minimal and the fractures did not elevate loss. The fractures are possible artifacts from sample collection and preparation rather than natural fractures within the material tested. Microscopic examination of the samples utilized in this study

show they contain few pores or channels other than those cited above to allow penetration by the sodium sulfate into the stone preventing breakage and loss.

Specific Gravity and Absorption

The testing results for bulk specific gravity ranged from 2.593 to 2.651 with an average of 2.616. The absorption of the samples tested ranges from 0.5% to 0.7% with an average of 0.6%. Sample N3-4-10 had a higher absorption than the other samples with an absorption of 0.7%. This is attributed to a combination of an elevated chlorite content, highly altered plagioclase with an increased clay content and porosity, and open fractures which formed along healed fractures during sample preparation. There is a correlation between rock density and porosity. As porosity increases rock density decreases. Low specific gravity and high absorption is important from a volume perspective. Many states restrict the maximum specific gravity to 2.90 or less. Stone is sold on a tonnage rather than a volume basis while most applications for aggregate are calculated on a volume basis. As specific gravity increases volume per ton decreases requiring a larger tonnage of stone to fill a given volume resulting in increased cost to the stone consumer. Specific gravity is controlled by mineralogy and porosity (absorption) of a stone. Stone with a higher absorption will create the need for more binder in hot mix asphalt and more water and cement in concrete increasing the cost. The petrographic examination of a stone permits the petrographer to estimate the specific gravity and absorption (porosity) of a particular stone sample.

CONCLUSIONS

This study has shown a direct relationship between physical testing results and aggregate properties observed petrographically. Properties influencing physical testing include the interlocking nature of grains within the aggregate, grain size, mineral cleavage, healed and open fractures within the aggregate, alteration of mineral grains, and porosity (absorption).

Grain size and grain boundaries have a direct influence on Los Angeles abrasion losses. As grain size increases there is a corresponding increase in Los Angeles abrasion loss. This can be attributed to a number of properties to include mineral cleavage, brittleness, and alteration. Well-developed cleavage in microcline and, to a lesser extent, plagioclase is particularly susceptible to breakage with increased grain size. Quartz has no well-defined cleavage but is brittle and tends to shatter during crushing or when impacted by steel balls and other stone particles in the Los Angeles abrasion machine. Interlocking grain boundaries that form a jig saw puzzle texture tend to lock mineral grains together increasing the stones resistance to breakage. Conversely, straight grain boundaries tend to fracture relatively easily along the grain boundaries increasing the Los Angeles abrasion loss. This is particularly evident in subhedral to euhedral grains within the matrix. Microcline, plagioclase, and micas tend to form straight boundaries and as their grain size increases the grains become more susceptible to breakage along the grain boundaries.

Healed and open fractures are planes of weakness and have a direct influence on both Los Angeles abrasion and sodium sulfate soundness losses. Impact by steel balls and other stone particles in the Los Angeles machine causes the stone to fracture along the healed and open fractures increasing the Los Angeles abrasion loss. The fractures also provide pathways for sodium sulfate solution to penetrate the stone particles. During the drying cycles the sodium sulfate is precipitated into the fractures and expands resulting in breakage and an increase in the sodium sulfate loss.

Mineral alteration has a significant effect on physical testing results. In igneous and metamorphic rocks plagioclase and biotite are often altered. The most common plagioclase alteration products are sericite (white mica), clay, epidote, and calcite along with the formation of small vacuoles (pores) within the plagioclase grains. The vacuoles allow penetration of sodium sulfate solution increasing sodium sulfate soundness losses and weaken the plagioclase grains increasing Los Angeles abrasion losses. Biotite commonly undergoes alteration to chlorite. Chlorite and clay have weak crystal plane that allow penetration by sodium sulfate solution between the plates which increases the sulfate soundness loss. In stone with small grains and interlocking grain boundaries penetration by sodium sulfate solution is minimal and sulfate soundness losses remain low.

Specific gravity and absorption are dependent upon mineral composition and porosity. As the percentage of minerals with higher specific gravity such as pyroxenes, amphiboles, sulfides, and iron oxide increases the specific gravity will also increase. Pore space and open fractures decrease specific gravity. By determining the identity and percentage of minerals present along with any pores, open fractures, or related features an

estimate of specific gravity and absorption can be made during the petrographic examination.

The physical testing results highlight the heterogeneity of most stone deposits which can vary considerably both laterally and vertically. Many specifying agencies approve quarries by benches and zones within the quarry addressing the vertical and lateral variation in stone quality. Therefore, to evaluate a particular potential quarry site petrographically, it is necessary to evaluate a large sample population that represents both vertical and lateral variations in the deposit. This may be a matter of sampling exposed outcrops along strike and across strike to account for possible lateral and vertical variations in stone properties. However, on sites with little outcrop exposures it may be necessary to consider alternate sampling techniques. One such technique is using an air track drill which is considerably cheaper than a core drill and allows the depth of the overburden and weathered stone to be determined while sampling. A grid is overlaid on a map of the potential site and a sampling interval is determined. Holes are drilled to a pre-determined depth with drill chip samples collected at predetermined intervals, normally ten feet. The drill chips are too small for physical testing but can be evaluated petrographically by preparing grain mount thin sections.

This study has demonstrated that a correlation exists between physical testing results and petrographic examination. The use of petrographic examinations early in the exploration process will allow mining companies to evaluate potential quarry sites without incurring the costs of core drilling and testing. Sites that are identified through petrographic examination as not containing quality stone can be eliminated without the high cost of core drilling and physical testing.

REFERENCES

- ASTM. (2008). ASTM Standards and Test Methods on CD. West Conshohocken, PA, USA.
- Barksdale, R. D. (2001). *The Aggregate Handbook*. Washington, D.C.: National Stone, Sand, and Gravel Association.
- Bell, F. G. (1978). The Physical and Mechanical Properties of the Fell Sandstone, Northumberland, England. *Engineering Geology*. p.1-29.
- Bentley, R. D., & Neathery, T. L. (1970). Geology of the Brevard Fault Zone and Rocks of the Inner Piedmont of Alabama. Alabama Geological Society 8th Annual Field Trip Guidebook. p.119
- Blatt, H., & Tracy, R. J. (1996). *Petrology, Igneous, Sedimentary, and Metamorphic; 2nd Edition*. New York: W.H. Freeman and Company.
- Bogdan, K. R. (2009). *Geology of the Farmville Metagranite and Associated Units as Exposed at the Notasulga Quarry*. Auburn, AL: Auburn University.
- Colberg, M. R. (1989). *The origin of the Auburn Formation migmatites, Lee County, Alabama*. Auburn, Alabama: Auburn University, p.169
- Cook, R. B., Fousek, R. S., Bogdan, K. R., & Steltenpohl, M. G. (2007). Geology of the Farmville Metagranite, Opelika Complex, Inner Piedmont at the Vulcan Materials Company Notasulga Quarry, Lee County, Alabama.. Alabama Geological Society, p. 93-101
- Dolar-Mantuanui, L. D. (1983). *Handbook of Concrete Aggregates: A Petrographic and Technological Evaluation*. Archridge, New Jersey: Noyes Publications.
- ESRI. (2012). ArcGIS. DEM
- Fahy, M. P., & Guccione, M. J. (1979). Estimating Strength of Sandstone using Petrographic Thin Section Data. *Engineering Geology*. p.467-485.
- Goldberg, S. A., & Burnell, J. R. (1987). Rubidium-strontium geochronology of the Farmville granite, Alabama Inner Piedmont. In M. S. Drummond, & N. L. Green, *Granites of Alabama*. Geological Survey of Alabama. p.251-258.

- Goldberg, S. A., & Steltenpohl, M. G. (1990). Timing and characteristics of Paleozoic deformation in the Alabama Inner Piedmont. *American Journal of Science*. p.1169-1200.
- Grimes, J.E., and Steltenpohl, M.G., 1993, Geology of the crystalline rocks along the fall line, on the Carrville, Notasulga, and Loachapoka quadrangles, Alabama, in Steltenpohl, M.G., and Salpas, P.A., eds., Geology of the southernmost exposed Appalachian Piedmont rocks along the fall line: Geological Society of America, Southeastern Section 42nd Annual Meeting Field Trip Guidebook, p. 67-94.
- Handlin, J., & Hager, R. V. (1957). Experimental Deformation of Sedimentary Rock Under a Confining Pressure. *Am. Assoc. Petroleum Geology*. p.1-50.
- Hatcher, R.D., Jr., Osberg, P.H., Drake, A.A., Jr., Robinson, P., and Thomas, W.A., 1989, Tectonic map of the U.S. Appalachians, in Hatcher, R.D., Jr., et al., eds., The Appalachian-Ouachita orogen in the United States: Boulder, Colorado, Geological Society of America, Geology of North America, v. F-2, Plate 1.
- Langer, W. H., & Knepper, D. H. (1995). *Geologic Characterization of Natural Aggregate: A Field Geologist's Guide to Natural Aggregate Resource Assessment*. Denver, CO: U.S. Geological Survey.
- MacKenzie, W. S., Donaldson, C. H., & Guilford, C. (1987). *Atlas of Igneous Rocks and Their Textures; Longman Scientific & Technical*. New York: John Wiley & Sons, Inc.
- Mielenz, R. C. (1946). *Petrographic Examination of Concrete Aggregates*.
- Mielenz, R. C., & Witte, L. P. (1948). Tests Used by the Bureau of Reclamation for Identifying Reactive Concrete Aggregates.
- Mielenz, R. (1955). Petrographic Examination. In A. S. 169, *Significance of Tests and Properties of Concrete and Concrete Aggregates*. Philadelphia, PA: American Society for Testing Materials. p. 253-273.
- Onodera, T. F., & Asoka, K. M. (1980). Relationship Between Texture and Mechanical Properties of Crystalline Rocks. *Bill. Int. Assoc. Engineering Geology*. p.173-177.
- Osborne, W. E., Szabo, M. W., Neathery, T. L., & Copeland, C. W. (1988). *Geologic Map of Alabama, Northeast Sheet*. Tuscaloosa, Alabama: Alabama Geological Survey.
- Patterson, S. R., & Tobisch, O. T. (1988). Using pluton ages to date regional deformations: problems with commonly used criteria. *Geology*. p.1108-1111.

- Steltenpohl, M. G., & Moore, W. B. (1988). Metamorphism in the Alabama Piedmont. *Alabama Geological Survey Circular 138*. p.29.
- Steltenpohl, M. G., Neilson, M. J., Bittner, E. I., Colberg, M. R., & Cook, R. B. (1990). Geology of the Alabama Piedmont terrane. *Geological Survey of Alabama Bulletin*. p.1-80.
- Steltenpohl, M. G., Heatherington, A., Mueller, P., & Miller, B. V. (2005). New Isotopic dates on crystalline rocks from Alabama and Georgia. In M. G. Steltenpohl, *Southernmost Appalachian terranes, Alabama and Georgia*. Geological Society of America Field Trip Guidebook. p.51-69.
- Steltenpohl, M.G., ed., 2005, New perspectives on southernmost Appalachian terranes, Alabama and Georgia: Alabama Geological Society 42nd Annual Field Trip Guidebook. p.212.
- Sterling, W., & Steltenpohl, M. G. (2004). Geologic map of the Notasulga quadrangle, Lee and Macon counties, Alabama. *Geological Survey of America, Open File Map*.
- Tugrul, A., & Zarif, I. H. (1999). Correlation of Mineral and Textural Characteristics with Engineering Properties of Selected Granitic Rocks from Turkey. *Engineering Geology*. p.303-317.
- Ulusay, R., Tureli, K., & Ider, M. H. (1994). Prediction of Engineering Properties of a Selected Litharenite Sandstone from its Petrographic Characteristics Using Correlation and Multivariable Statistical Techniques. *Engineering Geology*. p.135-157.
- White, W. W. (2007). Geology of the 1:24,000 Tallassee, Alabama, Quadrangle and its implications for southern Appalachian tectonics. Auburn, Alabama: Auburn University, p.89

APPENDIX A

Sieve Analysis for Coarse and Fine Aggregate

National Center for Asphalt Technology
Sieve Analysis for Fine and Coarse Aggregate (Washed or Dry)
(ASTM C136)

Project: Thesis Date: 2/10/2011

Tested By: Nick Nuno Calculated By: _____

Sample Identification: N1-4-10

Sieve Size		Sample #			Sample #			Average % Passing
std.	metric	Cumulative Wt. Retained	% Retained	% Passing	Cumulative Wt. Retained	% Retained	% Passing	
2"	50.0							
1 1/2"	37.5							
1"	25.0	8.0	7.6	92.4				
3/4"	19.0	33.8	31.8	68.2				
1/2"	12.5	73.7	69.4	30.6				
3/8"	9.5	82.6	77.8	22.2				
#4	4.75	92.0	86.6	13.4				
#8	2.36	106.2	100.0	0.0				
#16	1.18							
#30	0.600							
#50	0.300							
#100	0.150							
#200	0.075							
-200	-0.075			----			----	----

<p>Check if Wetting Agent Used. _____</p> <p>(A) Total Wt. of original sample, gm <u>106.2</u></p> <p>(B) Wt. after wash, gm _____</p> <p>(C) Loss due to wash, gm (A - B) _____</p> <p>(D) -200 in pan, gm _____</p> <p>Total -200 material, gm (C + D) _____</p>	<p>Check if Wetting Agent Used. _____</p> <p>(A) Total Wt. of original sample, gm _____</p> <p>(B) Wt. after wash, gm _____</p> <p>(C) Loss due to wash, gm (A - B) _____</p> <p>(D) -200 in pan, gm _____</p> <p>Total -200 material, gm (C + D) _____</p>
--	---

National Center for Asphalt Technology
Sieve Analysis for Fine and Coarse Aggregate (Washed or Dry)
(ASTM C136)

Project: Thesis Date: 2/10/2011

Tested By: Nick Nuno Calculated By: _____

Sample Identification: N2-4-10

Sieve Size		Sample #			Sample #			Average % Passing
std.	metric	Cumulative Wt. Retained	% Retained	% Passing	Cumulative Wt. Retained	% Retained	% Passing	
2"	50.0							
1 1/2"	37.5							
1"	25.0	8.2	7.2	92.8				
3/4"	19.0	34.9	30.6	69.4				
1/2"	12.5	79.9	70.2	29.8				
3/8"	9.5	89.7	78.7	21.3				
#4	4.75	99.5	87.3	12.7				
#8	2.36	113.9	100.0	0.0				
#16	1.18							
#30	0.600							
#50	0.300							
#100	0.150							
#200	0.075							
-200	-0.075			----			----	----
Check if Wetting Agent Used. _____ (A) Total Wt. of original sample, gm <u>113.9</u> (B) Wt. after wash, gm _____ (C) Loss due to wash, gm (A - B) _____ (D) -200 in pan, gm _____ Total -200 material, gm (C + D) _____					Check if Wetting Agent Used. _____ (A) Total Wt. of original sample, gm _____ (B) Wt. after wash, gm _____ (C) Loss due to wash, gm (A - B) _____ (D) -200 in pan, gm _____ Total -200 material, gm (C + D) _____			

National Center for Asphalt Technology
Sieve Analysis for Fine and Coarse Aggregate (Washed or Dry)
(ASTM C136)

Project: Thesis Date: 2/10/2011

Tested By: Nick Nuno Calculated By: _____

Sample Identification: N3-4-10

		Sample #			Sample #			
Sieve Size	std. metric	Cumulative Wt. Retained	% Retained	% Passing	Cumulative Wt. Retained	% Retained	% Passing	Average % Passing
2"	50.0							
1 1/2"	37.5							
1"	25.0	5.0	4.2	95.8				
3/4"	19.0	26.1	22.0	78.0				
1/2"	12.5	72.2	60.8	39.2				
3/8"	9.5	83.1	70.0	30.0				
#4	4.75	96.8	81.5	18.5				
#8	2.36	118.7	100.0	0.0				
#16	1.18							
#30	0.600							
#50	0.300							
#100	0.150							
#200	0.075							
-200	-0.075			----			----	----
Check if Wetting Agent Used. _____ (A) Total Wt. of original sample, gm <u>118.7</u> (B) Wt. after wash, gm _____ (C) Loss due to wash, gm (A - B) _____ (D) -200 in pan, gm _____ Total -200 material, gm (C + D) _____					Check if Wetting Agent Used. _____ (A) Total Wt. of original sample, gm _____ (B) Wt. after wash, gm _____ (C) Loss due to wash, gm (A - B) _____ (D) -200 in pan, gm _____ Total -200 material, gm (C + D) _____			

National Center for Asphalt Technology
Sieve Analysis for Fine and Coarse Aggregate (Washed or Dry)
(ASTM C136)

Project: Thesis Date: 2/10/2011

Tested By: Nick Nuno Calculated By: _____

Sample Identification: N4-4-10

		Sample #			Sample #			
Sieve Size	std. metric	Cumulative Wt. Retained	% Retained	% Passing	Cumulative Wt. Retained	% Retained	% Passing	Average % Passing
2"	50.0							
1 1/2"	37.5							
1"	25.0	4.4	5.0	95.0				
3/4"	19.0	23.7	27.0	73.0				
1/2"	12.5	59.4	67.5	32.5				
3/8"	9.5	68.3	77.7	22.3				
#4	4.75	79.7	90.5	9.5				
#8	2.36	88.0	100.0	0.0				
#16	1.18							
#30	0.600							
#50	0.300							
#100	0.150							
#200	0.075							
-200	-0.075			----			----	----
Check if Wetting Agent Used. _____ (A) Total Wt. of original sample, gm <u>88.0</u> (B) Wt. after wash, gm _____ (C) Loss due to wash, gm (A - B) _____ (D) -200 in pan, gm _____ Total -200 material, gm (C + D) _____					Check if Wetting Agent Used. _____ (A) Total Wt. of original sample, gm _____ (B) Wt. after wash, gm _____ (C) Loss due to wash, gm (A - B) _____ (D) -200 in pan, gm _____ Total -200 material, gm (C + D) _____			

National Center for Asphalt Technology
Sieve Analysis for Fine and Coarse Aggregate (Washed or Dry)
(ASTM C136)

Project: Thesis Date: 2/10/2011

Tested By: Nick Nuno Calculated By: _____

Sample Identification: N1A-4-10

Sieve Size		Sample #			Sample #			Average % Passing
std.	metric	Cumulative Wt. Retained	% Retained	% Passing	Cumulative Wt. Retained	% Retained	% Passing	
2"	50.0							
1 1/2"	37.5							
1"	25.0	1.9	1.5	98.5				
3/4"	19.0	16.6	13.6	86.4				
1/2"	12.5	74.4	61.2	38.8				
3/8"	9.5	89.1	73.3	26.7				
#4	4.75	103.1	84.8	15.2				
#8	2.36	121.5	100.0	0.0				
#16	1.18							
#30	0.600							
#50	0.300							
#100	0.150							
#200	0.075							
-200	-0.075			----			----	----
Check if Wetting Agent Used. _____ (A) Total Wt. of original sample, gm <u>121.5</u> (B) Wt. after wash, gm _____ (C) Loss due to wash, gm (A - B) _____ (D) -200 in pan, gm _____ Total -200 material, gm (C + D) _____					Check if Wetting Agent Used. _____ (A) Total Wt. of original sample, gm _____ (B) Wt. after wash, gm _____ (C) Loss due to wash, gm (A - B) _____ (D) -200 in pan, gm _____ Total -200 material, gm (C + D) _____			

National Center for Asphalt Technology
Sieve Analysis for Fine and Coarse Aggregate (Washed or Dry)
(ASTM C136)

Project: Thesis Date: 2/10/2011

Tested By: Nick Nuno Calculated By: _____

Sample Identification: N2A-4-10

Sieve Size		Sample #			Sample #			Average % Passing
std.	metric	Cumulative Wt. Retained	% Retained	% Passing	Cumulative Wt. Retained	% Retained	% Passing	
2"	50.0							
1 1/2"	37.5							
1"	25.0	7.0	5.0	95.0				
3/4"	19.0	32.6	23.2	76.8				
1/2"	12.5	94.2	67.1	32.9				
3/8"	9.5	107.8	76.8	23.2				
#4	4.75	121.4	86.5	13.5				
#8	2.36	140.4	100.0	0.0				
#16	1.18							
#30	0.600							
#50	0.300							
#100	0.150							
#200	0.075							
-200	-0.075			----			----	----
Check if Wetting Agent Used. _____ (A) Total Wt. of original sample, gm <u>140.4</u> (B) Wt. after wash, gm _____ (C) Loss due to wash, gm (A - B) _____ (D) -200 in pan, gm _____ Total -200 material, gm (C + D) _____					Check if Wetting Agent Used. _____ (A) Total Wt. of original sample, gm _____ (B) Wt. after wash, gm _____ (C) Loss due to wash, gm (A - B) _____ (D) -200 in pan, gm _____ Total -200 material, gm (C + D) _____			

National Center for Asphalt Technology
Sieve Analysis for Fine and Coarse Aggregate (Washed or Dry)
(ASTM C136)

Project: Thesis Date: 2/10/2011

Tested By: Nick Nuno Calculated By: _____

Sample Identification: N3A-4-10

Sieve Size		Sample #			Sample #			Average % Passing
std.	metric	Cumulative Wt. Retained	% Retained	% Passing	Cumulative Wt. Retained	% Retained	% Passing	
2"	50.0							
1 1/2"	37.5							
1"	25.0	2.2	2.0	98.0				
3/4"	19.0	15.7	14.0	86.0				
1/2"	12.5	62.6	55.8	44.2				
3/8"	9.5	78.1	69.6	30.4				
#4	4.75	92.4	82.4	17.6				
#8	2.36	112.2	100.0	0.0				
#16	1.18							
#30	0.600							
#50	0.300							
#100	0.150							
#200	0.075							
-200	-0.075			----			----	----
Check if Wetting Agent Used. _____ (A) Total Wt. of original sample, gm <u>112.2</u> (B) Wt. after wash, gm _____ (C) Loss due to wash, gm (A - B) _____ (D) -200 in pan, gm _____ Total -200 material, gm (C + D) _____					Check if Wetting Agent Used. _____ (A) Total Wt. of original sample, gm _____ (B) Wt. after wash, gm _____ (C) Loss due to wash, gm (A - B) _____ (D) -200 in pan, gm _____ Total -200 material, gm (C + D) _____			

National Center for Asphalt Technology
Sieve Analysis for Fine and Coarse Aggregate (Washed or Dry)
(ASTM C136)

Project: Thesis Date: 2/10/2011

Tested By: Nick Nuno Calculated By: _____

Sample Identification: N4A-4-10

Sieve Size		Sample #			Sample #			Average % Passing
std.	metric	Cumulative Wt. Retained	% Retained	% Passing	Cumulative Wt. Retained	% Retained	% Passing	
2"	50.0							
1 1/2"	37.5							
1"	25.0	2.4	2.6	97.4				
3/4"	19.0	15.2	16.6	83.4				
1/2"	12.5	54.9	59.9	40.1				
3/8"	9.5	66.5	72.6	27.4				
#4	4.75	76.7	83.7	16.3				
#8	2.36	91.6	100.0	0.0				
#16	1.18							
#30	0.600							
#50	0.300							
#100	0.150							
#200	0.075							
-200	-0.075			----			----	----

<p>Check if Wetting Agent Used. _____</p> <p>(A) Total Wt. of original sample, gm <u>91.6</u></p> <p>(B) Wt. after wash, gm _____</p> <p>(C) Loss due to wash, gm (A - B) _____</p> <p>(D) -200 in pan, gm _____</p> <p>Total -200 material, gm (C + D) _____</p>	<p>Check if Wetting Agent Used. _____</p> <p>(A) Total Wt. of original sample, gm _____</p> <p>(B) Wt. after wash, gm _____</p> <p>(C) Loss due to wash, gm (A - B) _____</p> <p>(D) -200 in pan, gm _____</p> <p>Total -200 material, gm (C + D) _____</p>
---	---

APPENDIX B

Sodium Sulfate Soundness

NATIONAL CENTER FOR ASPHALT TECHNOLOGY

Soundness of Aggregate by Use of Sodium Sulfate or Magnesium Sulfate

AASHTO Designation: T 104-99

ASTM Designation: C 88-99a

Project: Thesis Date: 4/4/2011

Tested By: Nick Nuno Calculated By: _____

Sample Identification: N1-4-10

Soundness - Coarse - 1500g - 1.5" to 3/4"				
Sample Description and Tag ID	Particle Size	Initial	Final	Weighted % Loss
A-5	3/4" - 500 +/-30 g	499.8	499.6	0.040
	1" - 1000 +/- 50g			
	Total	499.8	499.6	0.040
A-13	3/4" - 500 +/-30 g	506.4	506.3	0.020
	1" - 1000 +/- 50g			
	Total	506.4	506.3	0.020
			Avg	0.030

NATIONAL CENTER FOR ASPHALT TECHNOLOGY

Soundness of Aggregate by Use of Sodium Sulfate or Magnesium Sulfate

AASHTO Designation: T 104-99

ASTM Designation: C 88-99a

Project: Thesis Date: 4/4/2011

Tested By: Nick Nuno Calculated By: _____

Sample Identification: N2-4-10

Soundness - Coarse - 1500g - 1.5" to 3/4"				
Sample Description and Tag ID	Particle Size	Initial	Final	Weighted % Loss
L-1	3/4" - 500 +/-30 g	505.4		
	1" - 1000 +/- 50g	1002.0		
	Total	1507.4	1507.4	0.000
L-2	3/4" - 500 +/-30 g	506.5		
	1" - 1000 +/- 50g	996.4		
	Total	1502.9	1502.9	0.000
			Avg	0

NATIONAL CENTER FOR ASPHALT TECHNOLOGY

Soundness of Aggregate by Use of Sodium Sulfate or Magnesium Sulfate

AASHTO Designation: T 104-99

ASTM Designation: C 88-99a

Project: Thesis Date: 4/4/2011

Tested By: Nick Nuno Calculated By: _____

Sample Identification: N3-4-10

Soundness - Coarse - 1500g - 1.5" to 3/4"				
Sample Description and Tag ID	Particle Size	Initial	Final	Weighted % Loss
X-2	3/4" - 500 +/-30 g	497.6	497.3	0.060
	1" - 1000 +/- 50g			
	Total	497.6	497.3	0.060
E-1	3/4" - 500 +/-30 g	504.2	504.2	0.000
	1" - 1000 +/- 50g			
	Total	504.2	504.2	0.000
			Avg	0.030

NATIONAL CENTER FOR ASPHALT TECHNOLOGY

Soundness of Aggregate by Use of Sodium Sulfate or Magnesium Sulfate

AASHTO Designation: T 104-99

ASTM Designation: C 88-99a

Project: Thesis Date: 4/4/2011

Tested By: Nick Nuno Calculated By: _____

Sample Identification: N4-4-10

Soundness - Coarse - 1500g - 1.5" to 3/4"				
Sample Description and Tag ID	Particle Size	Initial	Final	Weighted % Loss
D-2	3/4" - 500 +/-30 g	501.0	500.9	0.020
	1" - 1000 +/- 50g			
	Total	501.0	500.9	0.020
6	3/4" - 500 +/-30 g	503.9	503.8	0.020
	1" - 1000 +/- 50g			
	Total	503.9	503.8	0.020
			Avg	0.020

NATIONAL CENTER FOR ASPHALT TECHNOLOGY

Soundness of Aggregate by Use of Sodium Sulfate or Magnesium Sulfate

AASHTO Designation: T 104-99

ASTM Designation: C 88-99a

Project: Thesis Date: 4/4/2011

Tested By: Nick Nuno Calculated By: _____

Sample Identification: N1A-4-10

Soundness - Coarse - 1500g - 1.5" to 3/4"				
Sample Description and Tag ID	Particle Size	Initial	Final	Weighted % Loss
K-2	3/4" - 500 +/-30 g	503.9	503.9	0.000
	1" - 1000 +/- 50g			
	Total	503.9	503.9	0.000
3	3/4" - 500 +/-30 g	504.6	499.6	0.991
	1" - 1000 +/- 50g			
	Total	504.6	499.6	0.991
			Avg	0.495

NATIONAL CENTER FOR ASPHALT TECHNOLOGY
Soundness of Aggregate by Use of Sodium Sulfate or Magnesium Sulfate
AASHTO Designation: T 104-99
 ASTM Designation: C 88-99a

Project: Thesis Date: 4/4/2011

Tested By: Nick Nuno Calculated By: _____

Sample Identification: N2A-4-10

Soundness - Coarse - 1500g - 1.5" to 3/4"				
Sample Description and Tag ID	Particle Size	Initial	Final	Weighted % Loss
E-2	3/4" - 500 +/-30 g	500.1		
	1" - 1000 +/- 50g	1008.5		
	Total	1508.6	1508.1	0.033
F-2	3/4" - 500 +/-30 g	501.7		
	1" - 1000 +/- 50g	1000.6		
	Total	1502.3	1502.1	0.013
			Avg	0.023

NATIONAL CENTER FOR ASPHALT TECHNOLOGY

Soundness of Aggregate by Use of Sodium Sulfate or Magnesium Sulfate

AASHTO Designation: T 104-99

ASTM Designation: C 88-99a

Project: Thesis Date: 4/4/2011

Tested By: Nick Nuno Calculated By: _____

Sample Identification: N3A-4-10

Soundness - Coarse - 1500g - 1.5" to 3/4"				
Sample Description and Tag ID	Particle Size	Initial	Final	Weighted % Loss
I-2	3/4" - 500 +/-30 g	505.8		
	1" - 1000 +/- 50g			
	Total	505.8	505.6	0.040
V-2	3/4" - 500 +/-30 g	502.1		
	1" - 1000 +/- 50g			
	Total	502.1	501.8	0.060
			Avg	0.050

NATIONAL CENTER FOR ASPHALT TECHNOLOGY

Soundness of Aggregate by Use of Sodium Sulfate or Magnesium Sulfate

AASHTO Designation: T 104-99

ASTM Designation: C 88-99a

Project: Thesis Date: 4/4/2011

Tested By: Nick Nuno Calculated By: _____

Sample Identification: N4A-4-10

Soundness - Coarse - 1500g - 1.5" to 3/4"				
Sample Description and Tag ID	Particle Size	Initial	Final	Weighted % Loss
C-1	3/4" - 500 +/-30 g	509.5	507.6	0.373
	1" - 1000 +/- 50g			
	Total	509.5	507.6	0.373
B-9 PIECE JUST SMALL ENOUGH TO FIT THROUGH THE 5/8 HOLE	3/4" - 500 +/-30 g	499.8	489	2.161
	1" - 1000 +/- 50g			
	Total	499.8	489	2.161
			Avg	1.267

APPENDIX C

Specific Gravity and Absorption

NATIONAL CENTER FOR ASPHALT TECHNOLOGY
Specific Gravity and Absorption of Coarse Aggregate and
Specific Gravity and Absorption of Fine Aggregate
(AASHTO T85 and AASHTO T84)

Project: Thesis Date: 2/11/2011

Tested By: Nick Nuno Calculated By: _____

Sample Identification: N1-4-10

Coarse Aggregate (AASHTO T85)			
Passing _____ Sieve & Retained on _____ Sieve	Sample 1	Sample 2	Average
A) Wt. of Oven Dry Aggregate, gm	4706.1	4698.6	
B) Wt. of Saturated Surface Dry Aggregate, gm	4731.1	4727.5	
C) Wt. of Saturated Aggregate in Water, gm	2943.0	2935.1	
Apparent Specific Gravity, $G_{sa} = A/(A - C)$	2.669	2.664	2.667
Bulk Specific Gravity, $G_{sb} = A/(B - C)$	2.632	2.621	2.627
Bulk SSD Specific Gravity, $G_{ssd} = B/(B - C)$	2.646	2.638	2.642
Absorption, % = $(B - A)/A$	0.5	0.6	0.6

NATIONAL CENTER FOR ASPHALT TECHNOLOGY
Specific Gravity and Absorption of Coarse Aggregate and
Specific Gravity and Absorption of Fine Aggregate
(AASHTO T85 and AASHTO T84)

Project: Thesis Date: 2/11/2011

Tested By: Nick Nuno Calculated By: _____

Sample Identification: N2-4-10

Coarse Aggregate (AASHTO T85)			
Passing _____ Sieve & Retained on _____ Sieve	Sample 1	Sample 2	Average
A) Wt. of Oven Dry Aggregate, gm	4761.1	4743.6	
B) Wt. of Saturated Surface Dry Aggregate, gm	4790.1	4772.3	
C) Wt. of Saturated Aggregate in Water, gm	2972.4	2961.5	
Apparent Specific Gravity, $G_{sa} = A/(A - C)$	2.662	2.662	2.662
Bulk Specific Gravity, $G_{sb} = A/(B - C)$	2.619	2.620	2.619
Bulk SSD Specific Gravity, $G_{ssd} = B/(B - C)$	2.635	2.635	2.635
Absorption, % = $(B - A)/A$	0.6	0.6	0.6

NATIONAL CENTER FOR ASPHALT TECHNOLOGY
Specific Gravity and Absorption of Coarse Aggregate and
Specific Gravity and Absorption of Fine Aggregate
(AASHTO T85 and AASHTO T84)

Project: Thesis Date: 2/11/2011

Tested By: Nick Nuno Calculated By: _____

Sample Identification: N3-4-10

Coarse Aggregate (AASHTO T85)			
Passing	Sieve & Retained on	Sieve	Average
		Sample 1	Sample 2
A) Wt. of Oven Dry Aggregate, gm		4160.3	4161.8
B) Wt. of Saturated Surface Dry Aggregate, gm		4189.3	4188.1
C) Wt. of Saturated Aggregate in Water, gm		2591.9	2591.7
Apparent Specific Gravity, $G_{sa} = A/(A - C)$		2.653	2.651
Bulk Specific Gravity, $G_{sb} = A/(B - C)$		2.604	2.607
Bulk SSD Specific Gravity, $G_{ssd} = B/(B - C)$		2.623	2.623
Absorption, % = $(B - A)/A$		0.7	0.6

NATIONAL CENTER FOR ASPHALT TECHNOLOGY
Specific Gravity and Absorption of Coarse Aggregate and
Specific Gravity and Absorption of Fine Aggregate
(AASHTO T85 and AASHTO T84)

Project: Thesis Date: 2/11/2011

Tested By: Nick Nuno Calculated By: _____

Sample Identification: N4-4-10

Coarse Aggregate (AASHTO T85)			
Passing _____ Sieve & Retained on _____ Sieve	Sample 1	Sample 2	Average
A) Wt. of Oven Dry Aggregate, gm	4917.8	4920.3	
B) Wt. of Saturated Surface Dry Aggregate, gm	4943.0	4945.0	
C) Wt. of Saturated Aggregate in Water, gm	3059.1	3060.5	
Apparent Specific Gravity, $G_{sa} = A/(A - C)$	2.646	2.646	2.646
Bulk Specific Gravity, $G_{sb} = A/(B - C)$	2.610	2.611	2.611
Bulk SSD Specific Gravity, $G_{ssd} = B/(B - C)$	2.624	2.624	2.624
Absorption, % = $(B - A)/A$	0.5	0.5	0.5

NATIONAL CENTER FOR ASPHALT TECHNOLOGY
Specific Gravity and Absorption of Coarse Aggregate and
Specific Gravity and Absorption of Fine Aggregate
(AASHTO T85 and AASHTO T84)

Project: Thesis Date: 2/16/2011

Tested By: Nick Nuno Calculated By: _____

Sample Identification: N1A-4-10

Coarse Aggregate (AASHTO T85)			
Passing _____ Sieve & Retained on _____ Sieve	Sample 1	Sample 2	Average
A) Wt. of Oven Dry Aggregate, gm	4616.7	4620.3	
B) Wt. of Saturated Surface Dry Aggregate, gm	4646.6	4648.4	
C) Wt. of Saturated Aggregate in Water, gm	2867.2	2869.4	
Apparent Specific Gravity, $G_{sa} = A/(A - C)$	2.639	2.639	2.639
Bulk Specific Gravity, $G_{sb} = A/(B - C)$	2.595	2.597	2.596
Bulk SSD Specific Gravity, $G_{ssd} = B/(B - C)$	2.611	2.613	2.612
Absorption, % = $(B - A)/A$	0.6	0.6	0.6

NATIONAL CENTER FOR ASPHALT TECHNOLOGY
Specific Gravity and Absorption of Coarse Aggregate and
Specific Gravity and Absorption of Fine Aggregate
(AASHTO T85 and AASHTO T84)

Project: Thesis Date: 2/16/2011

Tested By: Nick Nuno Calculated By: _____

Sample Identification: N2A-4-10

Coarse Aggregate (AASHTO T85)			
Passing _____ Sieve & Retained on _____ Sieve	Sample 1	Sample 2	Average
A) Wt. of Oven Dry Aggregate, gm	4987.3	4990.0	
B) Wt. of Saturated Surface Dry Aggregate, gm	5021.1	5016.2	
C) Wt. of Saturated Aggregate in Water, gm	3138.5	3135.1	
Apparent Specific Gravity, $G_{sa} = A/(A - C)$	2.698	2.690	2.694
Bulk Specific Gravity, $G_{sb} = A/(B - C)$	2.649	2.653	2.651
Bulk SSD Specific Gravity, $G_{ssd} = B/(B - C)$	2.667	2.667	2.667
Absorption, % = $(B - A)/A$	0.7	0.5	0.6

NATIONAL CENTER FOR ASPHALT TECHNOLOGY
Specific Gravity and Absorption of Coarse Aggregate and
Specific Gravity and Absorption of Fine Aggregate
(AASHTO T85 and AASHTO T84)

Project: Thesis Date: 2/16/2011

Tested By: Nick Nuno Calculated By: _____

Sample Identification: N3A-4-10

Coarse Aggregate (AASHTO T85)			
Passing _____ Sieve & Retained on _____ Sieve	Sample 1	Sample 2	Average
A) Wt. of Oven Dry Aggregate, gm	4818.2	4795.9	
B) Wt. of Saturated Surface Dry Aggregate, gm	4848.2	4826.5	
C) Wt. of Saturated Aggregate in Water, gm	2991.1	2975.4	
Apparent Specific Gravity, $G_{sa} = A/(A - C)$	2.637	2.634	2.636
Bulk Specific Gravity, $G_{sb} = A/(B - C)$	2.594	2.591	2.593
Bulk SSD Specific Gravity, $G_{ssd} = B/(B - C)$	2.611	2.607	2.609
Absorption, % = $(B - A)/A$	0.6	0.6	0.6

NATIONAL CENTER FOR ASPHALT TECHNOLOGY
Specific Gravity and Absorption of Coarse Aggregate and
Specific Gravity and Absorption of Fine Aggregate
(AASHTO T85 and AASHTO T84)

Project: Thesis Date: 2/16/2011

Tested By: Nick Nuno Calculated By: _____

Sample Identification: N4A-4-10

Coarse Aggregate (AASHTO T85)			
Passing _____ Sieve & Retained on _____ Sieve	Sample 1	Sample 2	Average
A) Wt. of Oven Dry Aggregate, gm	4550.7	4573.7	
B) Wt. of Saturated Surface Dry Aggregate, gm	4573.6	4597.2	
C) Wt. of Saturated Aggregate in Water, gm	2840.0	2854.4	
Apparent Specific Gravity, $G_{sa} = A/(A - C)$	2.660	2.660	2.660
Bulk Specific Gravity, $G_{sb} = A/(B - C)$	2.625	2.624	2.625
Bulk SSD Specific Gravity, $G_{ssd} = B/(B - C)$	2.638	2.638	2.638
Absorption, % = $(B - A)/A$	0.5	0.5	0.5

APPENDIX D

Los Angeles Abrasion

NATIONAL CENTER FOR ASPHALT TECHNOLOGY

Resistance to Degradation of Small-Size Coarse Aggregate by Abrasion and Impact in the Los Angeles Machine

Project: Thesis Date: 3/7/2011

Tested By: Nick Nuno Calculated By: Nick Nuno

Sample Identification: N1-4-10

LA Abrasion				
Sample ID #:		Sample A	Sample B	Average
	Initial Weight (grams), A	5000.6	5000.5	
	Final Weight (grams), B	3302.1	3263.4	
	Percent Loss (%) $[(A-B)/A]*100$	33.966	34.739	34.4

NATIONAL CENTER FOR ASPHALT TECHNOLOGY
Resistance to Degradation of Small-Size Coarse Aggregate by Abrasion and Impact in the Los Angeles Machine

Project: Thesis Date: 3/7/2011

Tested By: Nick Nuno Calculated By: Nick Nuno

Sample Identification: N2-4-10

LA Abrasion				
Sample ID #:		Sample A	Sample B	Average
	Initial Weight (grams), A	5000.1	5000.1	
	Final Weight (grams), B	3213.8	3132.6	
	Percent Loss (%) $[(A-B)/A]*100$	35.725	37.349	36.5

NATIONAL CENTER FOR ASPHALT TECHNOLOGY

Resistance to Degradation of Small-Size Coarse Aggregate by Abrasion and Impact in the Los Angeles Machine

Project: Thesis Date: 3/7/2011

Tested By: Nick Nuno Calculated By: Nick Nuno

Sample Identification: N3-4-10

LA Abrasion				
Sample ID #:		Sample A	Sample B	Average
	Initial Weight (grams), A	5002.5	5000.7	
	Final Weight (grams), B	2894.4	2911.3	
	Percent Loss (%) $[(A-B)/A]*100$	42.141	41.782	42.0

NATIONAL CENTER FOR ASPHALT TECHNOLOGY

Resistance to Degradation of Small-Size Coarse Aggregate by Abrasion and Impact in the Los Angeles Machine

Project: Thesis Date: 3/7/2011

Tested By: Nick Nuno Calculated By: Nick Nuno

Sample Identification: N4-4-10

LA Abrasion				
Sample ID #:		Sample A	Sample B	Average
	Initial Weight (grams), A	5002.5	5000.1	
	Final Weight (grams), B	2871.6	2859.1	
	Percent Loss (%) $[(A-B)/A]*100$	42.597	42.819	42.7

NATIONAL CENTER FOR ASPHALT TECHNOLOGY

Resistance to Degradation of Small-Size Coarse Aggregate by Abrasion and Impact in the Los Angeles Machine

Project: Thesis Date: 3/7/2011

Tested By: Nick Nuno Calculated By: Nick Nuno

Sample Identification: N1A-4-10

LA Abrasion				
Sample ID #:		Sample A	Sample B	Average
	Initial Weight (grams), A	5000.7	5001.9	
	Final Weight (grams), B	3274.9	3254.7	
	Percent Loss (%) $[(A-B)/A]*100$	34.511	34.931	34.7

NATIONAL CENTER FOR ASPHALT TECHNOLOGY

Resistance to Degradation of Small-Size Coarse Aggregate by Abrasion and Impact in the Los Angeles Machine

Project: Thesis Date: 3/7/2011

Tested By: Nick Nuno Calculated By: Nick Nuno

Sample Identification: N2A-4-10

LA Abrasion				
Sample ID #:		Sample A	Sample B	Average
	Initial Weight (grams), A	5000.4	4999.6	
	Final Weight (grams), B	3574.6	3555.6	
	Percent Loss (%) $[(A-B)/A]*100$	28.514	28.882	28.7

NATIONAL CENTER FOR ASPHALT TECHNOLOGY

Resistance to Degradation of Small-Size Coarse Aggregate by Abrasion and Impact in the Los Angeles Machine

Project: Thesis Date: 3/7/2011

Tested By: Nick Nuno Calculated By: Nick Nuno

Sample Identification: N3A-4-10

LA Abrasion				
Sample ID #:		Sample A	Sample B	Average
	Initial Weight (grams), A	5002.7	5000.9	
	Final Weight (grams), B	2782.5	2780.3	
	Percent Loss (%) $[(A-B)/A]*100$	44.380	44.404	44.4

NATIONAL CENTER FOR ASPHALT TECHNOLOGY

Resistance to Degradation of Small-Size Coarse Aggregate by Abrasion and Impact in the Los Angeles Machine

Project: Thesis Date: 3/7/2011

Tested By: Nick Nuno Calculated By: Nick Nuno

Sample Identification: N4A-4-10

LA Abrasion				
Sample ID #:		Sample A	Sample B	Average
	Initial Weight (grams), A	5001.3	4999.1	
	Final Weight (grams), B	3098.9	3122.4	
	Percent Loss (%) $[(A-B)/A]*100$	38.038	37.541	37.8

